Aalborg Universitet

AALBORG UNIVERSITY
DENMARK

Analysis of Waves

Technical documentation for WaveLab 3

Frigaard, Peter; Andersen, Thomas Lykke

[Link to publication from Aalborg University](#)

Analysis of Waves

Technical documentation for WaveLab 3

Peter Frigaard
Thomas Lykke Andersen

AALBORG UNIVERSITY
Department of Civil Engineering

Aalborg University
Department of Civil Engineering
Water and Soil

DCE Lecture Notes No. 33

Analysis of Waves
Technical documentation for WaveLab 3

by

Peter Frigaard
Thomas Lykke Andersen

October 2014

Scientific Publications at the Department of Civil Engineering

Technical Reports are published for timely dissemination of research results and scientific work carried out at the Department of Civil Engineering (DCE) at Aalborg University. This medium allows publication of more detailed explanations and results than typically allowed in scientific journals.

Technical Memoranda are produced to enable the preliminary dissemination of scientific work by the personnel of the DCE where such release is deemed to be appropriate. Documents of this kind may be incomplete or temporary versions of papers—or part of continuing work. This should be kept in mind when references are given to publications of this kind.

Contract Reports are produced to report scientific work carried out under contract. Publications of this kind contain confidential matter and are reserved for the sponsors and the DCE. Therefore, Contract Reports are generally not available for public circulation.

Lecture Notes contain material produced by the lecturers at the DCE for educational purposes. This may be scientific notes, lecture books, example problems or manuals for laboratory work, or computer programs developed at the DCE.

Theses are monograms or collections of papers published to report the scientific work carried out at the DCE to obtain a degree as either PhD or Doctor of Technology. The thesis is publicly available after the defence of the degree.

Latest News is published to enable rapid communication of information about scientific work carried out at the DCE. This includes the status of research projects, developments in the laboratories, information about collaborative work and recent research results.

Contents

Chapter 1

Introduction

The present book describes the most important aspects of wave analysis techniques applied to physical model tests. Moreover, the book serves as technical documentation for the wave analysis software WaveLab 3, cf. Aalborg University (2012). In that respect it should be mentioned that supplementary to the present technical documentation exists also the online help document describing the WaveLab software in detail including all the inputs and output fields. In addition to the two main authors also Tue Hald, Jacob Helm-Ptersen and Morten Møller Jakobsen have contributed to the note. Their input is highly acknowledged.

The outline of the book is as follows:

- Chapter 2 and 3 describes analysis of waves in time and frequency domain.

- Chapter 4 and 5 describes the separation of incident and reflected waves for the two-dimensional case.

- Chapter 6 describes the estimation of the directional spectra which also includes the separation of incident and reflected waves for multi-directional waves.

- Chapter 7 describes the analysis of wave groups and calculation of the groupiness factor.

Chapter 2

Time-Domain Analysis of Waves

2.1 Definition of the individual wave : Zero-down crossing

The individual wave is defined by two successive zero-down crossings, cf. 2.1. For many years it was common to use zero-up crossings to define a wave, but due to the asymmetry of natural waves, the greatest wave forces are often experienced when the wave front hits a structure. That's one of the main reasons why IAHR (1986) recommended that the height of a wave is defined as the height from a trough to the following crest in a time series. Fig. 2.2 is an example of surface elevation recordings. The application of
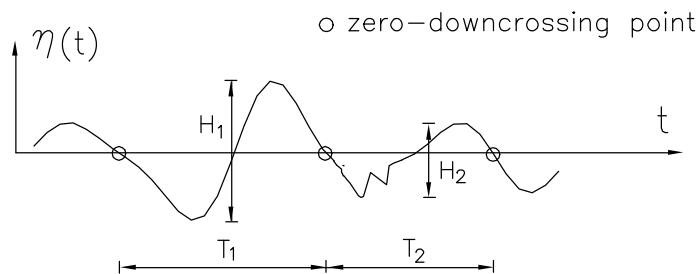
Figure 2.1: Individual waves defined by zero-down crossing.

zero-downcrossing gives 15 individual waves (N=15). In Table 4.1 the data are arranged according to the descending order of wave height.
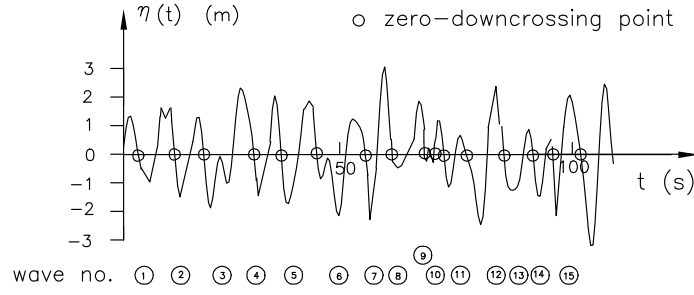
Figure 2.2: Application of zero-down crossing.

Table 4.1. Ranked individual wave heights and corresponding periods in Fig. 2.2.

rank i	1	2	3	4	5	6	7	8	9	10	11	12	13	14	15
H (m)	5.5	4.8	4.2	3.9	3.8	3.4	2.9	2.8	2.7	2.3	2.2	1.9	1.8	1.1	0.23
T (s)	12.5	13.0	12.0	11.2	15.2	8.5	11.9	11.0	9.3	10.1	7.2	5.6	6.3	4.0	0.9
wave no. in 2.2	7	12	15	3	5	4	2	11	6	1	10	8	13	14	9

2.2 Characteristic wave heights and periods

Usually a surface elevation recording, exemplified in Fig. 2.2, contains more than several hundred individual waves.

Both wave height and wave period can be considered as random variables, which have certain probability distributions.

Before these distributions are discussed, some definitions of characteristic waves will be given.

Mean wave: $\overline{H}, \overline{T}$

$\overline{H}$ and $\overline{T}$ are the mean values of the heights and periods , respectively, of all

8

individual waves. Table 4.1 yields

$$\overline{H} \;=\; \frac{1}{15} \sum_{i=1}^{15} H_i \;=\; 2.9 \text{ m} \qquad\qquad \overline{T} \;=\; \frac{1}{15} \sum_{i=1}^{15} T_i \;=\; 9.25 \text{ s}$$

Root-mean-square wave: H_{rms}

This wave has a height defined as

$$H_{rms} \;=\; \sqrt{\frac{1}{N} \sum_{i=1}^{N} H_i^2}$$

From Table 4.1 is found

$$H_{rms} \;=\; \sqrt{\frac{1}{15} \sum_{i=1}^{15} H_i^2} \;=\; 3.20 \text{ m}$$

Significant wave: H_s, T_s or $H_{1/3}$, $T_{H_{1/3}}$

The significant wave height is the average of the wave heights of the one-third highest waves. The significant wave period is the average of the wave periods of the one-third highest waves. From Table 4.1 one finds

$$H_s \;=\; \frac{1}{5} \sum_{i=1}^{5} H_i \;=\; 4.44 \text{ m} \qquad T_s \;=\; \frac{1}{5} \sum_{j=1}^{5} T_j \;=\; 12.8 \text{ s} \qquad i, j \text{ are the rank no.}$$

The significant wave is very often used as the design wave. The reason might be that in old days structures were designed an a basis of visually observed waves. Experiences show that often the wave height and period reported by visual observation correspond approximately to the measured significant wave. Therefore the choice of significant wave as design wave can make use of the existing engineering experience.

<u>Maximum wave: H_{max}, $T_{H_{max}}$</u>

This is the wave, which has the maximum wave height. In Table 4.1,

$$H_{max} = 5.5 \text{ m} \qquad\qquad T_{H_{max}} = 12.5 \text{ s}$$

Note, however, that H_{max} is a random variable which depends on the number of individual waves in the time series.

The maximum wave from a long time series corresponding to a storm with a return period of e.g. 100 years is often chosen as the design wave for structures which are very important and very sensitive to wave loads.

<u>Highest one-tenth wave: $H_{1/10}$, $T_{H_{1/10}}$</u>

$H_{1/10}$ is the average of the wave heights of the one-tenth highest waves. $T_{H_{1/10}}$ is the average of the wave periods of the one-tenth highest wave.

<u>Wave height with exceedence probability of $\alpha\%$: $H_{\alpha\%}$</u>

It is often practical to denote a wave height according to the probability of exceedence. Examples are $H_{0.1\%}$, $H_{1\%}$, $H_{2\%}$ etc. In many situations $H_{0.1\%}$ in the 100 year storm is used as the design wave.

2.3 Distribution of individual wave heights

<u>Histogram of wave heights</u>

Instead of showing all individual wave heights, it is easier to use the wave height histogram which gives information about the number of waves in various wave height intervals. Fig. 2.3 is the histogram of wave heights corresponding to Table 4.1.

<u>Non-dimensionalized histogram</u>

In order to compare the distribution of wave heights at different locations, the histogram of wave heights is non-dimensionalized, cf. Fig. 2.4.

When $\Delta(H/\overline{H})$ approaches zero, the probability density becomes a smooth curve. Experience and theory have shown that this curve is very close to
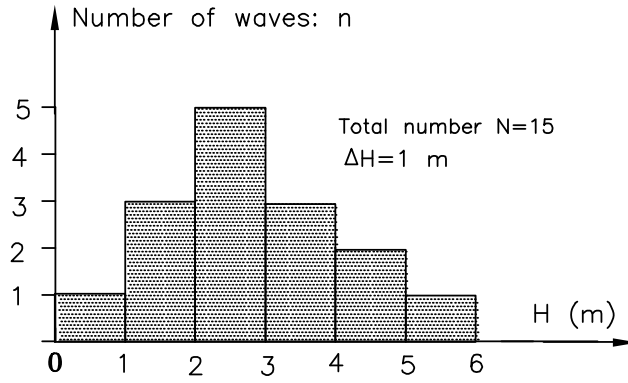
Figure 2.3: Wave height histogram.
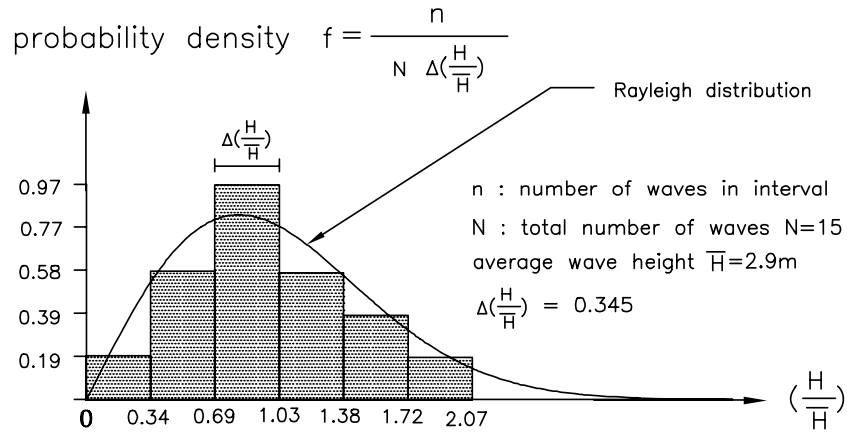
Figure 2.4: Non-dimensionalized wave height histogram.

the Rayleigh distribution in case of deep water waves. In other words, the individual wave heights follow the Rayleigh distribution.

Rayleigh distribution

The Rayleigh probability density function is defined as

$$f(x) \; = \; \frac{\pi}{2} \, x \, \exp\left(-\frac{\pi}{4}x^2\right) \qquad \text{where} \qquad x = \frac{H}{\overline{H}} \qquad (2.1)$$

11

The Rayleigh distribution function is

$$F(x) \;=\; \mathrm{Prob}\{X < x\} \;=\; 1 \;-\; \exp\left(-\frac{\pi}{4}x^2\right) \tag{2.2}$$

Relation between characteristic wave heights
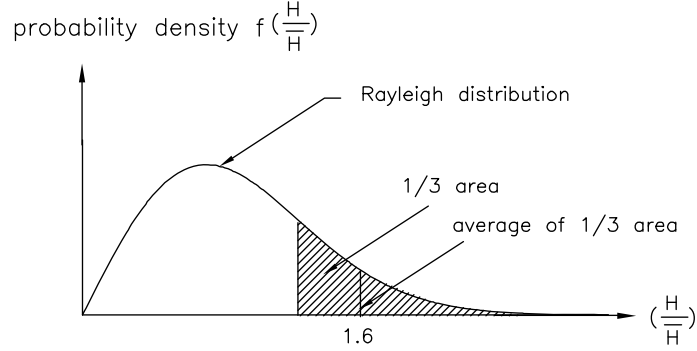
Figure 2.5: Relation between H_s and $\overline{H}$.

If we adopt the Rayleigh distribution as an approximation to the distribution of individual wave heights, then the characteristic wave heights $H_{1/10}$, $H_{1/3}$, H_{rms} and $H_{\alpha\%}$ can be expressed by $\overline{H}$ through the manipulation of the Rayleigh probability density function.

$$
\begin{aligned}
H_{1/10} &= 2.03\,\overline{H} \\
H_{1/3} &= 1.60\,\overline{H} \\
H_{rms} &= 1.13\,\overline{H} \\
H_{2\%} &= 2.23\,\overline{H} \\
H_{0.1\%} &= 2.97\,\overline{H}
\end{aligned}
\tag{2.3}
$$

Fig. 2.5 illustrates how to obtain the relation between H_s and $\overline{H}$.

The Rayleigh distribution function given by H_s instead of $\overline{H}$ reads

$$F(H) \;=\; 1 \;-\; \exp\left(-2\left(\frac{H}{H_s}\right)^2\right) \tag{2.4}$$

Individual wave height distribution in shallow water

Only in relatively deep water, the Rayleigh distribution is a good approxima-
tion to the distribution of individual wave heights. When wave breaking takes
place due to limited water depth, the individual wave height distribution will
differ from the Rayleigh distribution.

Stive (1986), proposed the following empirical correction to the Rayleigh
distribution based on model tests and also roughly checked against some
prototype data.

$$H_{1\%} = H_{m0} \left(\frac{ln100}{2}\right)^{\frac{1}{2}} \left(1 + \frac{H_{m0}}{h}\right)^{-\frac{1}{3}} \qquad (2.5)$$

$$H_{0.1\%} = H_{m0} \left(\frac{ln1000}{2}\right)^{\frac{1}{2}} \left(1 + \frac{H_{m0}}{h}\right)^{-\frac{1}{2}} \qquad (2.6)$$

where h is the water depth, $H_{1\%}$ means the 1% exceedence value of the wave
height determined by zero-down-crossing analysis, whereas the significant
wave height H_{m0} is determined from the surface elevataion spectrum, cf.
chapter 3. The correction formulae are very useful for checking the wave
height distribution in small scale physical model tests, cf. Fig. 2.6.
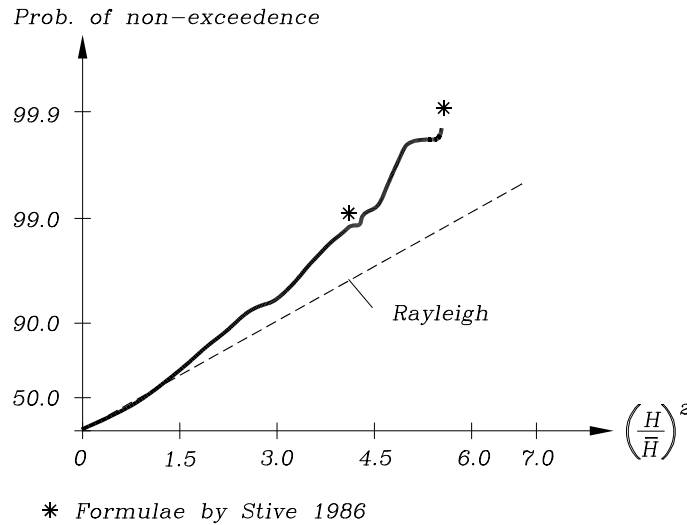
Figure 2.6: Comparison of the expression by Stive, 1986, for shallow water
wave height distribution with model test results. Aalborg University Hy-
draulics Laboratory 1990.

Klopmann et al. (1989) proposed also a semi-empirical expression for the individual wave height distribution. Worth mentioning is also the very much used method of Battjes and Groenendijk (2000) which was calibrated against a lot of physical model test data, but the numerical procedure is somewhat more complicated.

Chapter 3 gives a more detailed discussion on the validity of the Rayleigh distribution, based on energy spectrum width parameter.

2.4   Maximum wave height H_{max}

As mentioned above H_{max} is a random variable that depends on the number of waves in the timeseries. Below some facts about the distribution of H_{max} are given.

Distribution of H_{max}

The distribution function of $X = H/\overline{H}$ is the Rayleigh distribution

$$F_X(x) \;=\; \mathrm{Prob}\{X < x\} \;=\; 1 \;-\; \exp\left(-\frac{\pi}{4}x^2\right) \tag{2.7}$$

If there are N individual waves in a storm[1], the distribution function of $X_{max} = H_{max}/\overline{H}$ is

$$
\begin{aligned}
F_{X_{max}}(x) \;&=\; \mathrm{Prob}\{X_{max} < x\} \;=\; \left(\,F_X(x)\,\right)^N \\
&=\; \left(\,1 \;-\; \exp\left(-\frac{\pi}{4}x^2\right)\,\right)^N
\end{aligned}
\tag{2.8}
$$

Note that $F_{X_{max}}(x)$ can be interpreted as the probability of the non-occurrence of the event $(\,X > x\,)$ in any of N independent trials. The probability density function of X_{max} is

$$
\begin{aligned}
f_{X_{max}}(x) \;&=\; \frac{\mathrm{d}F_{X_{max}}}{\mathrm{d}x} \\
&=\; \frac{\pi}{2}\,N\,x\,\exp\left(-\frac{\pi}{4}x^2\right)\left(\,1 \;-\; \exp\left(-\frac{\pi}{4}x^2\right)\,\right)^{N-1}
\end{aligned}
\tag{2.9}
$$

---

[1]A storm usually lasts some days. The significant wave height is varying during a storm. However we are more interested in the maximum significant wave height in a short period of time. In practice, N is often assumed to be 1000.

The density function of X and the density function of X_{max} are sketched in Fig. 2.7.
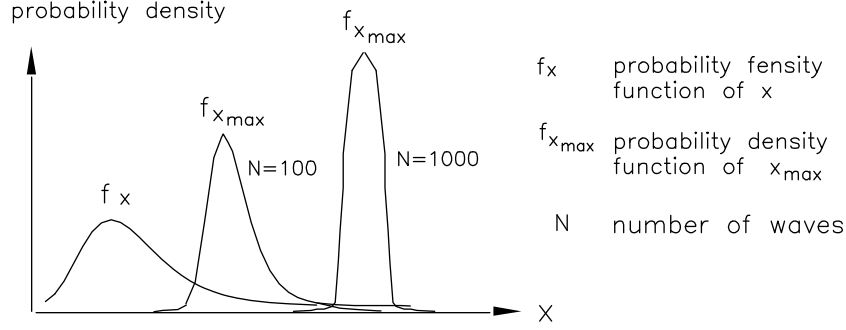
Figure 2.7: Probability density function of X and X_{max}.

Mean, median and mode of H_{max}

Mean, median and mode are often used as the characteristic values of a random variable. Their definitions are given in Fig. 2.8.
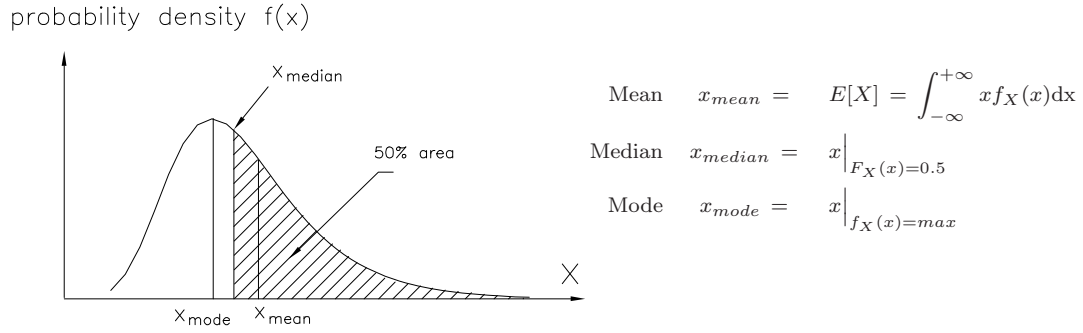
Figure 2.8: Probability density function of X and X_{max}.

By putting eqs (2.8) and (2.9) into the definitions, we obtain

$$(H_{max})_{mean} \approx \left(\sqrt{\frac{\ln N}{2}} + \frac{0.577}{\sqrt{8 \ln N}} \right) H_s \tag{2.10}$$

$$(H_{max})_{mode} \approx \sqrt{\frac{\ln N}{2}} H_s \tag{2.11}$$

15

Furthermore, $(H_{max})_\mu$, defined as the maximum wave height with exceedence probability of μ (cf. Fig. 2.9), is

$$(H_{max})_\mu \approx \sqrt{\frac{1}{2} \ln \left(\frac{N}{\ln \left(\frac{1}{1-\mu} \right)} \right)} H_s \qquad (2.12)$$

Obviously $(H_{max})_{median} = (H_{max})_{0.5}$.

We get for the commonly used $N = 1000$ the following maximum wave heights:

$$(H_{max})_{mode} \approx 1.86 H_s = 2.97\overline{H} \qquad (2.13)$$
$$(H_{max})_{mean} \approx 1.94 H_s = 3.10\overline{H} \qquad (2.14)$$
$$(H_{max})_{10\%} \approx 2.14 H_s = 3.42\overline{H} \qquad (2.15)$$
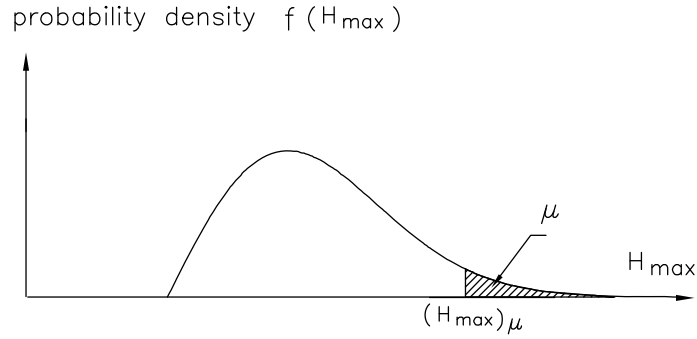
Figure 2.9: Definition of $(H_{max})_\mu$.

Monte-Carlo simulation of H_{max} distribution

The distribution of H_{max} can also be studied by the Monte-Carlo simulation. Individual wave heights follow the Rayleigh distribution

$$F(H) = 1 - exp\left(-2 \left(\frac{H}{H_s} \right)^2 \right) \qquad (2.16)$$

The storm duration corresponds to N individual waves.

1) Generate randomly a data between 0 and 1. Let the non-exceedence probability $F(H)$ equal to that data. One individual wave height H is obtained by (cf. Fig. 2.10)

$$H = F^{-1}(F(H)) = H_s \sqrt{\frac{- \ln(1 - F(H))}{2}} \qquad (2.17)$$

2) Repeat step 1) N times. Thus we obtain a sample belonging to the distribution of eq (2.16) and the sample size is N.

3) Pick up H_{max} from the sample.

4) Repeat steps 2) and 3), say, 10,000 times. Thus we get 10,000 values of H_{max}.

5) Draw the probability density of H_{max}.
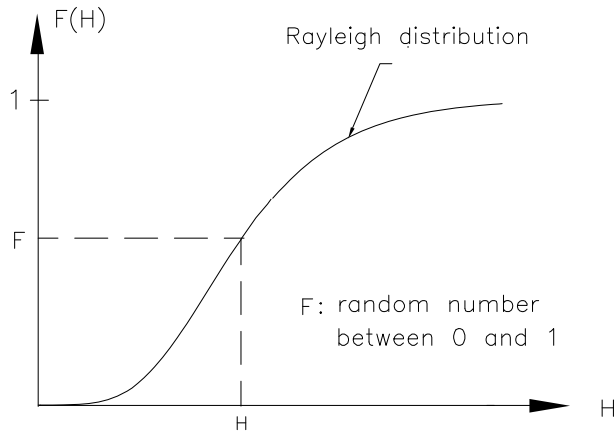
Figure 2.10: Simulated wave height from the Rayleigh distribution.

2.5 Distribution of wave periods

It is summarized as

- When we talk about the distribution of wave periods, we often mean the joint distribution of significant wave height and significant wave period. Until now there is no general theoretical expression for the joint distribution, even though there are some so-called *scatter diagrams* based on wave recording. Such a diagram is valid only for the measurement location. The relation between H_s and T_s is often simplified as $T_s = \alpha H_s^\beta$, e.g. in Canadian Atlantic waters $\alpha = 4.43$ and $\beta = 0.5$ (Neu 1982).

- The distribution of wave periods is narrower than that of wave height.

- The empirical relation $T_{max} \approx T_{1/10} \approx T_{1/3} \approx 1.2\,\overline{T}$ (Goda 2010).

2.6 Skewness, kurtosis and atiltness

Non-linear waves do not have a gaussian distributed surface as the waves are assymetric with higher and narrower crests and wider and less deep troughs. This distortion of the distribution of the surface can be described by the skewness (β_1) and kurtosis (β_2) defined as:

$$\sqrt{\beta_1} = \frac{1}{\eta_{rms}^3} \cdot \frac{1}{N} \sum_{i=1}^{N} (\eta_i - \overline{\eta})^3 \tag{2.18}$$

$$\beta_2 = \frac{1}{\eta_{rms}^4} \cdot \frac{1}{N} \sum_{i=1}^{N} (\eta_i - \overline{\eta})^4 \tag{2.19}$$

For a Gaussian surface the skewness is zero. Positive skewness indicate that the median value is below the mean value and a heavy positive tail which will be the case for non-linear waves. Huang and Long (1980) found that in deep water the skewness is proportional to the wave skewness. The kurtosis describes the peakedness of the statistical distribution. A gaussian process has a kurtosis of 3 and higher values indicate high narrow peak and heavier tails than given by the gaussian distribution.

Goda (1986) introduced the overall atiltness paramter (β_3) which describes

the assymetry in the direction of propagation.

$$\beta_3 \;=\; \frac{\frac{1}{N-1} \sum_{i=1}^{N-1} (\dot{\eta}_i - \overline{\eta})^3}{\left(\frac{1}{N-1} \sum_{i=1}^{N-1} (\dot{\eta}_i - \overline{\eta})^2 \right)^{3/2}} \qquad (2.20)$$

Waves in the near shore zone as the waves tend to have a steep front slope and a gentle rear slope. Such waves would have a positive atiltness and the atiltness paramter can exceed unity within the surf zone.

Chapter 3

Frequency-Domain Analysis

The concept of a spectrum can be attributed to Newton, who discovered that sunlight can be decomposed into a spectrum of colors from red to violet, based on the principle that white light consists of numerous components of light of various colors (wave length or wave frequency).

Energy spectrum means the energy distribution over frequency. Spectral analysis is a technique of decomposing a complex physical phenomenon into individual components with respect to frequency.

Spectral analysis of irregular waves is very important for the design of structures. For example, in the oil-drilling platform design where wave forces plays an important role, it is of importance to design the structure in such a way that the natural frequency of the structure is rather far away from the frequency band where the main part of wave energy concentrates. In this way resonance phenomenon and the corresponding dynamic amplification of force and deformation can be avoided.

3.1   Basic concepts of linear waves

<u>Surface elevation</u>

The surface elevation of a linear wave is:

$$\eta(x,t) \;=\; \frac{H}{2}\cos(\omega t - kx + \delta) \;=\; a\ \cos(\omega t - kx + \delta) \tag{3.1}$$

where H wave height

           a amplitude, $a = H/2$

           ω angular frequency, $\omega = 2\pi/T$

           T wave period.

           k wave number, $k = 2\pi/L$

           L wave length

           δ initial phase

We can also define the observation location to $x = 0$ and obtain

$$\eta(t) = a \; \cos(\omega t + \delta) \tag{3.2}$$

The relation between wave period and wave length (dispersion relationship) is

$$L = \frac{g\,T^2}{2\pi} \; \tanh\left(\frac{2\pi h}{L}\right) \tag{3.3}$$

where h is water depth.

Wave energy

The average wave energy per unit area is:

$$E = \frac{1}{8}\rho\,g\,H^2 = \frac{1}{2}\rho\,g\,a^2 \quad \text{(Joule/m}^2 \text{ in SI unit)} \tag{3.4}$$

Variance of surface elevation of a linear wave

The variance of the surface elevation of a sinus wave is:

$$\mathrm{Var}[\eta(t)] = E\left[\left(\eta(t) - \overline{\eta(t)}\right)^2\right] \quad \text{(E: Expectation)}$$

$$= E\left[(\eta(t))^2\right]$$

$$= \tfrac{1}{T} \int_0^T \eta^2(t)\, dt \quad \text{(T: wave period)}$$

$$= \tfrac{1}{2}\,a^2$$

Superposition of linear waves

Since the governing equation (Laplace equation) and boundary conditions are linear in small amplitude wave theory, it is known from mathematics that small amplitude waves are superposable. This means that the superposition of a number of linear waves with different wave height and wave period will be:

	superposition		wave 1		wave 2		$\cdots$		wave N
velocity potential	φ	$=$	φ_1	$+$	φ_2	$+$	$\cdots$	$+$	φ_N
surface elevation	η	$=$	η_1	$+$	η_2	$+$	$\cdots$	$+$	η_N
particle velocity	u	$=$	u_1	$+$	u_2	$+$	$\cdots$	$+$	u_N
dynamic pressure	p	$=$	p_1	$+$	p_2	$+$	$\cdots$	$+$	p_N

3.2   Example of variance spectrum

First we will make use of an example to demonstrate what a variance spectrum is.

Surface elevation of irregular wave

Fig. 3.1 gives an example of an irregular wave surface elevation which is constructed by adding 4 linear waves (component waves) of different wave height and wave period. The superposed wave surface elevation is

$$\eta(t) \;=\; \sum_{i=1}^{4} \eta_i(t) \;=\; \sum_{i=1}^{4} a_i \, \cos(\omega_i t + \delta_i) \tag{3.5}$$
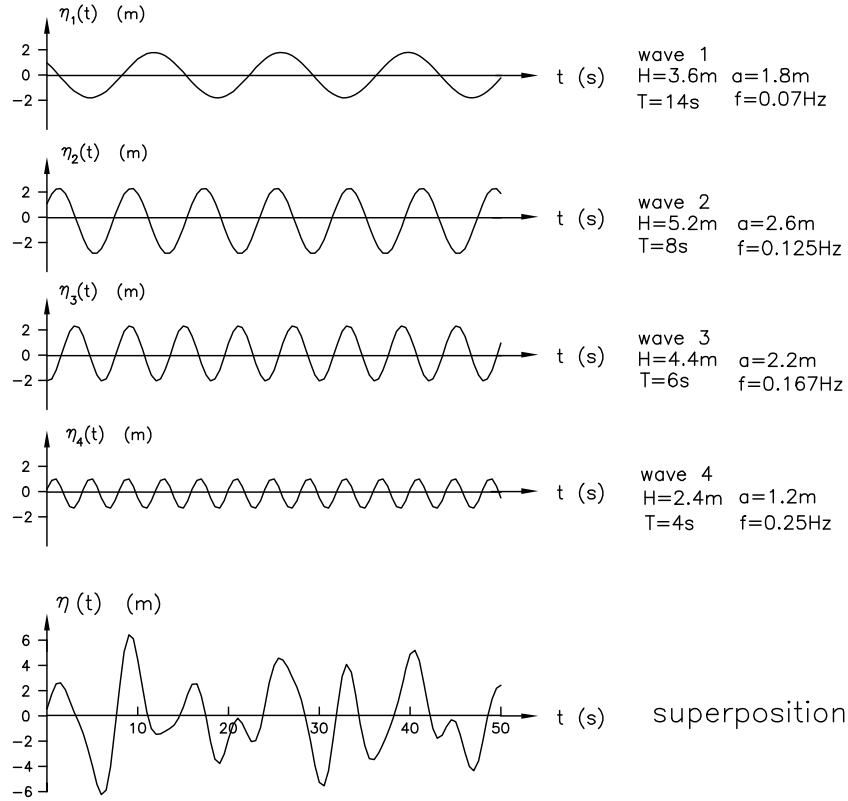
Figure 3.1: Simulation of irregular waves by superposition of linear waves.

Variance diagram

Instead of Fig. 3.1, we can use a variance diagram, shown in Fig. 3.2, to describe the irregular wave.
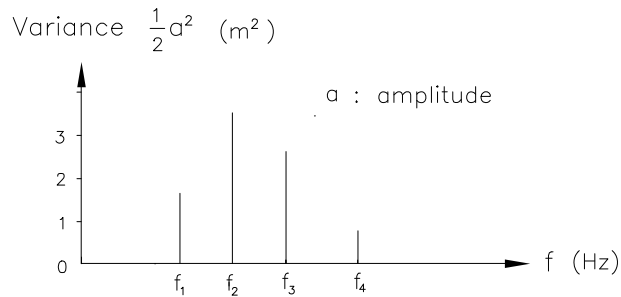
Figure 3.2: Variance diagram.

In comparison with Fig. 3.1, the variance diagram keeps the information on amplitude (a_i) and frequency $(f_i$, hence T_i and L_i) of each component, while the information on initial phase (δ_i) is lost. This information loss does not

matter because the surface elevation of irregular wave is a random process. We can simply assign a random initial phase to each component.

Variance spectral density $S_\eta(f)$

The variance diagram can be converted to variance spectrum, The spectral density is defined as

$$S_\eta(f) = \frac{\frac{1}{2}a^2}{\Delta f} \qquad (\text{m}^2 \text{ s}) \tag{3.6}$$

where Δf is the frequency band width[1], cf. Fig. 3.3.
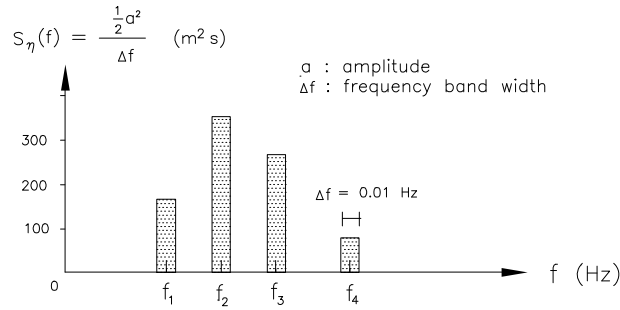
Figure 3.3: Stepped Variance spectrum.

In reality an irregular wave is composed of infinite number of linear waves with different frequency. Fig. 3.4 gives an example of stepped variance spectrum.
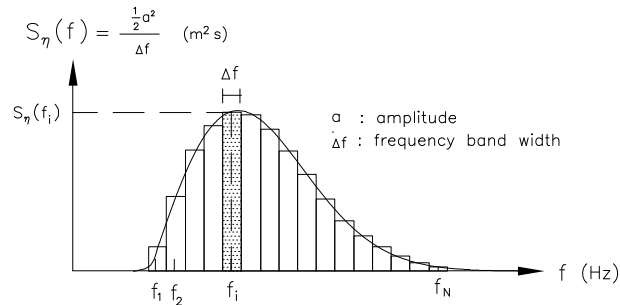
Figure 3.4: Continuous variance spectrum (wave energy spectrum).

[1]we will see later that Δf depends on signal recording duration. In the figure it is assumed that $\Delta f = 0.01 Hz$

25

When Δf approaches zero, the variance spectrum becomes a continuous curve. A variance spectrum is also called energy spectrum. But strictly speaking, the energy spectral density should be defined as

$$S(f) = \frac{\frac{1}{2}\rho\, g\, a^2}{\Delta f} \qquad (\tfrac{J\ s}{m^2}) \tag{3.7}$$

Construction of time series from variance spectrum

We can also construct time series of surface elevation from variance spectrum. In Fig. 3.4 the known variance spectral density $S_\eta(f)$ is divided into N parts by the frequency band width Δf. This means that the irregular wave is composed of N linear waves

$$\eta(t) = \sum_{i=1}^{N} \eta_i(t) = \sum_{i=1}^{N} a_i\, \cos(\omega_i t + \delta_i) \tag{3.8}$$

The variance of each linear wave is

$$S_\eta(f_i)\, \Delta f = \frac{1}{2}a_i^2 \qquad i = 1, 2, \cdots, N \tag{3.9}$$

Therefore the amplitude is

$$a_i = \sqrt{2\, S_\eta(f_i)\, \Delta f} \qquad i = 1, 2, \cdots, N \tag{3.10}$$

The angular frequency is

$$\omega_i = \frac{2\pi}{T_i} = 2\pi f_i \qquad i = 1, 2, \cdots, N \tag{3.11}$$

The initial phase δ_i is assigned a random number between 0 and 2π. Hence by use of Eq. (3.8) we can draw the time-series of the surface elevation of the irregular wave which has the variance spectrum as shown in Fig. 3.4.

3.3   Fourier series

Conversion of irregular surface elevation into variance spectrum is not as simple as the above example, where the linear components of the irregular wave are pre-defined (cf. Fig. 3.1). We need to decompose the irregular wave into its linear components. First let's see how it can be done with a known continuous function $x(t)$.

Fourier series is used to represent any arbitrary function[2].
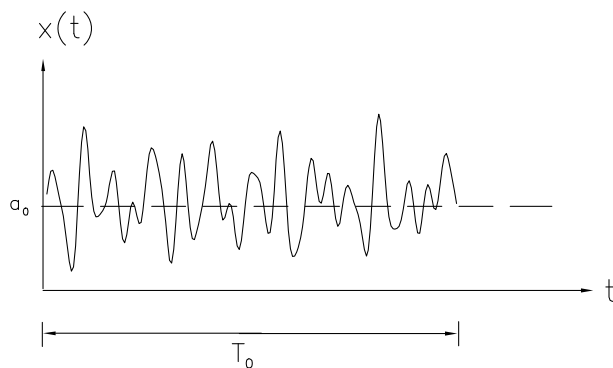
Figure 3.5: Arbitrary periodic function of time.

$$
\begin{aligned}
x(t) &= a_0 + \sum_{i=1}^{\infty} \left(a_i \cos\left(\frac{2\pi i}{T_0}t\right) + b_i \sin\left(\frac{2\pi i}{T_0}t\right) \right) \\
&= \sum_{i=0}^{\infty} \left(a_i \cos\omega_i t + b_i \sin\omega_i t \right)
\end{aligned}
\tag{3.12}
$$

---

[2] Not all mathematicians agree that an arbitrary function can be represented by a Fourier series. However, all agree that if $x(t)$ is a periodic function of time t, with period T_0 then $x(t)$ can be expressed as a Fourier series. In our case $x(t)$ is the surface elevation of irregular wave, which is a random process. if T_0 is large enough, we can assume that $x(t)$ is a periodic function with period T_0.

where a_i and b_i are Fourier coefficients given by

$$
\begin{aligned}
a_0 &= \tfrac{1}{T_0} \int_0^{T_0} x(t)\ \mathrm{dt} \quad \text{and} \quad b_0 = 0 \\
a_i &= \tfrac{2}{T_0} \int_0^{T_0} x(t)\ \cos\omega_i t\ \mathrm{dt} \\
b_i &= \tfrac{2}{T_0} \int_0^{T_0} x(t)\ \sin\omega_i t\ \mathrm{dt}
\end{aligned}
\left.\vphantom{\begin{aligned}a\\a\\a\end{aligned}}\right\}
\quad i = 1, 2, 3, \cdots, \infty
\qquad (3.13)
$$

Physical interpretation

Now we say that the continuous function $x(t)$ is the surface elevation of irregular wave. $\eta(t)$ can be expanded as a Fourier series.

$$
\eta(t) = \sum_{i=0}^{\infty} (a_i \cos\omega_i t\ +\ b_i \sin\omega_i t)
$$

a_i b_i : Fourier coefficients

$$
c_i = \sqrt{a_i^2 + b_i^2}
$$

$$
\delta_i' = \operatorname{arctg}\frac{a_i}{b_i}
$$
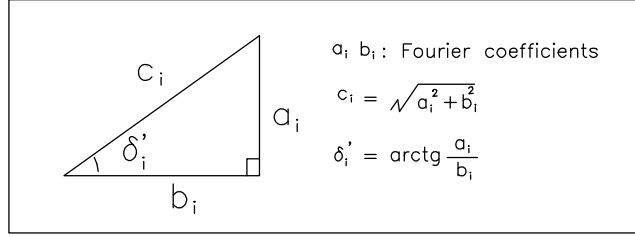
$$
= \sum_{i=0}^{\infty} \left(c_i \sin\delta_i'\ \cos\omega_i t\ +\ c_i \cos\delta_i'\ \sin\omega_i t \right)
$$

$$
= \sum_{i=0}^{\infty} c_i (\sin\delta_i'\ \cos\omega_i t\ +\ \cos\delta_i'\ \sin\omega_i t)
$$

$$
= \sum_{i=0}^{\infty} c_i\ \sin(\omega_i t\ +\ \delta_i')
$$

$$
= \sum_{i=0}^{\infty} c_i\ \cos(\omega_i t\ +\ \delta_i) \qquad (3.14)
$$

where $\delta_i = \delta_i' - \frac{\pi}{2}$ and $\sin(x+y) = \sin(x)\cos(y) + \cos(x)\sin(y)$ have been used.

That is to say, any irregular wave surface elevation, expressed as a continues

28

function, is composed of infinite number of linear waves with

$$\left.\begin{array}{rll}\text{amplitude} & c_i & = \sqrt{a_i^2 + b_i^2} \\ \text{period} & T_i & = \frac{2\pi}{\omega_i} = \frac{T_0}{i}\end{array}\right\} \quad i = 0, 1, \cdots, \infty \qquad (3.15)$$

$\{a_i,\ b_i\},\ i = 0, 1, 2, \cdots, \infty$, are given in Eq. (3.13).

3.4 Discrete signal analysis

The measurement of surface elevation is carried out digitally. We do not have, neither necessary, a continuous function of the surface elevation. Instead we have a series of surface elevation measurement equally spaced in time, cf. Fig. 3.6.
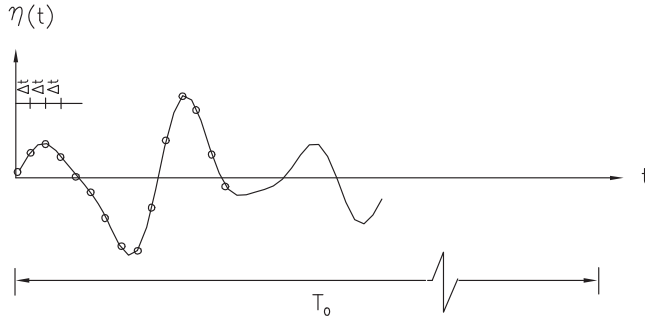
Figure 3.6: Sampling of surface elevation at regular intervals.

If the sampling frequency is f_s, then the time interval between two succeeding points is $\Delta t = 1/f_s$. Corresponding to the sample duration T_0 the total number of sample is $N = T_0/\Delta t$. Thus we obtain a discrete time series of surface elevation

$$\eta_0, \quad \eta_1, \quad \cdots, \quad \eta_{N-1}$$

The Fourier coefficients

$$(a_0,\ b_0), \quad (a_1,\ b_1), \quad \cdots, \quad (a_{N-1},\ b_{N-1})$$

29

can be obtained by Fast Fourier Transforms (FFT)[3]. That is to say, the irregular wave surface elevation, expressed by digital time series, is composed of N linear waves

$$\eta(t) \;=\; \sum_{i=0}^{N-1} \eta_i(t) \;=\; \sum_{i=0}^{N-1} \sqrt{a_i^2 + b_i^2}\;\cos(\omega_i t + \delta_i) \tag{3.16}$$

$$\left.\begin{array}{lll}
\text{amplitude} & \sqrt{a_i^2 + b_i^2} & \\[4pt]
\text{angular frequency} & \omega_i \;=\; \frac{2\pi i}{T_0} & \\[4pt]
\text{period} & T_i \;=\; \frac{2\pi}{\omega_i} \;=\; \frac{T_0}{i} & \\[4pt]
\text{frequency} & f_i \;=\; \frac{1}{T_i} \;=\; \frac{i}{T_0} &
\end{array}\right\} \quad i = 0, 1, \cdots, N-1 \tag{3.17}$$

Therefore we obtain the variance spectrum

$$\text{frequency width} \quad \Delta f \;=\; f_{i+1} - f_i \;=\; \frac{1}{T_0}$$

$$\text{spectral density} \quad S_\eta(f_i) \;=\; \frac{\frac{1}{2}(amplitude)^2}{\Delta f} \;=\; \frac{\frac{1}{2}(a_i^2 + b_i^2)}{\Delta f} \tag{3.18}$$

An example of variance spectrum is shown in Fig. 3.7.
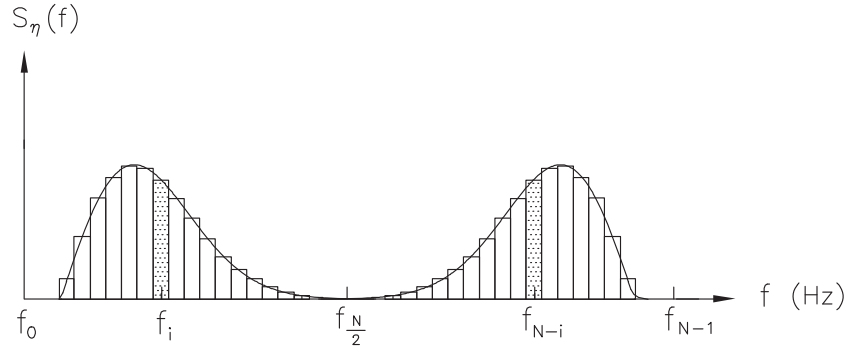
Figure 3.7: Variance spectrum.

---

[3]FFT is a computer algorithm for calculating DFT. It offers an enormous reduction in computer processing time. For details of DFT and FFT, refer to Newland (1975)

Nyquist frequency $f_{nyquist}$ is the maximum frequency which can be detected by the Fourier analysis.

Fourier analysis decomposes N digital data into N linear components. The frequency of each component is

$$f_i = \frac{i}{T_0} \qquad i = 0, 1, \cdots, N-1 \tag{3.19}$$

The Nyquist frequency is

$$f_{nyquist} = f_{\frac{N}{2}} = \frac{\frac{N}{2}}{T_0} = \frac{\frac{1}{2}\frac{T_0}{\Delta}}{T_0} = \frac{f_s}{2} \tag{3.20}$$

where f_s sample frequency

Δ time interval between two succeeding sample points, $\Delta = 1/f_s$

T_0 sample duration

N total number of sample, $N = T_0/\Delta$

The concept of Nyquist frequency means that the Fourier coefficients { a_i, b_i }, $i = 0, 1, \cdots, N-1$, contains two parts, the first half part below the Nyquist frequency ($i = 0, 1, \cdots, N/2 - 1$) represents true components while the second half part ($i = N/2, N/2+1, \cdots, N-1$) is the folding components (aliasing).

Fig. 3.8 gives an example on aliasing after the Fourier analysis of discrete time series of a linear wave.

The solution to aliasing is simple: let { a_i, b_i }, $i = N/2, N/2+1, \cdots, N-1$, equal to zero, cf. Fig. 3.9. That is the reason why $f_{nyquist}$ is also called cut-off frequency. In doing so we are actually assuming that irregular wave contains no linear components whose frequency is higher than $f_{nyquist}$. This assumption can be assured by choosing sufficiently high sample frequency f_s in combination with an analog low-pass filter, cf. Eq. 3.20.

surface elevation (cm)

O digital sample points

time (s)

original discrete
time series

$S_\eta(f)$

aliasing

f (Hz)

f_i $f_{\frac{N}{2}}$ f_{N-i}

spectrum from
discrete time series

surface elevation (cm)

aliasing

time (s)

time series of
linear components
given by spectrum

(Both linear components go through all sample points)
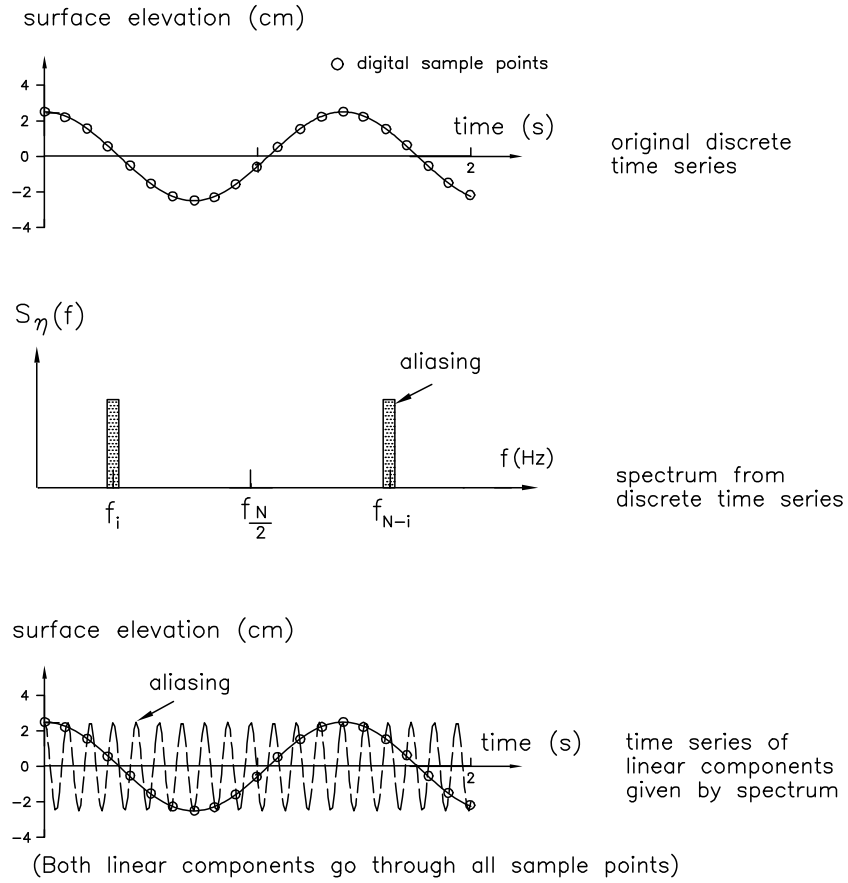
Figure 3.8: Aliasing after Fourier analysis.

$S_\eta(f) = \dfrac{\frac{1}{2}a^2}{\Delta f}$ $(m^2\,s)$

a : amplitude
Δf : frequency band width
N : total number of sample

Δf

f (Hz)

f_0 f_1 f_i $f_{\frac{N}{2}-1}$
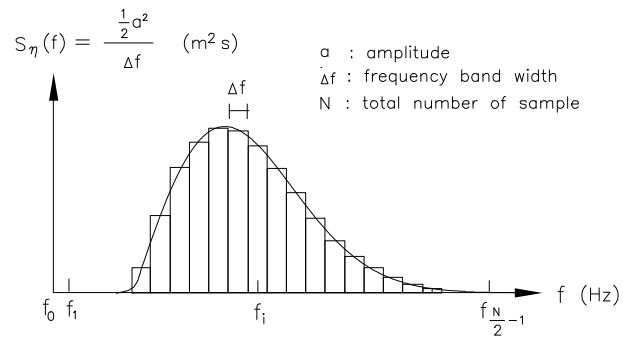
Figure 3.9: Variance spectrum after cut-off (refer to Fig. 3.7).

32

Taper data window

Fourier analysis requires that $\eta(t)$ is a periodic function with period T_0, it may be desirable to modify the recorded time series before Fourier analysis, so that the signal looks like a periodic function. The modification is carried out with the help of taper data window.

The widely-used cosine taper data window reads

$$
d(t) \;=\; \begin{cases} \frac{1}{2}\left(1 - \cos\frac{10\pi t}{T_0}\right) & 0 \le t \le \frac{T_0}{10} \\[2mm] 1 & \frac{T_0}{10} \le t \le \frac{9T_0}{10} \\[2mm] \frac{1}{2}\left(1 + \cos\frac{10\pi\left(t - \frac{9T_0}{10}\right)}{T_0}\right) & \frac{9T_0}{10} \le t \le T_0 \end{cases}
\qquad (3.21)
$$
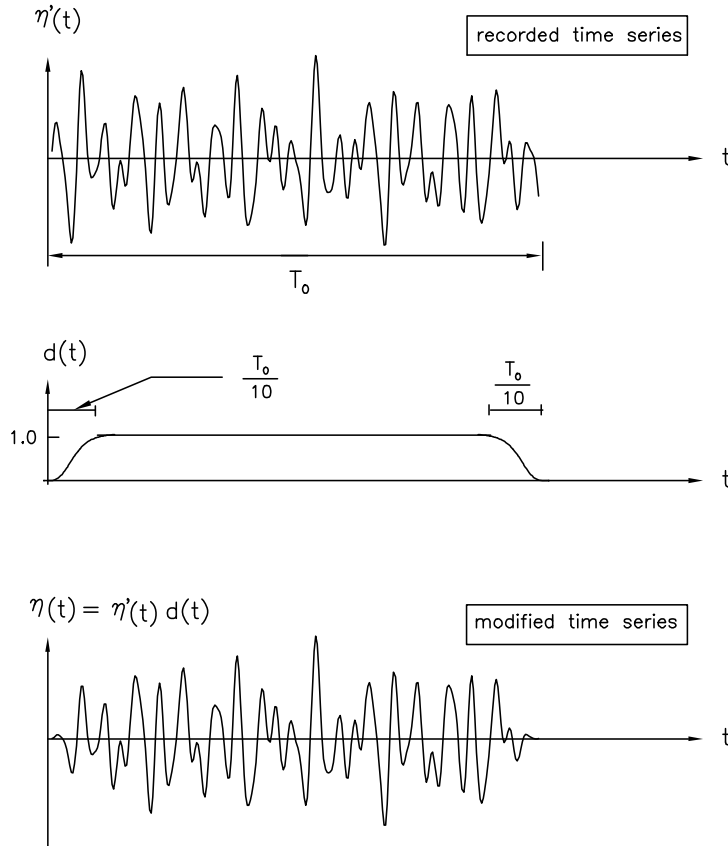
Figure 3.10: Taper data window.

33

3.5 Characteristic wave height and period

The variance spectrum, illustrated in Fig. 3.11, says nothing about how high the individual waves will be. Now we will see how to estimate the characteristic wave height and period based on the variance spectrum.
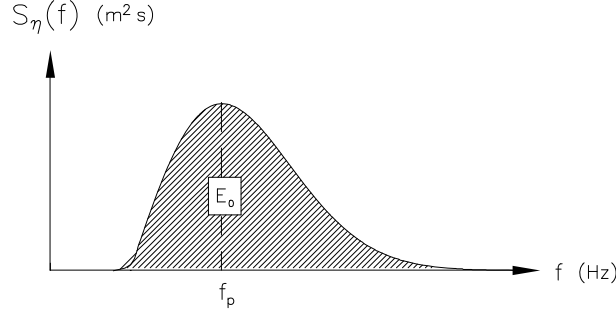
Figure 3.11: Variance spectrum.

<u>n order moment m_n</u>

m_n is defined as

$$ m_n = \int_0^\infty f^n \, S_\eta(f) \, \mathrm{df} \tag{3.22} $$

The zero moment is

$$ m_0 = \int_0^\infty S_\eta(f) \, \mathrm{df} \tag{3.23} $$

which is actually the area under the curve, cf. Fig. 3.11.

<u>Spectrum width parameter and validity of the Rayleigh distribution</u>

From the definition of m_n, it can be seen that the higher the order of moment, the more weight is put on the higher frequency portion of the spectrum. With the same m_0, a wider spectrum gives larger values of the higher order moment ($n \geq 2$). Longuet-Higgins has defined a broadness parameter:

$$ \varepsilon_4 = \sqrt{1 - \frac{m_2^2}{m_0 m_4}} \tag{3.24} $$

An alternative parameter is the narrowness paramter:

$$\varepsilon_2 = \sqrt{\frac{m_0 m_2}{m_1^2} - 1} \qquad (3.25)$$

It has been proven theoretically that:

spectrum width parameter		wave height distribution
$\varepsilon = 0$	narrow spectrum	Rayleigh distribution
$\varepsilon = 1$	wide spectrum	Normal distribution

In reality ε lies in the range of 0.4-0.5. It has been found that Rayleigh distribution is a very good approximation and furthermore conservative, as the Rayleigh distribution gives slightly larger wave height for any given probability level.

Significant wave height H_{m_0} and peak wave period T_p

When wave height follows the Rayleigh distribution, i.e. $\varepsilon = 0$, the significant wave height H_s[4] can theoretically be expressed as

$$H_s \approx H_{m_0} \equiv 4\sqrt{m_0} \qquad (3.26)$$

In reality where $\varepsilon = 0.4 - 0.5$, a good estimate of significant wave height from energy spectrum is

$$H_s = 3.7\sqrt{m_0} \qquad (3.27)$$

Peak frequency is defined as (cf. Fig. 3.11)

$$f_p = f\Big|_{S_\eta(f)=max} \qquad (3.28)$$

Wave peak period $(T_p = 1/f_p)$ is approximately equal to significant wave period defined in time-domain analysis.

---

[4] H_{m_0} denotes a wave height determined from spectrum while H_s or $H_{1/3}$ is significant wave height determined from time-domain analysis. They are equal to each other when wave height follows the Rayleigh distribution.

Chapter 4

Reflection Analysis of Long-Crested Waves

4.1 Introduction

Coastal and offshore engineering cover a wide spectrum in the field of civil engineering. Some of the major subjects involved are the construction of harbours and breakwaters.

Design of breakwaters and breakwater lay-outs are based on the need for an acceptable wave climate in the harbour and in the harbour entrance. However, the complex behaviour of waves propagating into a more or less closed basin makes the design of the quaywalls and breakwaters important.

When a physical or numerical model is used for wave climate investigations it is important that the model will provide reliable results. Naturally this depends upon whether the boundary conditions in the model are correct.

Establishing the correct boundary conditions is a problem due to scale effects. However the important properties of a boundary are the absorption, transmission and reflection of waves.

In order to provide correct reflection characteristics in the models one must know the true reflection characteristics for the structure under study.

The wave field in front of a structure consist of both incident waves and reflected waves. As one cannot first measure the incident waves and then the reflected waves, methods are required to separate or distinguish between the incident and reflected waves.

4.2 Wave Reflection

Wave reflection occurs when waves are propagating onto breakwaters and quaywalls.

Separating the incident waves and the reflected waves from a recorded wave elevation time series has several purposes. Either:

- The reflection characteristic for a structure is wanted, or

- The incident wave characteristic for a given site is wanted

The reflection characteristics for a structure are mainly wanted in sheltered areas, e.g. inside harbours, where the level of wave disturbance plays an important role in the design situation. Though, also the reflection characteristics of breakwaters are wanted, because it is important for the wave climate in the harbour entrance.

Generally a low reflection is wanted.

In order to apply physical models and numerical models the reflection characteristics must be modeled correct.

The incident waves are wanted where response of a structure (breakwater) is wanted as function of the incomming waves in front (seaward) of the reflecting structure.

In the following several different methods for separating incident waves and reflected waves will be presented. After separation of the incident waves and the reflected waves it is easy to calculate the reflection characteristics for the structure.

The following methods for separating the waves will be divided into two main groups:

- 2D methods (treated in this lection)
  The waves are assumed to be 2-dimensional (long crested)

- 3D methods (treated in lection 14)
  The waves are assumed to be 3-dimensional (short crested)

There is a wide need for 2D methods due to the amount of experiments carried out in wave flumes. In wave flumes reflection and re-reflection influence upon the validity of measurements if it is not possible to extract the incident

waves. Further when operating in the near shore environment the wave-field will often be approximately two-dimensional as the waves refract, i.e. they bend towards orthogonals to the shore.

The 2D methods presented herein are all based on surface elevation measurements at a number of positions.

Three of the 2D methods are derived from the same principles but for various number of probes. The simplest method requires two probes. The other methods need three or more probes. The three first methods work in *frequency domain* and give the incident wave spectrum as well as the reflected wave spectrum. The last 2D method works in *time domain* and gives the incident wave timeserie.

There is a considerable step from 2D methods to 3D methods. This is due to the circumstance that 3D methods for estimation of random sea states even without reflection are tedious and not as reliable as 2D methods. In principle, all methods for estimating directional wavespectra may be considered as a tool to determine reflection coefficients. However, only a few methods are capable of handling reflected seas as the reflected waves propagate with the same frequency as the incident waves, and thereby makes it impossible or at least difficult to distinguish. One should also recall that the direction of the waves is unknown in contrast to a 2D case.

As an intermediate case there is oblique long crested waves. This may be considered as a 3D case having a very narrow peak in the directional spreading function. This justifies the assumption that only one direction is present. Furthermore in laboratories real oblique waves can be generated. This may be used to determine the 3D reflection characteristics for e.g. a breakwater by use of physical models.

4.3   Methods

In the following four methods for separation of incident and reflected waves in a two-dimensional wave field will be presented.

The first three methods are all working in the *frequency domain* and have the same basic principle. They assume the wave elevation to be a sum of regular waves travelling with different frequency and phase. The first method by Goda & Suzuki needs measurements of the wave elevation in two distinct points. Hence by use of Fourier analysis the amplitude of the incident and reflected waves for a given frequency can be estimated. This procedure does not account for the noise which probably is contaminated in the measured

39

wave signals, i.e. the measured wave elevations.

The method presented by Mansard & Funke takes this into account, but also requires the wave elevation to be measured in three distinct points. By applying Fourier analysis this should result in the same waves except that the measured noise varies from wave gauge to wave gauge. That is, 10 Fourier coefficients are needed but only 6 are available. Instead the noise is expressed in terms of the Fourier coefficients for the incident and reflected waves and the measured coefficients. The best estimate of the Fourier coefficients is then found by minimising the noise.

The method by Zelt & Skjelbreia extents the method to apply to an arbitrary number (though larger than one) of wave gauges. Further a weighting of each frequency component is introduced. This is to control the possible influence of singularities which occur for some geometric relations between the distances between the probes. Grønbech et. al (1996) presented a revised version of the Zelt & Skjelbreia method to separate cross-modes from the incident and reflected waves. The method is good to quantify the amount of cross-mode activity and if neglectable the standard method can be applied. However, due to the more degrees of freedom more gauges are needed to give reliable results.

Finally a method by Frigaard & Brorsen is presented in the following chapter. This method is based on another approach than the previously mentioned methods. The method has the advantage that it works in the *time domain* and can be applied in real time as it is based on digital filters. The other methods can in post analyses also be used to get the time domain results by the use of InvFFT on the Fourrier coefficients. However, they cannot be applied in real time.

Other methods have been published to account for sloping bottoms and non-linear waves, but they will not be presented herein. The methods by Goda & Suzuki and Mansard & Funke are the methods being used most often as they are relatively simple to apply and yield reliable results within most applications.

4.4   Goda & Suzuki's method

The method presented by Goda & Suzuki (1976) is the most simple method. It is based on the assumption that the wave elevation can be considered as a sum of waves travelling with different frequency, amplitude and phase. Further for each wave a reflected wave will travel in the opposite direction. The method makes use of Fourier analysis and will due to singularities put con-

straint to the distance between the waveprobes. The method is very easy to implement but has a lack of accuracy as no measuring errors are accounted for.

The surface elevation in a two-dimensional wave field is assumed to be a summation of a number of waves, say N waves, i.e.

$$\eta(x,t) = \sum_{n=1}^{N} a_n \cos(k_n x - \omega_n t + \Phi_n) \tag{4.1}$$

where η is the surface elevation relative to MWL
      x is the position of the wave gauge in a predefined coordinatesystem
      t is time
      a_n is the amplitude
      k_n is the wavenumber
      ω_n is the angular frequency of the waves
      Φ_n is the phase

If reflection happens 4.1 may be expanded to

$$\eta(x,t) = \sum_{n=1}^{N} a_{I,n} \cos(k_n x - \omega_n t + \Phi_{I,n}) + \sum_{n=1}^{N} a_{R,n} \cos(k_n x + \omega_n t + \Phi_{R,n}) \tag{4.2}$$

where indices I and R denotes incident and reflected respectively.

In the following the index n will be omitted for simplicity, that is, only one frequency is considered. Hence eq. (4.2) will consist of only two terms:

$$\eta(x,t) \;\; = \;\; a_I \cos(kx - \omega t + \Phi_I) + a_R \cos(kx + \omega t + \Phi_R) \tag{4.3}$$

Sampling the surface elevation at two positions within a distance of $x_{1,2}$ measured in the direction of propagation of the waves, as illustrated in fig.
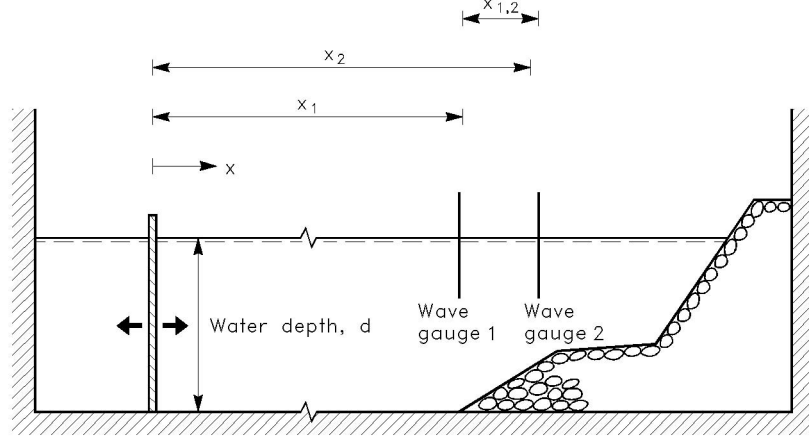
Figure 4.1: Definition sketch showing $x_{1,2}$.

(4.1), yields:

$$
\begin{aligned}
\eta_1 = \eta(x_1, t) &= a_I \cos(kx_1 - \omega t + \Phi_I) + a_R \cos(kx_1 + \omega t + \Phi_R) \\
\eta_2 = \eta(x_2, t) &= a_I \cos(kx_2 - \omega t + \Phi_I) + a_R \cos(kx_2 + \omega t + \Phi_R)
\end{aligned}
\tag{4.4}
$$

Decomposing the trigonometric terms in eq. (4.4) by use of

$$
\cos A \cos B \pm \sin A \sin B = \cos(A \mp B)
\tag{4.5}
$$

leads to

$$
\begin{aligned}
\eta_1 &= a_I \left(\sin(kx_1 + \Phi_I) \sin(\omega t) + \cos(kx_1 + \Phi_I) \cos(\omega t) \right) \\
&\quad + a_R \left(\cos(kx_1 + \Phi_R) \cos(\omega t) - \sin(kx_1 + \Phi_R) \sin(\omega t) \right) \\
\eta_2 &= a_I \left(\sin(kx_2 + \Phi_I) \sin(\omega t) + \cos(kx_2 + \Phi_I) \cos(\omega t) \right) \\
&\quad + a_R \left(\cos(kx_2 + \Phi_R) \cos(\omega t) - \sin(kx_2 + \Phi_R) \sin(\omega t) \right)
\end{aligned}
\tag{4.6}
\tag{4.7}
$$

which is rearranged to

$$
\begin{aligned}
\eta_1 &= A_1 \cos(\omega t) + B_1 \sin(\omega t) \\
\eta_2 &= A_2 \cos(\omega t) + B_2 \sin(\omega t)
\end{aligned}
\tag{4.8}
$$

where

$$\begin{aligned}
A_1 &= a_I \cos(kx_1 + \Phi_I) + a_R \cos(kx_1 + \Phi_R) \\
B_1 &= a_I \sin(kx_1 + \Phi_I) - a_R \sin(kx_1 + \Phi_R) \\
A_2 &= a_I \cos(kx_2 + \Phi_I) + a_R \cos(kx_2 + \Phi_R) \\
B_2 &= a_I \sin(kx_2 + \Phi_I) - a_R \sin(kx_2 + \Phi_R)
\end{aligned} \tag{4.9}$$

In eq. (4.8) the elevation is seen to be a composite signal of a sine and cosine signal having different time-constant amplitude, i.e. the LHS of eq. (4.9) must correspond to the Fourier coefficients which can be obtained from Fourier analysis of the recorded time series.

Thus eq. (4.9) contains four equations with four unknowns, i.e. a_I, a_R, Φ_I and Φ_R. The solution giving the amplitudes is given by Goda & Suzuki (1976) as:

$$\begin{aligned}
a_I &= \frac{1}{2|\sin(kx_{1,2})|} \sqrt{(A_2 - A_1 \cos(kx_{1,2}) - B_1 \sin(kx_{1,2}))^2} \\
&\quad \overline{+(B_2 + A_1 \sin(kx_{1,2}) - B_1 \cos(kx_{1,2}))^2} \\
a_R &= \frac{1}{2|\sin(kx_{1,2})|} \sqrt{(A_2 - A_1 \cos(kx_{1,2}) + B_1 \sin(kx_{1,2}))^2} \\
&\quad \overline{+(B_2 - A_1 \sin(kx_{1,2}) - B_1 \cos(kx_{1,2}))^2}
\end{aligned} \tag{4.10}$$

where $x_{1,2} = x_2 - x_1$.

It is seen from eq. (4.10) that singularities will occur for $\sin(kx_{1,2}) = 0$. Hence it should be avoided that

$$\frac{x_{1,2}}{L} = \frac{n}{2} \qquad \text{where} \qquad n = 0, 1, 2, ...$$

Further Goda & Suzuki (1976) suggest to avoid values in the range $\pm 0.05 \frac{x_{1,2}}{L}$ at the singularity points. For a wide wave spectrum this will be impossible for all frequencies, but of course values applying for the peak frequencies should be weighted highest.

For regular waves the method is quite accurate but for irregular waves the confidence of the FFT analysis plays a significant role. However in both cases noise may be the dominant error as it cannot be accounted for.

4.5 Mansard & Funke's method

As a natural extension to the method by Goda & Suzuki, Mansard & Funke (1980) presented a three-points method. Here an additional probe is taken into use which makes it possible to add an error to the measurements and hence minimise it in a least squares sense.

The general equation for a progressive wave field is obtained as in the previous method, i.e. eq. (4.1):

$$\eta(x,t) = \sum_{n=1}^{N} a_n \cos(k_n x - \omega_n t + \Phi_n) \tag{4.11}$$

The wave elevation given by eq. (4.1) and eq. (4.11) is separated into incident waves and reflected waves, also as previously, but now a noise function is added. This leads to:

$$\eta(x,t) = \sum_{n=1}^{N} a_{I,n} \cos(k_n x - \omega_n t + \Phi_{I,n}) + \sum_{n=1}^{N} a_{R,n} \cos(k_n x + \omega_n t + \Phi_{R,n})$$

or

$$\begin{aligned} \eta(x,t) &= \sum_{n=1}^{N} a_{I,n} \cos(k_n x - \omega_n t + \Phi_n) \\ &+ \sum_{n=1}^{N} a_{R,n} \cos(k_n(x + 2x_R) + \omega_n t + \Phi_n + \theta_s) + \Omega(t) \end{aligned} \tag{4.12}$$

Here in contrary to Goda & Suzuki (1976) the distance from the point of observation to the reflecting structure is assumed known. However as the distance may be impossible to determine (e.g. for a slope) a phase θ_s is introduced to compensate herefore. This has the consequence that the phase Φ_n remains the same for the incident and reflected wave. $\Omega(t)$ is the noise function and expresses all kinds of errors. x_R is the distance from the wave probe to the reflecting structure.

Mansard & Funke allow a phaseshift θ_s to occur at the reflecting structure. For three probes placed as indicated on fig 4.2 eq. (4.12) can be applied for
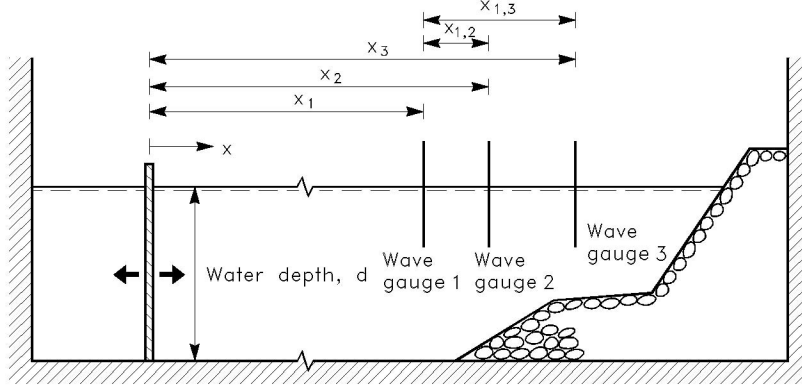
Figure 4.2: Definition sketch.

each probe.

Hence

$$
\begin{aligned}
\eta_p &= \eta(x_p, t) \\
&= \sum_{n=1}^{N} a_{I,n} \cos(k_n x_p - \omega_n t + \Phi_n) \\
&\quad + \sum_{n=1}^{N} a_{R,n} \cos(k_n(x_p + 2x_{R,p}) + \omega_n t + \Phi_n + \theta_s) + \Omega_p(t) \quad (4.13)
\end{aligned}
$$

where index p refer to probe number.

Inserting $x_{1,p}$, which is the distance from the 1st probe to the p'th probe, eq. (4.13) can be modified to

$$
\begin{aligned}
\eta_p &= \sum_{n=1}^{N} a_{I,n} \cos(k_n(x_1 + x_{1,p}) - \omega_n t + \Phi_n) \\
&\quad + \sum_{n=1}^{N} a_{R,n} \cos(k_n(x_1 + 2x_{R,1} - x_{1,p}) + \omega_n t + \Phi_n + \theta_s) + \Omega_p(t) \quad (4.14)
\end{aligned}
$$

In the following until eq. (4.25) only one frequency will be considered, i.e. in-

45

dex n will be omitted. Thus

$$
\begin{aligned}
\eta_p \;=\; & a_I \cos(k(x_1 + x_{1,p}) - \omega t + \Phi) \\
& + a_R \cos(k(x_1 + 2x_{R,1} - x_{1,p}) + \omega t + \Phi + \theta_s) + \Omega_p(t) \qquad (4.15)
\end{aligned}
$$

The following manipulations have the purpose to derive an algebraic solution, which is based on a minimisation of the noise function.

Fourier transformation of eq. (4.15) yields

$$
\begin{aligned}
A_p + iB_p \;=\; & a_I \exp\left(ik(x_1 + x_{1,p}) + i\Phi\right) \\
& + a_R \exp\left(ik(x_1 + 2x_{R,1} - x_{1,p}) + i(\Phi + \theta_s)\right) \\
& + Y_p \exp(i\rho_p) \qquad (4.16)
\end{aligned}
$$

where A_p and B_p are the Fourier coefficients.

Let

$$
\begin{aligned}
Z_I \;&=\; a_I \exp(ikx_1 + i\Phi) & (4.17) \\
Z_R \;&=\; a_R \exp(ik(x_1 + 2x_{R,1}) + i(\Phi + \theta_s)) & (4.18) \\
Z_{N,p} \;&=\; Y_p \exp(i\rho_p) & (4.19)
\end{aligned}
$$

where index N refer to noise.

Now, eq. (4.16) can be applied to each probe yielding

$$
\begin{aligned}
A_1 + iB_1 \;&=\; Z_I + Z_R + Z_{N,1} \\
A_2 + iB_2 \;&=\; Z_I \exp(ikx_{1,2}) + Z_R \exp(-ikx_{1,2}) + Z_{N,2} \\
A_3 + iB_3 \;&=\; Z_I \exp(ikx_{1,3}) + Z_R \exp(-ikx_{1,3}) + Z_{N,3}
\end{aligned}
$$

or in general form

$$
A_p + iB_p \;=\; Z_I \exp\left(ikx_{1,p}\right) + Z_R \exp\left(-ikx_{1,p}\right) + Z_{N,p} \qquad (4.20)
$$

One is interested in solving 4.20 with regard to Z_I and Z_R as they contain information of the reflection coefficients.

Now eq. (4.20) can be rearranged to

$$
\begin{aligned}
\varepsilon_1 &= Z_I + Z_R - (A_1 + iB_1) \\
\varepsilon_2 &= Z_I \exp(ikx_{1,2}) + Z_R \exp(-ikx_{1,2}) - (A_2 + iB_2) \\
\varepsilon_3 &= Z_I \exp(ikx_{1,3}) + Z_R \exp(-ikx_{1,3}) - (A_3 + iB_3)
\end{aligned}
\tag{4.21}
$$

where

$$
\varepsilon_p = -Z_{N,p} + f_e(Z_I, Z_R)
$$

Minimising the noise function $\Omega_p(t)$ introduced in eq. (4.12) correspond to minimising the sum of squares of ε_p for all p, i.e.

$$
\sum_{p=1}^{3} (\varepsilon_p)^2 = \sum_{p=1}^{3} (Z_I \exp(ikx_{1,p}) + Z_R \exp(-ikx_{1,p}) - (A_p + iB_p))^2 \tag{4.22}
$$

should be minimised.

Assuming that the minimum of eq. (4.22) is achieved when both partial derivatives are zero, i.e.

$$
\frac{\partial \sum_{p=1}^{3} \varepsilon_p^2}{\partial Z_I} = \frac{\partial \sum_{p=1}^{3} \varepsilon_p^2}{\partial Z_R} = 0 \tag{4.23}
$$

Hence one obtains:

$$
\tag{4.24}
$$

$$
\begin{aligned}
0 &= 2\sum_{p=1}^{3} (Z_I \exp(ikx_{1,p}) + Z_R \exp(-ikx_{1,p}) - (A_p + iB_p)) \exp(ikx_{1,p}) \\
0 &= 2\sum_{p=1}^{3} (Z_I \exp(ikx_{1,p}) + Z_R \exp(-ikx_{1,p}) - (A_p + iB_p)) \exp(-ikx_{1,p})
\end{aligned}
$$

When written out and again including index n eq. (4.24) leads to

$$Z_{I,n}(1 + \exp(i2k_n x_{1,2}) + \exp(i2k_n x_{1,3})) + 3Z_{R,n} =$$
$$(A_{1,n} + iB_{1,n}) + (A_{2,n} + iB_{2,n})\exp(ik_n x_{1,2}) + (A_{3,n} + iB_{3,n})\exp(ik_n x_{1,3})$$
$$Z_{R,n}(1 + \exp(-i2k_n x_{1,2}) + \exp(-i2k_n x_{1,3})) + 3Z_{I,n} =$$
$$(A_{1,n} + iB_{1,n}) + (A_{2,n} + iB_{2,n})\exp(-ik_n x_{1,2}) + (A_{3,n} + iB_{3,n})\exp(-ik_n x_{1,3}) \tag{4.25}$$

The solution is given by Mansard & Funke (1980) as:

$$
\begin{aligned}
Z_{I,n} &= \tfrac{1}{D_n}((A_{1,n} + iB_{1,n})(R_{1,n} + iQ_{1,n}) \\
&\quad + (A_{2,n} + B_{2,n})(R_{2,n} + iQ_{2,n}) + (A_{3,n} + iB_{3,n})(R_{3,n} + iQ_{3,n})) \\
Z_{R,n} &= \tfrac{1}{D_n}((A_{1,n} + iB_{1,n})(R_{1,n} - iQ_{1,n}) \\
&\quad + (A_{2,n} + iB_{2,n})(R_{2,n} - iQ_{2,n}) + (A_{3,n} + iB_{3,n})(R_{3,n} - iQ_{3,n}))
\end{aligned} \tag{4.26}
$$

where

$$
\begin{aligned}
D_n &= 2(\sin^2(k_n x_{1,2}) + \sin^2(k_n x_{1,3}) + \sin^2((k_n x_{1,3}) - k_n x_{1,2})) \\
R_{1,n} &= \sin^2(k_n x_{1,2}) + \sin^2(k_n x_{1,3}) \\
Q_{1,n} &= \sin(k_n x_{1,2})\cos(k_n x_{1,2}) + \sin(k_n x_{1,3})\cos(k_n x_{1,3}) \\
R_{2,n} &= \sin(k_n x_{1,3})\sin(k_n x_{1,3} - k_n x_{1,2}) \\
Q_{2,n} &= \sin(k_n x_{1,3})\cos(k_n x_{1,3} - k_n x_{1,2}) - 2\sin(k_n x_{1,2}) \\
R_{3,n} &= -\sin(k_n x_{1,2})\sin(k_n x_{1,3} - k_n x_{1,2}) \\
Q_{3,n} &= \sin(k_n x_{1,2})\cos(k_n x_{1,3} - k_n x_{1,2}) - 2\sin(k_n x_{1,3})
\end{aligned}
$$

The only unknowns in eq. (4.26) are the Fourier coefficients of the measured wave elevations. These are obtained by use of FFT analysis of the measurements.

Compared to the previously discussed method this method has the advantage that it minimises the noise contaminated to the elevation measurements.

Thus instead of obtaining an exact solution a fitted solution is obtained.

Problems due to singularities, however, occur as well. Singularity will occur when

$$D_n = 0$$

i.e.

$$\sin^2(k_n x_{1,2}) + \sin^2(k_n x_{1,3}) + \sin^2(k_n x_{1,3} - k_n x_{1,2}) = 0$$

As all the terms are positive the solution is solution to

$$\sin(k_n x_{1,2}) = \sin(k_n x_{1,3}) = \sin(k_n x_{1,3} - k_n x_{1,2}) = 0$$

but if $\sin(k_n x_{1,2}) = \sin(k_n x_{1,3}) = 0$ then $\sin(k_n x_{1,3} - k_n x_{1,2}) = 0$ whereas the solution is reduced to

$$\sin(k_n x_{1,2}) = \sin(k_n x_{1,3}) = 0$$

which is obtained for

$$
\begin{aligned}
k_n x_{1,2} &= m\pi &\wedge\quad k_n x_{1,3} &= l\pi & m &= 1, 2, 3, ... \\
& & & & l &= m+1, m+2, ...
\end{aligned}
$$

$$
\begin{aligned}
k_n x_{1,2} &= m\pi &\wedge\quad k_n x_{1,3} &= l\pi \\
x_{1,2} &= \tfrac{m}{2} L_n &\wedge\quad x_{1,3} &= \tfrac{l}{2} L_n = \tfrac{l}{m} x_{1,2}
\end{aligned}
$$

as by definition $0 < x_{1,2} < x_{1,3}$. Mansard & Funke (1980) suggest that

$$
\begin{aligned}
x_{1,2} &= \frac{L_n}{10} \\
\frac{L_n}{6} < \; x_{1,3} \; &< \frac{L_n}{3} \\
x_{1,3} &\neq \frac{L_n}{5} \\
x_{1,3} &\neq \frac{3L_n}{10}
\end{aligned}
$$

4.6   Zelt & Skjelbreia's method

Zelt and Skjelbreia (1992) introduced a method based on the same principles as the previously described methods.

This method applies for an arbitrary number p of probes and further introduces a weighting of the measurements from the gauges. The latter facility takes into account the spacing between each pair of wave gauges. However

determining the weighting coefficients is a rather subjective process and requires some additional work.

For $p = 2$ the method corresponds to the method by Goda & Suzuki. For $p = 3$ and a uniform weighting, the method corresponds to the method by Mansard & Funke.

Once again the wave elevation is considered as a sum of incident and reflected waves, i.e. for the pth probe at position x_p utilising eq. (4.2)

$$\eta_p = \eta(x_p, t) = \sum_{n=1}^{N} a_{I,n} \cos(k_n x_p - \omega_n t + \Phi_{I,n}) + \sum_{n=1}^{N} a_{R,n} \cos(k_n x_p + \omega_n t + \Phi_{R,n})$$

or by use of eq. (4.14)

$$\eta_p = \sum_{n=1}^{N} a_{I,n} \cos(k_n(x_1 + x_{1,p}) - \omega_n t + \Phi_n)$$

$$+ \sum_{n=1}^{N} a_{R,n} \cos(k_n(x_1 + 2x_{R,1} - x_{1,p}) + \omega_n t + \Phi_n + \theta_s) + \Omega_p(t)$$

As in the method of Mansard & Funke (1980) this is by use of the Fourier coefficients rearranged to eq. (4.21) which has the general form

$$\varepsilon_{p,n} = Z_{I,n} \exp(ik_n x_{1,p}) + Z_{R,n} \exp(-ik_n x_{1,p}) - (A_{p,n} + iB_{p,n}) \qquad (4.27)$$

That is, if the estimated coefficients are correct there will be no error, i.e. $\varepsilon_{p,n} = 0$. A function is chosen to be a weighted sum of the squares of $\varepsilon_{p,n}$, i.e.

$$E_n = \sum_{p=1}^{P} W_{p,n} \varepsilon_{p,n} \varepsilon_{p,n}^* \qquad (4.28)$$

where $W_{p,n} > 0$ are weighting coefficients.

It is assumed that the minimum of eq. (4.28) occurs where the partial deriva-

tives with regard to $Z_{I,n}$ and $Z_{R,n}$ are zero. Thus

$$\sum_{p=1}^{P} W_{p,n}\varepsilon_{p,n}\exp(\pm ik_n x_{1,p}) = 0 \tag{4.29}$$

Inserting eq. (4.27) into eq. (4.29) gives:

$$
\begin{aligned}
\sum_{p=1}^{P} W_{p,n}Z_{I,n}\exp(i2k_n x_{1,p}) + \sum_{p=1}^{P} W_{p,n}Z_{R,n} &= \\
\sum_{p=1}^{P} W_{p,n}(A_{p,n} + iB_{p,n})\exp(ik_n x_{1,p}) & \\
\sum_{p=1}^{P} W_{p,n}Z_{I,n} + \sum_{p=1}^{P} W_{p,n}Z_{R,n}\exp(-i2k_n x_{1,p}) &= \\
\sum_{p=1}^{P} W_{p,n}(A_{p,n} + iB_{p,n})\exp(-ik_n x_{1,p}) &
\end{aligned}
\tag{4.30}
$$

This, eq. (4.30) can be solved with regard to $Z_{I,n}$ and $Z_{R,n}$ as a linear system of equations. Simply isolate $a_{I,n}$ and $a_{R,n}$ in both equations in eq. (4.30) and substitute into the other equation respectively. Hence the following solution is obtained

$$
\begin{aligned}
Z_{I,n} &= \frac{1}{D_n}\Big(S_n \sum_{p=1}^{P} W_{p,n}(A_{p,n} + iB_{p,n})\exp(-ik_n x_{1,p}) \\
&\quad - \sum_{p=1}^{P} W_{p,n}(A_{p,n} + iB_{p,n})\exp(ik_n x_{1,p})\sum_{q=1}^{P} W_{q,n}\exp(-i2k_n x_{1,q}) \Big) \\
Z_{R,n} &= \frac{1}{D_n}\Big(S_n \sum_{p=1}^{P} W_{p,n}(A_{p,n} + iB_{p,n})\exp(ik_n x_{1,p}) \\
&\quad - \sum_{p=1}^{P} W_{p,n}(A_{p,n} + iB_{p,n})\exp(-ik_n x_{1,p})\sum_{q=1}^{P} W_{q,n}\exp(i2k_n x_{1,q}) \Big)
\end{aligned}
$$

$$\tag{4.31}$$

where

$$D_n = S_n^2 - \sum_{p=1}^{P} W_{p,n}\exp(i2k_n x_{1,p})\sum_{q=1}^{P} W_{q,n}\exp(-i2k_n x_{1,q})$$

$$S_n = \sum_{p=1}^{P} W_{p,n}$$

It is seen from eq. (4.31) that $D_n = 0$ will lead to singularity whereas it should be avoided that $x_{q,p} = 0$ for all p and q where $p > q$.

51

4.7 Robustness to possible errors

In order to evaluate the performance of the proposed methods for estimating reflection, the methods are tested upon numerical data, where possible errors are introduced.

The possible errors are:

- Random noise on signals

- Non-linear effects in the waves

- Phase locked waves

- Three-dimensional waves in cases where a two-dimensional method is used

- Divergens in the estimation due to numerical problems in solving the system of equations

4.7.1 Random noise on signals

The following section describes a numerical test, where the elevations are calculated for monochromatic waves according to the shown equation:

$$\eta(x,t) = a_I \cos(kx - \omega t) + \alpha a_I \cos(kx + \omega t) + random \cdot \beta \cdot a_I$$

where α is reflection coefficient
β is noise coefficient
$random$ is a random number in $[-1; 1]$

Goda & Suzuki								
β	ω	Δt	a_I	α	$\tilde{\alpha}_{12}$	$\tilde{\alpha}_{13}$	$\tilde{\alpha}_{23}$	$\tilde{\alpha}_{average}$
%	rad/sec	sec	metre	%	%	%	%	%
10	2π	0.0625	0.10	50.00	50.88	50.92	50.24	50.68
10	2π	0.0625	0.10	10.00	11.03	10.98	10.14	10.72

Goda & Suzuki								
β	ω	Δt	a_I	α	$\tilde{\alpha}_{12}$	$\tilde{\alpha}_{13}$	$\tilde{\alpha}_{23}$	$\tilde{\alpha}_{average}$
%	rad/sec	sec	metre	%	%	%	%	%
30	2π	0.0625	0.10	50.00	52.26	52.34	51.13	51.91
30	2π	0.0625	0.10	10.00	12.78	13.65	11.57	12.67

Mansard & Funke						
β	ω	Δt	a_I	α	$\tilde{\alpha}_{123}$	$\tilde{\alpha}_{average}$
%	rad/sec	sec	metre	%	%	%
10	2π	0.0625	0.10	50.00	50.50	50.50
10	2π	0.0625	0.10	10.00	10.42	10.42

Mansard & Funke						
β	ω	Δt	a_I	α	$\tilde{\alpha}_{123}$	$\tilde{\alpha}_{average}$
%	rad/sec	sec	metre	%	%	%
30	2π	0.0625	0.10	50.00	51.49	51.49
30	2π	0.0625	0.10	10.00	11.32	11.32

where Δt is sampling interval

    α is reflection coefficient

    ~   indicates estimated

All tests were performed with water depth $d = 0.50$ metre with a 160 sec. long time series. Distances between wave gauges were $x_{1,2} = 0.25$ metre and $x_{1,3} = 0.60$ metre .

The tests show good restistance to random noise. Though, the method proposed by Mansard & Funke gives sligthly better results than the method proposed by Goda & Suzuki.

The tests were repeated for 15 different wave periods and all tests showed the same tendency as described in the examples above.

4.7.2 Non-linear effects in the waves

All the described methods assume linear waves. In order to examine the effect from non-linearites a 2-order wave were generated. First with a free 2-harmonic eq. (4.32), and then with a bounded 2-harmonics eq. (4.33):

$$
\begin{aligned}
\eta(x,t) = a_I \cos(kx - \omega t) + 0.2 \cdot a_I \cos(2k^* x - 2\omega t) + \\
\alpha a_I \cos(kx + \omega t) + \alpha \cdot 0.2 \cdot a_I \cos(2k^* x - 2\omega t) \quad (4.32) \\
\eta(x,t) = a_I \cos(kx - \omega t) + 0.2 \cdot a_I \cos(2kx - 2\omega t) + \\
\alpha a_I \cos(kx + \omega t) + \alpha \cdot 0.2 \cdot a_I \cos(2kx - 2\omega t) \quad (4.33)
\end{aligned}
$$

where k is wave number corresponding to ω
k^* is wave number corresponding to $2 \cdot \omega$

Goda & Suzuki								
					Free 2-harmonics		Bounded 2-harm	
ω	Δt	a_I	a_I^{2-harm}	α	$\tilde{\alpha}_{average}^{1-harm}$	$\tilde{\alpha}_{average}^{2-harm}$	$\tilde{\alpha}_{average}^{1-harm}$	$\tilde{\alpha}_{average}^{2-harm}$
rad/sec	sec	metre	metre	%	%	%	%	%
π	0.0625	0.10	0.02	50.00	50.04	49.78	50.12	61.10
π	0.0625	0.10	0.02	10.00	10.22	10.18	10.18	26.33

Mansard & Funke								
					Free 2-harmonics		Bounded 2-harm	
ω	Δt	a_I	a_I^{2-harm}	α	$\tilde{\alpha}_{average}^{1-harm}$	$\tilde{\alpha}_{average}^{2-harm}$	$\tilde{\alpha}_{average}^{1-harm}$	$\tilde{\alpha}_{average}^{2-harm}$
rad/sec	sec	metre	metre	%	%	%	%	%
π	0.0625	0.10	0.02	50.00			50.00	53.14
π	0.0625	0.10	0.02	10.00			10.00	19.42

4.7.3 Numerical problems

Numerical problems due to the discretisation of the signal and the succeeding FFT-analysis.

Timeseries were calculated from:

$$\eta(x,t) = a_I \cos(kx - \omega t) + \alpha a_I \cos(kx + \omega t) \tag{4.34}$$

where α is reflection coefficient

Goda & Suzuki							
ω	Δt	a_I	α	$\tilde{\alpha}_{12}$	$\tilde{\alpha}_{13}$	$\tilde{\alpha}_{23}$	$\tilde{\alpha}_{average}$
rad/sec	sec	metre	%	%	%	%	%
2π	0.0625	0.10	50.00	50.21	50.32	49.84	50.12
2π	0.0625	0.10	10.00	10.28	10.45	9.80	10.18
$0.98 \cdot 2\pi$	0.0625	0.10	50.00	48.92	49.78	53.00	49.20
$0.95 \cdot 2\pi$	0.0625	0.10	50.00	53.88	34.64	53.32	42.98

Mansard & Funke					
ω	Δt	a_I	α	$\tilde{\alpha}_{123}$	$\tilde{\alpha}_{average}$
rad/sec	sec	metre	%	%	%
2π	0.0625	0.10	50.00	50.00	50.00
2π	0.0625	0.10	10.00	10.00	10.00
$0.98 \cdot 2\pi$	0.0625	0.10	50.00	49.66	49.66
$0.95 \cdot 2\pi$	0.0625	0.10	50.00	48.70	48.70

All tests were performed with water depth $d = 0.50$ metre with a 80 sec. long time serie. The time serie were divided into 10 sub-series, which were cosine tapered. Distances between wave gauges were $x_{12} = 0.25$ metre and $x_{13} = 0.60$ metre .

In order to examine errors from comming from a wrong calibration constant on one or two of the wave gauges.

Timeseries were calculated from:

$$\eta(x,t) = a_I \cos(kx - \omega t) + \alpha a_I \cos(kx + \omega t)$$
$$\eta(x_1,t) = 1.00 \cdot a_I \cos(kx_1 - \omega t) + 1.00 \cdot \alpha a_I \cos(kx_1 + \omega t) \qquad (4.35)$$
$$\eta(x_2,t) = 1.05 \cdot a_I \cos(kx_2 - \omega t) + 1.05 \cdot \alpha a_I \cos(kx_2 + \omega t)$$
$$\eta(x_3,t) = 1.10 \cdot a_I \cos(kx_3 - \omega t) + 1.10 \cdot \alpha a_I \cos(kx_3 + \omega t)$$

	Goda & Suzuki						
ω	Δt	a_I	α	$\tilde{\alpha}_{12}$	$\tilde{\alpha}_{13}$	$\tilde{\alpha}_{23}$	$\tilde{\alpha}_{average}$
rad/sec	sec	metre	%	%	%	%	%
2π	0.0625	0.10	50.00	49.61	55.53	51.30	52.15
2π	0.0625	0.10	10.00	9.80	17.57	11.80	13.06

Mansard & Funke					
ω	Δt	a_I	α	$\tilde{\alpha}_{123}$	$\tilde{\alpha}_{average}$
rad/sec	sec	metre	%	%	%
2π	0.0625	0.10	50.00	51.40	51.40
2π	0.0625	0.10	10.00	18.90	18.90

Chapter 5

Seperation of Incident and Reflected Long-Crested Waves Using Digital Filters

In the hydraulic laboratory environment a separation of an irregular wave field into incident waves propagating towards a structure, and reflected waves propagating away from the structure is often wanted. This is due to the fact that the response of the structure to the incident waves is the target of the model test.

Goda and Suzuki (1976) presented a frequency domain method for estimation of irregular incident and reflected waves in random waves. Mansard and Funke (1980) improved this method using a least squares technique.

In the following a time-domain method for Separating the Incident waves and the Reflected Waves (SIRW-method) is presented. The method is based on the use of digital filters and can separate the wave fields in *real time*.

5.1   Principle

To illustrate the principle of the SIRW-method the set-up shown in Fig. 5.1 will be considered. The surface elevation $\eta(x, t)$ at a distance x from the wave generator may be written as the sum of the incident and reflected waves: the incident wave propagating away from the wave generator, and the reflected wave propagating towards the wave generator. Even though the method works for irregular waves it will be demonstrated in the following pages for
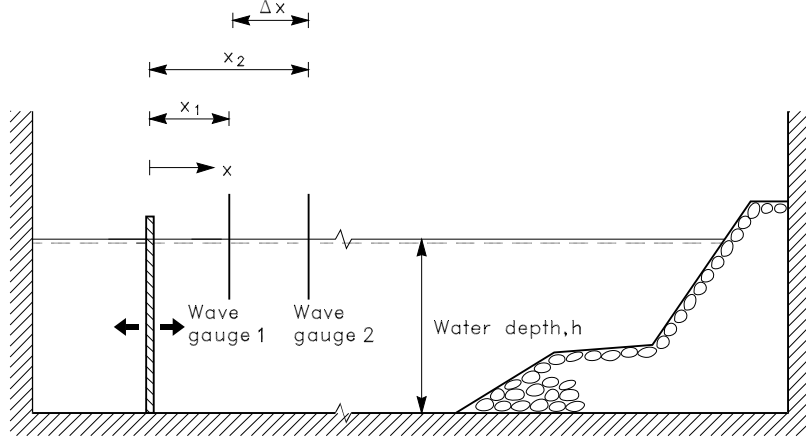
Figure 5.1: *Wave channel with piston-type wave generator.*

the case of monochromatic waves.

$$
\begin{aligned}
\eta(x,t) &= \eta_I(x,t) + \eta_R(x,t) \\
&= a_I \cos(2\pi f t - kx + \phi_I) + a_R \cos(2\pi f t + kx + \phi_R) \quad (5.1)
\end{aligned}
$$

where

f	: frequency
$a = a(f)$	: wave amplitude
$k = k(f)$	: wave number
$\phi = \phi(f)$	: phase

and indices I and R denote incident and reflected, respectively.

At the two wave gauges we have:

$$
\begin{aligned}
\eta(x_1,t) &= a_I \cos(2\pi f t - kx_1 + \phi_I) + a_R \cos(2\pi f t + kx_1 + \phi_R) \quad (5.2) \\
\eta(x_2,t) &= a_I \cos(2\pi f t - kx_2 + \phi_I) + a_R \cos(2\pi f t + kx_2 + \phi_R) \\
&= a_I \cos(2\pi f t - kx_1 - k\Delta x + \phi_I) + \\
&\quad a_R \cos(2\pi f t + kx_1 + k\Delta x + \phi_R) \quad (5.3)
\end{aligned}
$$

where $x_2 = x_1 + \Delta x$ has been substituted into Eq. 5.3.

It is seen that the incident wave is phase shifted $\Delta\phi = k\Delta x$ from signal $\eta(x_1,t)$ to signal $\eta(x_2,t)$, and the reflected wave is phase shifted $\Delta\phi = -k\Delta x$ due to opposite travel directions. These phase shifts are called the physical phase shifts and are denoted ϕ_I^{phys} and ϕ_R^{phys}, respectively.

58

The idea in the following manipulations of the elevation signals is to phase-shift the signals from the two wave gauges in such ways that the incident parts of the wave signals are in phase while the reflected parts of the signals are in mutual opposite phase. In this case the sum of the two manipulated signals is proportional to and in phase with the incident wave signal.

An amplification C and a theoretical phase shift ϕ^{theo} are introduced into the expressions for $\eta(x, t)$. The modified signal is denoted η^*. For the i'th wave gauge signal the modified signal is defined as:

$$
\begin{aligned}
\eta^*(x_i, t) &= Ca_I \cos(2\pi ft - kx_i + \phi_I + \phi_i^{theo}) + \\
&\quad Ca_R \cos(2\pi ft + kx_i + \phi_R + \phi_i^{theo})
\end{aligned} \tag{5.4}
$$

This gives at wave gauges 1 and 2:

$$
\begin{aligned}
\eta^*(x_1, t) &= Ca_I \cos(2\pi ft - kx_1 + \phi_I + \phi_1^{theo}) + \\
&\quad Ca_R \cos(2\pi ft + kx_1 + \phi_R + \phi_1^{theo})
\end{aligned} \tag{5.5}
$$

$$
\begin{aligned}
\eta^*(x_2, t) &= Ca_I \cos(2\pi ft - kx_2 + \phi_I + \phi_2^{theo}) + \\
&\quad Ca_R \cos(2\pi ft + kx_2 + \phi_R + \phi_2^{theo}) \\
&= Ca_I \cos(2\pi ft - kx_1 - k\Delta x + \phi_I + \phi_2^{theo}) + \\
&\quad Ca_R \cos(2\pi ft + kx_1 + k\Delta x + \phi_R + \phi_2^{theo})
\end{aligned} \tag{5.6}
$$

The sum of $\eta^*(x_1, t)$ and $\eta^*(x_2, t)$, which is denoted $\eta^{calc}(t)$, gives:

$$
\begin{aligned}
\eta^{calc}(t) &= \eta^*(x_1, t) + \eta^*(x_2, t) \\
\\
&= Ca_I \cos(2\pi ft - kx_1 + \phi_I + \phi_1^{theo}) + \\
&\quad Ca_R \cos(2\pi ft + kx_1 + \phi_R + \phi_1^{theo}) + \\
&\quad Ca_I \cos(2\pi ft - kx_1 - k\Delta x + \phi_I + \phi_2^{theo}) + \\
&\quad Ca_R \cos(2\pi ft + kx_1 + k\Delta x + \phi_R + \phi_2^{theo}) \\
\\
&= 2Ca_I \cos(0.5(-k\Delta x - \phi_1^{theo} + \phi_2^{theo})) \\
&\quad \cos(2\pi ft - kx_1 + \phi_I + 0.5(-k\Delta x + \phi_1^{theo} + \phi_2^{theo})) + \\
&\quad 2Ca_R \cos(0.5(-k\Delta x + \phi_1^{theo} - \phi_2^{theo})) \\
&\quad \cos(2\pi ft + kx_1 + \phi_R + 0.5(k\Delta x + \phi_1^{theo} + \phi_2^{theo}))
\end{aligned} \tag{5.7}
$$

It is seen that $\eta^{calc}(t)$ and $\eta_I(x_1, t) = a_I \cos(2\pi ft - kx_1 + \phi_I)$ are identical signals when the following three conditions are met:

$$2C \cos(0.5(-k\Delta x - \phi_1^{theo} + \phi_2^{theo})) = 1 \tag{5.8}$$

$$0.5(-k\Delta x + \phi_1^{theo} + \phi_2^{theo}) = n \cdot 2\pi \qquad n \in (0, \pm 1, \pm 2, ..) \tag{5.9}$$

$$0.5(-k\Delta x + \phi_1^{theo} - \phi_2^{theo}) = \frac{\pi}{2} + m \cdot \pi \qquad m \in (0, \pm 1, \pm 2, ..) \tag{5.10}$$

Solving Eqs. 5.8 - 5.10 with respect to $\phi_1^{theo}, \phi_2^{theo}$ and C gives Eqs. 5.11 - 5.13. n and m can still be chosen arbitrarily.

$$\phi_1^{theo} = k\Delta x + \pi/2 + m\pi + n2\pi \tag{5.11}$$

$$\phi_2^{theo} = -\pi/2 - m\pi + n2\pi \tag{5.12}$$

$$C = \frac{1}{2\cos(-k\Delta x - \pi/2 - m\pi)} \tag{5.13}$$

All the previous considerations and calculations were done in order to find an amplification and a phase shift for each of the two elevation signals η_1 and η_2. Eqs. 5.11 - 5.13 give the result of our efforts, i.e. $\eta_I(x_1, t) = \eta^{calc}(t)$. Remembering that $\phi_1^{theo} = \phi_1^{theo}(f), \phi_2^{theo} = \phi_2^{theo}(f)$ and $C = C(f)$, it is seen that the goal is already reached in the *frequency domain*. However, the implementation of the principle will be done in the *time domain* using digital filters. It is seen that singularities may occur. The consequences and the handling of the singularities will be treated later on in the chapter. Here it should just be mentioned that one way to bypass the singularities is to use a velocity meter instead of one of the two wave gauges. Such system is dealt with in the following chapter while the present chapter deals with two surface elevation signals only.

$\eta(x_1, t) \longrightarrow$ | FILTER 1 |

$\oplus \longrightarrow \eta_I(x_1, t)$

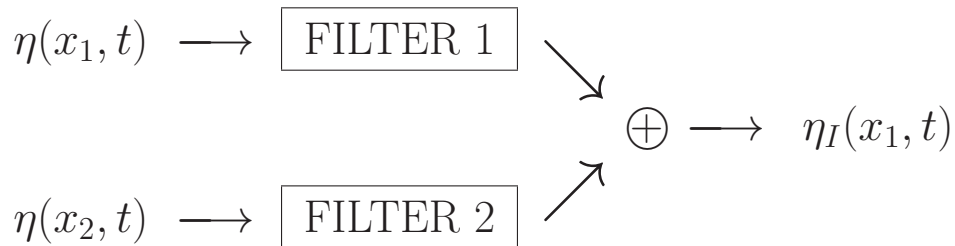$\eta(x_2, t) \longrightarrow$ | FILTER 2 |

Figure 5.2: *Flow diagram for signals in the SIRW-method.*

The purposes of the filters shown in Fig. 5.2 are exactly a frequency dependent amplification and a frequency dependent phase shift on each of the two elevation signals.

Taking $n = 0$ and $m = 0$ the frequency response functions $H_1(f)$ for filter 1 and $H_2(f)$ for filter 2 calculated due to Eqs. 5.11 - 5.13 are given below in complex notation:

$$\mathfrak{Re}\{H_1(f)\} = \frac{1}{2\cos(-k\Delta x - \pi/2)} \cdot \cos(k\Delta x + \pi/2)$$

$$\mathfrak{Im}\{H_1(f)\} = \frac{1}{2\cos(-k\Delta x - \pi/2)} \cdot \sin(k\Delta x + \pi/2) \qquad (5.14)$$

$$\mathfrak{Re}\{H_2(f)\} = \frac{1}{2\cos(-k\Delta x - \pi/2)} \cdot \cos(-\pi/2)$$

$$\mathfrak{Im}\{H_2(f)\} = \frac{1}{2\cos(-k\Delta x - \pi/2)} \cdot \sin(-\pi/2) \qquad (5.15)$$

Based on Eqs. 5.14 and 5.15 it is straightforward to design the time domain filters. The design of the filters will be given on the next pages.

5.2   Design of Filters

The impulse response of the filters is found by an inverse *discrete* Fourier transformation, which means that N discrete values of the complex frequency response are used in the transformation, see Fig. 5.3. This gives an impulse response of *finite* duration, i.e. the impulse response h^j or the filter coefficients are found by:

$$h^j = h(j \cdot \Delta t_{filter}) = \frac{1}{N} \sum_{r=0}^{N-1} H^r \cdot exp\left(i \frac{2\pi r j}{N}\right) \qquad (5.16)$$

where
$$r = 0,\ldots,\ N\text{-}1$$
$$j = 0,\ldots,\ N\text{-}1$$

and H^r is the complex frequency response given by Eqs. 5.14 and 5.15 at the frequency $f = r \cdot \Delta f$. Note that H^r should be hermitian, i.e. $H(f_n + f_i) = H^*(f_n - f_i)$.
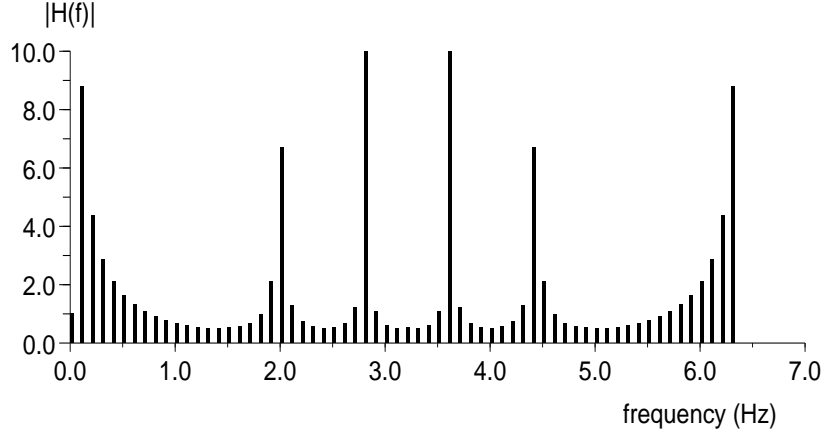
61

Figure 5.3:
Magnitude (gain) of the frequency responses of a discrete filter. $N = 64$, $h = 0.5$ m, $\Delta f = 0.10$ Hz, $\Delta t_{filter} = 0.16$ sec., $\Delta x = 0.2m$.

The frequency increment, Δf, in the frequency response is found by

$$\Delta f = \frac{1}{N \cdot \Delta t_{filter}} \tag{5.17}$$

where Δt_{filter} is the time increment of the filter.

 Fig. 5.4 gives an example on the filters. The price paid for handling only N frequencies in this transformation, is a minor inaccuracy in the performance of the filter at input frequencies, which do not coincide with one of the calculated frequencies in the discrete filter.

If the length of the filter (N) is increased, more frequencies are included, and in principle the overall accuracy of the filter is improved. In practice, however, there is a limit beyond which the accuracy of the filter starts to decrease due to other effects in the model.

The *convolution* integral (summation), Eq. 5.18, describes the input-output relationship for the filters. Notice that the output $\eta^*(x,t)$ is delayed $(N - 1)/2$ time steps relative to the input $\eta(x,t)$.
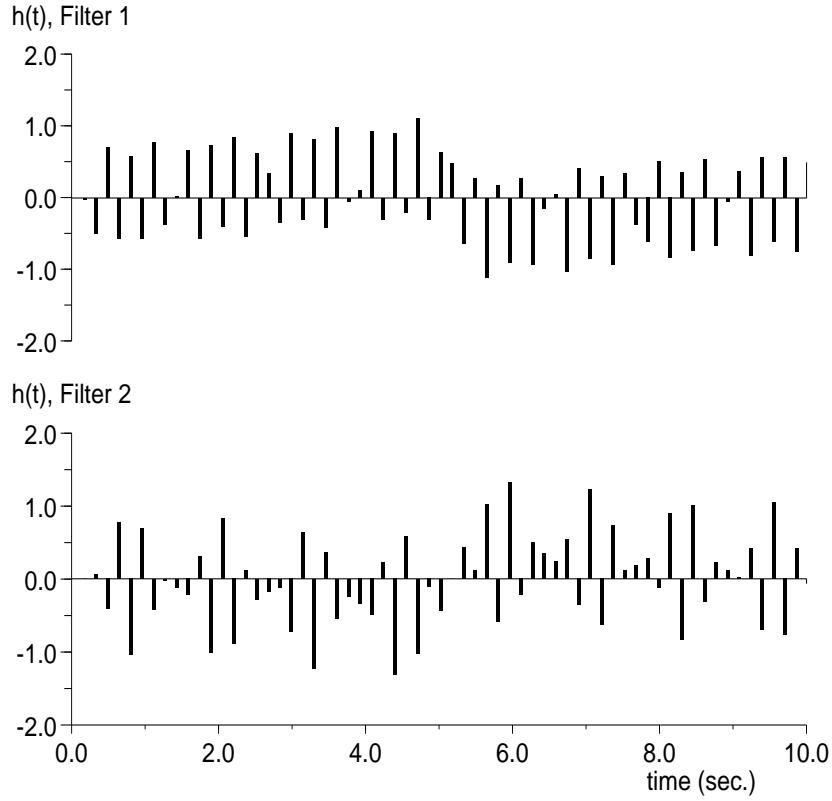
Figure 5.4: *Filter coefficients corresponding to Filter 1 and Filter 2. N = 64, water depth h = 0.5 m, Δf=0.10 Hz, Δt_{filter} = 0.16 sec.,Δx = 0.2m.*

$$\eta^{*p} = \sum_{j=0}^{N-1} h^j \cdot \eta^{p-j} \tag{5.18}$$

where

$j,p = 0,\ldots, N\text{-}1$

η^{p-j} : elevation at time $t = (p-j) \cdot \Delta t_{filter}$

η^{*p} : output from filter at time $t = p \cdot \Delta t_{filter}$

h^j : the filter coefficient corresponding to time $t = j \cdot \Delta t_{filter}$

Fig. 5.3 indicates that in the present example, singularities are present at frequencies of about 2.0 Hz and 2.8 Hz. The figure also shows that due to

63

the fact that the frequency response is calculated only at *discrete frequencies* in the filters, the singularities will not *destroy* the calculations. However, it is recommended to *cut off* the frequency responses whenever the value is larger than around 5. For practical use this means that, if $|H(f)| \geq 5$ when calculated, then $|H(f)|$ should be valued 5. Furthermore, it is recommended to *place* the singularities in a frequency range where the wave spectrum is without significant energy, for example 3 times the peak frequency of the spectrum. This can always be done by choosing appropriate values of Δx and Δt_{filter}, i.e. Δx smaller than a quarter of the shortest wave lengths.

5.2.1 Numerical Test Examples

In order to evaluate the SIRW-method we will look at two numerical examples with known incident and reflected waves. The error is described by the difference between the calculated incident wave signal η^{calc} and the actual incident wave signal η_I.

In the examples the total elevation due to two superimposed sine waves is described by Eq. 5.19, corresponding to 50 % reflection of the incident waves.

$$
\begin{aligned}
\eta(x,t) \;=\; & 0.01 \cdot \cos(2\pi f_1 t - k_1 x) + 0.01 \cdot \cos(2\pi f_2 t - k_2 x) + \\
& 0.01 \cdot 0.5 \cdot \cos(2\pi f_1 t + k_1 x) + \\
& 0.01 \cdot 0.5 \cdot \cos(2\pi f_2 t + k_2 x) \qquad\qquad (5.19)
\end{aligned}
$$

The signals are sampled with a frequency of 6.4 Hz. Fig. 5.5 illustrates the functionality of the method, when f_1 and f_2 are both coinciding with some frequencies of the discrete filter, i.e. $n \cdot \Delta f$.
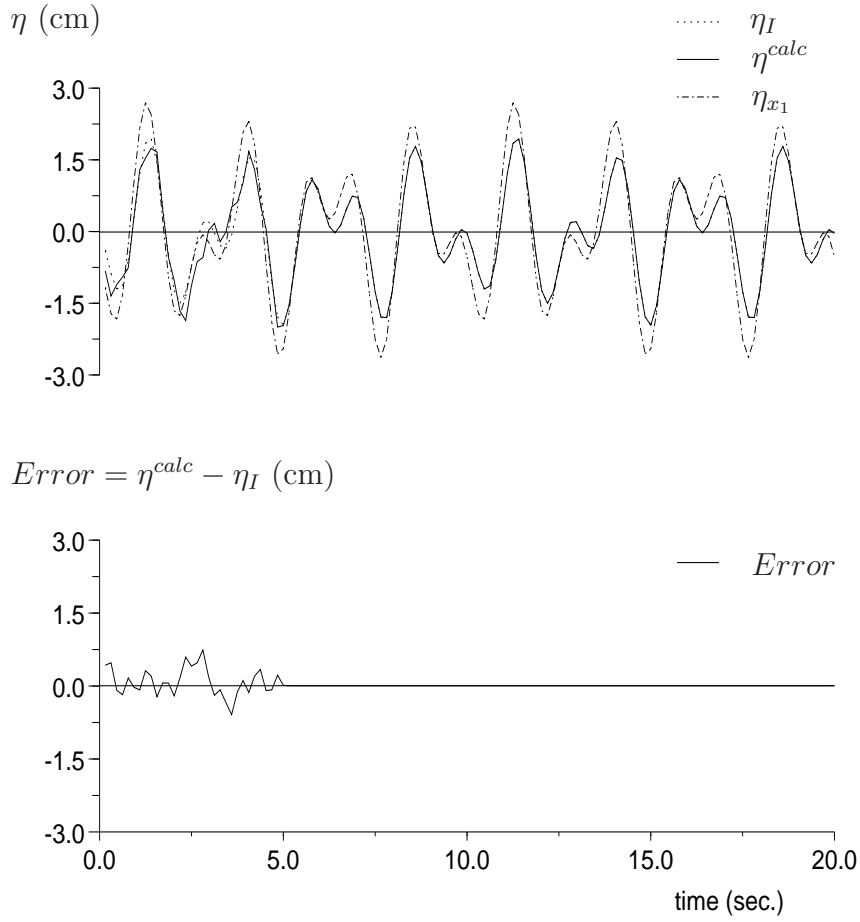
Figure 5.5: *A comparison between η_I, η^{calc} and η_{x_1}. $f_1 = 4\Delta f$, $f_2 = 7\Delta f$.*

As expected the method is exact for signals consisting only of energy placed at the discrete frequencies (Fig. 5.5), though it is seen that errors are present during *warm up* of the filters.

The second example (Fig. 5.6) is identical to the first example except that f_1 and f_2 are not coinciding with frequencies in the digital filter i.e. $f_1 = 4.2\Delta f$, $f_2 = 7.5\Delta f$. It must be stressed that the output signal shown in Fig. 5.6 corresponds to the worst case situation, where the wave frequencies are placed midway between filter frequencies.
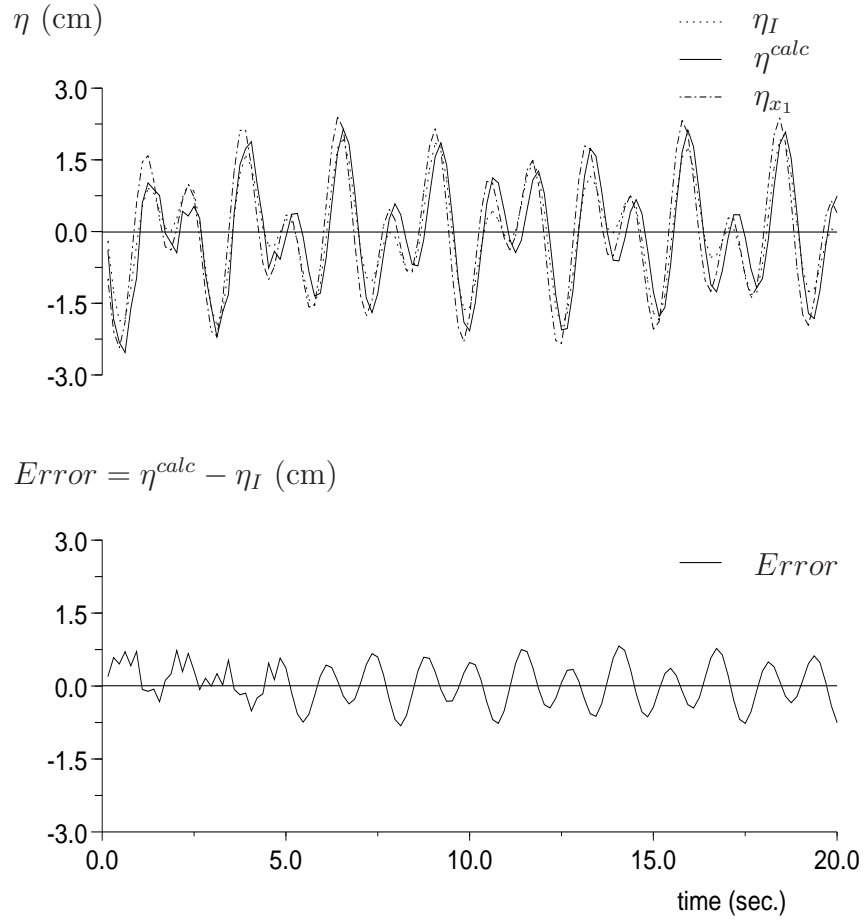
Figure 5.6: *A comparison between η_I, η^{calc} and η_{x_1}. $f_1 = 4.2\Delta f$, $f_2 = 7.5\Delta f$.*

One way to improve the results is to apply a tapering of the filter coefficients, because the output from a digital filter is more stable in case the absolute values of the filter coefficients are almost zero in both ends of the filter, Karl (1989). Cosine tapering of the filter coefficients improves the accuracy of the SIRW method as demonstrated in Fig. 5.7.
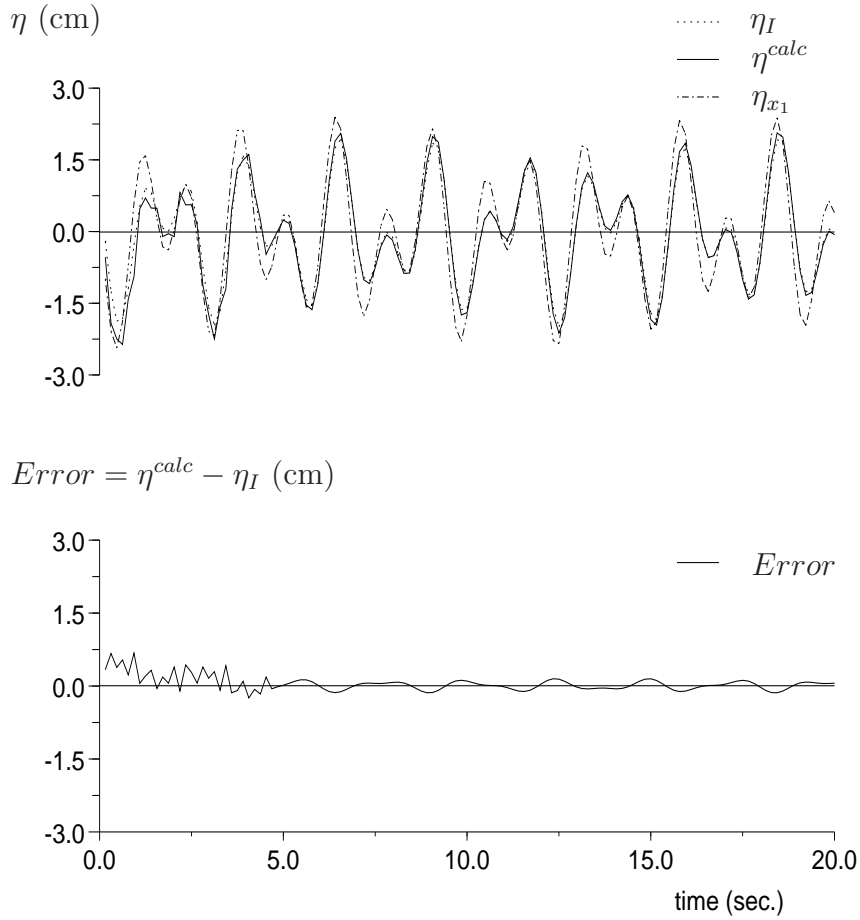
Figure 5.7: *A comparison between η_I, η^{calc} and η_{x_1}. The filters have been cosine tapered.* $f_1 = 4.2\Delta f$, $f_2 = 7.5\Delta f$.

5.2.2 Physical Model Tests

The SIRW-method previously described was also tested in a laboratory flume at the Hydraulics and Coastal Engineering Laboratory, Aalborg University, cf. Fig 5.8.

First, the waves (incident part of the timeseries) were generated and sent towards a spending permeable beach (slope 1:8) with low reflection (app. 5 %) in order to obtain a good estimate of the incident waves. Next, a reflecting wall was mounted in the flume giving a fairly high reflection (app. 50 %) and the same incident waves were reproduced by play back of the same digital steering signal to the wave maker. Notice, that the incident wave fields are identical only until re-reflection occurs. In Fig. 5.9 the output from the SIRW-filters is compared with the incident waves measured in the case of very low reflection.

Figure 5.8: *Set-up for physical model tests.*

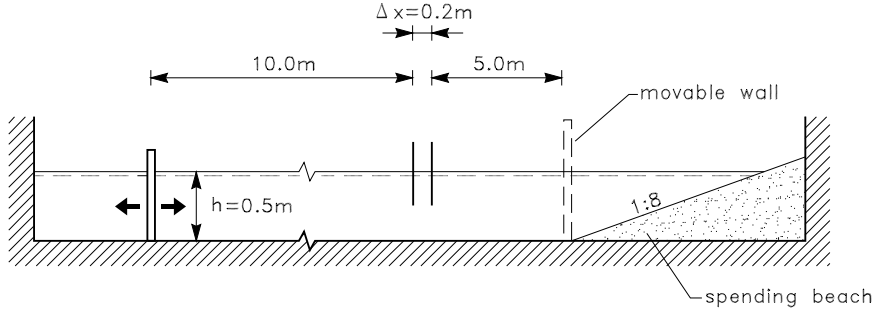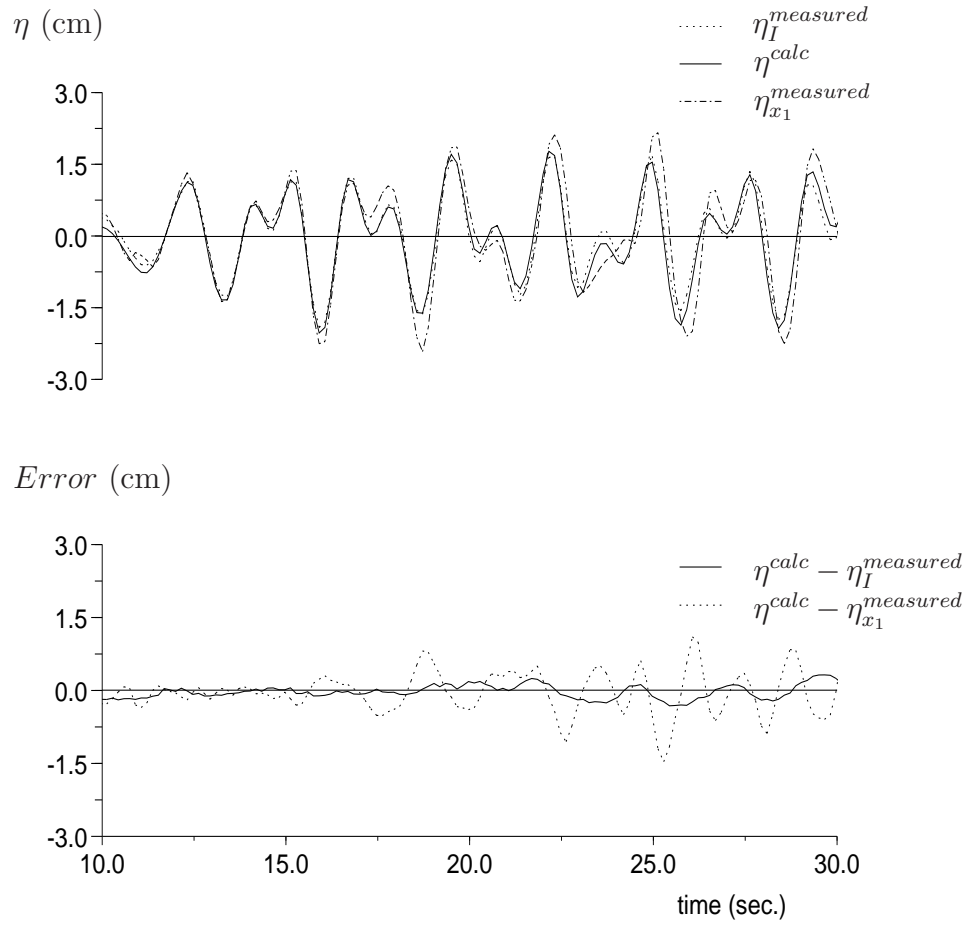Figure 5.9: *A comparison between* $\eta_I^{measured}, \eta^{calc}$ *and* $\eta_{x_1}^{measured}$. $f_1 = 4.2\Delta f$, $f_2 = 7.5\Delta f$.

The specific part of the signals, where reflection is present but re-reflection

68

from the wave paddle is still not present, is shown. Two different estimates of the incident waves are used, namely the measured elevation at gauge no 1 ($\eta_{x_1}^{measured}$) and the calculated elevation at gauge no 1 (η^{calc}). In the the specific example the SIRW-method reduces the error (variance of the difference $\eta^{calc} - \eta_{x_1}$) from 30 % of the incident energy to 3 % of the incident energy.

5.3   Conclusions

A time-domain method for Separating Incident and Reflected Irregular Waves (The SIRW-method) has been presented.

By numerical and physical model tests it is demonstrated that the method is quite efficient in separating the total wave field into incident and reflected waves. Please note, that all the tests shown were done with fairly small filters (few filter components), and that longer filters will improve the efficiency of the method. Taking the example shown in Fig. 5.6 and doubling the number of filter coefficients the error (variance) will decrease to 2/3 of the shown example.

The accuracy of the SIRW-method is comparable with the accuracy of the method proposed by Goda and Suzuki (1976), but the SIRW-method has the advantage that where the incident wave signal is wanted in *time domain* (i.e. for zero-crossing analysis) the singularity points are treated more properly than in the Goda-method. The SIRW-method can easily be extended to give the same accuracy as the method proposed by Mansard and Funke (1980).

The greatest advantage of the SIRW-method is that it works in *real time*. Brorsen and Frigaard (1992) previously used digital filters to make an open boundary condition in a Boundary Element Model, based on a filtering of the surface elevation. That boundary condition accumulated errors, because separation of the surface elevation into incident and reflected waves was not possible in *real time* at that moment and, consequently, the Boundary Element Model became unstable and could only run for a limited time. The SIRW-method will make it possible to use digital filters as boundary condition in these models.

At the moment the SIRW-method is implemented at Aalborg Hydraulics Laboratory, Aalborg University and the method is used in active absorption.

Chapter 6

Reflection Analysis of Oblique Long-Crested Waves

In the case of oblique waves, i.e. 2D-waves travelling along a line not perpendicular to the reflecting structure, the previous derived methods can all can be applied by assuming that the waves can be decomposed into two vectorial components, being respectively $\perp$ and $||$ to the structure.

$$
\begin{aligned}
\eta(\boldsymbol{x}, t) = \ & \sum_{n=1}^{N} a_{I,n} \cos(\boldsymbol{k}_n \boldsymbol{x} - \omega_n t + \Phi_{I,n}) + \\
& \sum_{n=1}^{N} a_{R,n} \cos(\boldsymbol{k}_n \boldsymbol{x} + \omega_n t + \Phi_{R,n})
\end{aligned}
\tag{6.1}
$$

where η is the surface elevation relative to MWL
$\boldsymbol{x}$ is the vectorial position of the wave gauge
t is time
a_n is the amplitude
$\boldsymbol{k}_n$ is the vectorial wavenumber
ω_n is the angular frequency of the waves
Φ_n is the phase

Omitting index n and rewriting eq. (6.1) in cartesian coordinates:

$$\eta(x, y, t) = \quad a_I \cos(\; kx \cos(\theta_I) + ky \sin(\theta_I) - \omega t + \Phi_I) +$$
$$a_R \cos(\; kx \cos(\theta_R) + ky \sin(\theta_R) + \omega t + \Phi_R) \qquad (6.2)$$

where x, y is the vectorial position of the wave gauge
       k is the wavenumber
       θ is direction of wave
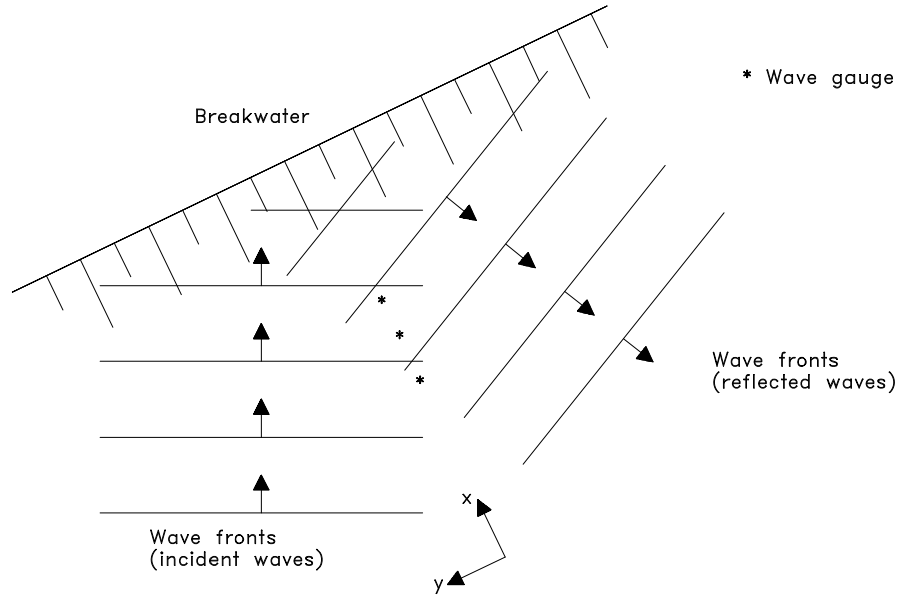
Figure 6.1: Placement of wave gauges in front of structure.

It is seen that if the angle of the incident wave is know, and the angle of the reflected wave is calculated using Snells law (incident angle = reflected angle) eq. (6.3) is very similar to the original expression for the wave elevation, eq(4.2).

The easiest way to solve the problem is to place the wave gauges on a line perpendicular to the reflecting structure (y-coordinate $\equiv 0$ for all gauges) as shown in fig 6. Eq. (6.2) will then simplify to:

$$\eta(x, 0, t) = \quad a_I \cos(kx \cos(\theta_I) - \omega t + \Phi_I) +$$
$$a_R \cos(kx \cos(\theta_R) + \omega t + \Phi_R) \qquad (6.3)$$

Which shows the with this positioning of the gauges the normal methods presented in the previous two chapters can be used when the geometrical gauge distances are modified by the factor $\cos(\theta)$.

Please notice that near the structure *edge-waves* will exist. These waves travel along the structure and can destroy the calculations because they are not included in the modelling of the waves.

Chapter 7

Methods for estimation of directional spectra

A short crested wave field is normally referred to as a three-dimensional wave field. This implies introduction of an additional parameter namely the direction of travel. A two dimensional wave field is commonly described in the frequency domain by use of the wave spectrum, i.e. the auto spectrum of the wave elevation process. Now in the three dimensional case a directional spreading function depending on frequency and direction of travel is introduced. The combination of the wave spectrum and the spreading function is the directional wave spectrum. Having determined the directional wave spectrum the wave field is fully described in the frequency domain.

For a two dimensional sea state the elevation was assumed to be a summation of a number of wavelets as stated in e.g. eq. (4.1). In a three dimensional case the corresponding expression is

$$
\eta(\boldsymbol{x}, t) = \sum_{n=1}^{N} \sum_{m=1}^{M} a_{mn} \cos(\boldsymbol{k}_{mn} \boldsymbol{x} - \omega_n t + \Phi_{mn}) \tag{7.1}
$$

where $\boldsymbol{k}$ is the wavenumber vector. Eq. (7.1) implies that for each pair of discrete values of frequency and direction of travel there exist a long crested wave propagating with these properties.

The amplitude a_{mn} can alternatively be described by use of the wavespectrum

as the variance of a sinusoidal wave is half the amplitude squared. Hence

$$
\begin{aligned}
\frac{1}{2}a_{mn}^2 &= S(\omega_m, \theta_n)\Delta\theta\Delta\omega \\
a_{mn} &= \sqrt{2S(\omega_m, \theta_n)\Delta\theta\Delta\omega}
\end{aligned}
\tag{7.2}
$$

Inserting eq. (7.2) into eq. (7.1) yields

$$
\eta(\boldsymbol{x}, t) = \sum_{n=1}^{N}\sum_{m=1}^{M}\sqrt{2S(\omega_m, \theta_n)\Delta\theta\Delta\omega}\cos(\boldsymbol{k}_{mn}\boldsymbol{x} - \omega_n t + \Phi_{mn})
\tag{7.3}
$$

Letting $\Delta\theta \to d\theta$ and $\Delta\omega \to d\omega$ eq. (7.3) turns into a double integral

$$
\eta(\boldsymbol{x}, t) = \int_0^\infty \int_{-\pi}^\pi \cos(\boldsymbol{k}\boldsymbol{x} - \omega t + \Phi(\omega, \theta))\sqrt{2S(\omega, \theta)d\theta d\omega}
\tag{7.4}
$$

The aim of the following is to establish an expression which relates known and measured numbers to the directional wave spectrum or the directional spreading function. These latter functions are related through

$$
S(\omega, \theta) = H(\omega, \theta)S(\omega)
\tag{7.5}
$$

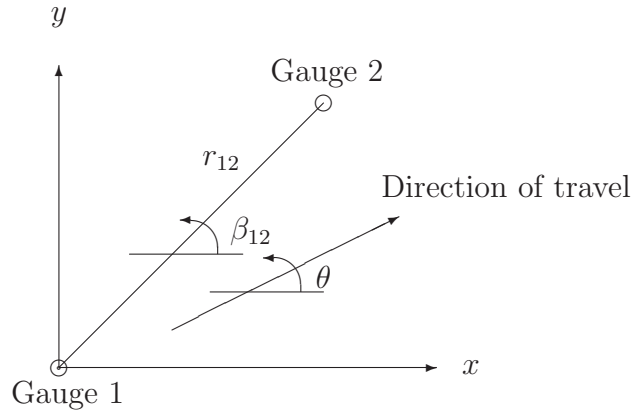Two wave gauges are considered. These are positioned as shown in fig. 7.

Figure 7.1: Definition of geometric parameters.

The elevations at gauge 1 and gauge 2, respectively, are

$$
\begin{aligned}
\eta_1 = \eta(\boldsymbol{x}_1, t) \ &= \ \int_0^\infty \int_{-\pi}^{\pi} \cos(\boldsymbol{k}\boldsymbol{x}_1 - \omega t + \Phi(\omega, \theta))\sqrt{2S(\omega, \theta)}d\theta d\omega \\
\eta_2 = \eta(\boldsymbol{x}_2, t) \ &= \ \int_0^\infty \int_{-\pi}^{\pi} \cos(\boldsymbol{k}\boldsymbol{x}_2 - \omega t + \Phi(\omega, \theta))\sqrt{2S(\omega, \theta)}d\theta d\omega \\
&= \ \int_0^\infty \int_{-\pi}^{\pi} \cos(\boldsymbol{k}\boldsymbol{x}_1 - \omega t + kr_{12}\cos(\theta - \beta_{12}) + \Phi(\omega, \theta)) \cdot \\
&\qquad \sqrt{2S(\omega, \theta)}d\theta d\omega
\end{aligned}
$$

The cross-correlation function is obtained as

$$
R_{\eta_1\eta_2}(\tau) \ = \ \frac{1}{T}\int_0^T \eta_1(t)\eta_2(t+\tau)dt \tag{7.6}
$$

Here it is necessary to specify the time argument, thus $\eta_1(t) = \eta_1$ and $\eta_2(t) = \eta_2$. Inserting into eq. (7.6) yields

$$
\begin{aligned}
R_{\eta_1\eta_2}(\tau) \ = \ &\frac{1}{T}\int_0^T \int_0^\infty \int_{-\pi}^{\pi} \cos(\boldsymbol{k}\boldsymbol{x}_1 - \omega t + \Phi(\omega, \theta)) \cdot \\
&\cos(\boldsymbol{k}\boldsymbol{x}_1 - \omega(t+\tau) + kr_{12}\cos(\theta - \beta_{12}) + \Phi(\omega, \theta)) \cdot \\
&2S(\omega, \theta)d\theta d\omega dt \tag{7.7}
\end{aligned}
$$

Applying the trigonometric relations

$$
\begin{aligned}
2\cos\alpha\cos\beta \ &= \ \cos(\alpha - \beta) + \cos(\alpha + \beta) \\
\cos(\alpha \pm \beta) \ &= \ \cos\alpha\cos\beta \mp \sin\alpha\sin\beta
\end{aligned}
$$

leads to

$$
\begin{aligned}
R_{\eta_1\eta_2}(\tau) \ = \ &\frac{1}{T}\int_0^T \int_0^\infty \int_{-\pi}^{\pi} [\cos(kr_{12}\cos(\theta - \beta_{12}) - \omega\tau) \\
&+ \cos(2\boldsymbol{k}\boldsymbol{x}_1 + kr_{12}\cos(\theta - \beta_{12}) - 2\omega t - \omega\tau + 2\Phi(\omega, \theta))] \cdot \\
&S(\omega, \theta)d\theta d\omega dt \\
= \ &\int_0^\infty \int_{-\pi}^{\pi} \cos(kr_{12}\cos(\theta - \beta_{12}) - \omega\tau)S(\omega, \theta)d\theta d\omega
\end{aligned}
$$

77

which can be written as

$$R_{\eta_1\eta_2}(\tau) = \int_0^\infty \int_{-\pi}^\pi [\cos(\omega\tau)\cos(kr_{12}\cos(\theta - \beta_{12}))$$
$$+ \sin(\omega\tau)\sin(kr_{12}\cos(\theta - \beta_{12}))] \, S(\omega,\theta)d\theta d\omega \qquad (7.8)$$

Because the cross-correlation is the inverse Fourier transform of the cross-spectrum, the cross-correlation can also be written

$$R_{\eta_1\eta_2}(\tau) = \int_0^\infty c_{12}(\omega)\cos(\omega\tau)d\omega + \int_0^\infty q_{12}(\omega)\sin(\omega\tau)d\omega \qquad (7.9)$$

where c_{12} is the co-spectrum and q_{12} the quad-spectrum in the cross-spectrum

$$S_{\eta_1\eta_2}(\omega) = c_{12}(\omega) - iq_{12}(\omega) \qquad (7.10)$$

A comparison between eq.(7.8) and eq.(7.9) leads to

$$c_{12}(\omega) = \int_{-\pi}^\pi S(\omega,\theta)\cos(kr_{12}\cos(\theta - \beta_{12}))d\theta$$
$$q_{12}(\omega) = \int_{-\pi}^\pi S(\omega,\theta)\sin(kr_{12}\cos(\theta - \beta_{12}))d\theta$$

Inserting these expressions for the co- and quad-spectrum into eq. (7.10) yields

$$S_{\eta_1\eta_2}(\omega) = \int_{-\pi}^\pi S(\omega,\theta)\exp(-ikr_{12}\cos(\theta - \beta_{12}))d\theta$$
$$\frac{S_{\eta_1\eta_2}(\omega)}{S_{\eta\eta}(\omega)} = \int_{-\pi}^\pi H(\omega,\theta)\exp(-ikr_{12}\cos(\theta - \beta_{12}))d\theta \qquad (7.11)$$

Eq. (7.11) relates data, which can be computed from wave elevation measurements, to the unknown directional spreading function. The geometry is represented by r_{12} and β_{12}.

Eq. (7.11) is the basic relation that was in demand. It cannot be solved analytically. Therefore methods have been proposed in order to make a reliable estimate.

Common for all methods is that they make assumptions about the shape of the directional spreading function. That may either be a parameterized

78

analytic expression or a number of discrete values making a step curve. This initial assumption is very important to the ability of the particular method. The next step is to fit the unknown parameters to the measured data. The reliability of the fit depends on the reliability of the measured data but also on the number of coefficients to fit, i.e. the more coefficients the less reliability. This is a problem as a high resolution requires many coefficients.

7.1 The Maximum Likelihood Method

In the Maximum Likelihood Method, MLM, the directional spectrum is calculated from minimizing the errors between measured wave data (cross-correlations) and fitted directional spectrum.

This is achieved by use of the Maximum Likelihood technique, which has named the method.

In it most simple form MLM applies for simultaneous wave elevations, but by use of transfer functions it can readily be extended to apply for various measurements. The MLM was originally presented by Capon (1969), but has since been modified by several authors. Especially the papers by Davis and Regier (1977) and Isobe et al. (1984) are of importance.

As an initial assumption the directional spectrum is expressed as a linear combination of the cross-spectra. The linear wave theory is assumed valid as well, i.e.

$$
\begin{aligned}
k &= 2\pi/L \\
L &= L_0 \tanh(kd)
\end{aligned}
$$

Hence the estimated directional spectrum, $\tilde{S}(\omega, \theta)$, can be written as

$$
\tilde{S}(\omega, \theta) = \sum_{m=1}^{N} \sum_{n=1}^{N} \alpha_{mn}(\omega, \theta) S_{mn}(\omega) \tag{7.12}
$$

Then using

$$
S_{mn}(\omega) = \int_0^{2\pi} \exp(-i\boldsymbol{k}(\boldsymbol{x}_n - \boldsymbol{x}_m)) S(\omega, \theta) d\theta \tag{7.13}
$$

79

eq. (7.12) leads to

$$\tilde{S}(\omega, \theta) = \sum_{m=1}^{N} \sum_{n=1}^{N} \alpha_{mn}(\omega, \theta) \int_{0}^{2\pi} \exp(-i\boldsymbol{k}'(\boldsymbol{x}_n - \boldsymbol{x}_m)) S(\omega, \theta') d\theta' \quad (7.14)$$

where $\boldsymbol{k}' = \left\{ \begin{array}{c} k \cos \theta' \\ k \sin \theta' \end{array} \right\}$.

Eq. (7.14) is expressed as

$$\tilde{S}(\omega, \theta) = \int_{0}^{2\pi} w(\omega, \theta, \theta') S(\omega, \theta') d\theta' \quad (7.15)$$

where

$$w(\omega, \theta, \theta') = \sum_{m=1}^{N} \sum_{n=1}^{N} \alpha_{mn}(\omega, \theta) \exp(-i\boldsymbol{k}'(\boldsymbol{x}_n - \boldsymbol{x}_m)) \quad (7.16)$$

From eq. (7.15) it is seen that the estimated directional spectrum is a convolution of the true directional spectrum and the window function $w(\omega, \theta, \theta')$ given by eq. (7.16).

It is assumed that the coefficients $\alpha_{mn}(\omega, \theta)$ can be expressed as

$$\alpha_{mn}(\omega, \theta) = \gamma_m(\omega, \theta) \gamma_n^*(\omega, \theta) \quad (7.17)$$

Inserting this into eq. (7.12) and eq. (7.16) yields

$$\tilde{S}(\omega, \theta) = \sum_{m=1}^{N}\sum_{n=1}^{N}\gamma_m(\omega,\theta)\gamma_n^*(\omega,\theta)S_{mn}(\omega) \tag{7.18}$$

$$w(\omega, \theta, \theta') = \sum_{m=1}^{N}\sum_{n=1}^{N}\gamma_m(\omega,\theta)\gamma_n^*(\omega,\theta)\exp(-i\boldsymbol{k}'(\boldsymbol{x}_n - \boldsymbol{x}_m))$$

$$= \sum_{m=1}^{N}\sum_{n=1}^{N}\gamma_m(\omega,\theta)\gamma_n^*(\omega,\theta)\exp(i\boldsymbol{k}'\boldsymbol{x}_m)\exp(-i\boldsymbol{k}'\boldsymbol{x}_n)$$

$$= \sum_{m=1}^{N}\gamma_m(\omega,\theta)\exp(i\boldsymbol{k}'\boldsymbol{x}_m)\sum_{n=1}^{N}\gamma_n^*(\omega,\theta)\exp(-i\boldsymbol{k}'\boldsymbol{x}_n)$$

$$= \sum_{m=1}^{N}\gamma_m(\omega,\theta)\exp(i\boldsymbol{k}'\boldsymbol{x}_m)\sum_{n=1}^{N}(\gamma_n(\omega,\theta)\exp(i\boldsymbol{k}'\boldsymbol{x}_n))^*$$

$$= |\sum_{m=1}^{N}\gamma_m(\omega,\theta)\exp(i\boldsymbol{k}'\boldsymbol{x}_m)|^2 \tag{7.19}$$

The window function is normalised by setting $w(\omega, \theta, \theta) = 1$. Having done this it is seen from eq. (7.15) that if the window function is Diracs delta function, then the estimated directional spectrum is equal to the true directional spectrum. As both the window function and the true directional spectrum is non-negative the aim is to minimise $\tilde{S}(\omega, \theta)$ as given in eq. (7.18) i.e.

$$\text{minimise}\left(\sum_{m=1}^{N}\sum_{n=1}^{N}\gamma_m(\omega,\theta)\gamma_n^*(\omega,\theta)S_{mn}(\omega)\right)$$

The same problem can be formulated as

$$\text{maximise}\left(\frac{w(\omega,\theta,\theta)}{\tilde{S}(\omega,\theta)} = \frac{\sum_{m=1}^{N}\sum_{n=1}^{N}\gamma_m(\omega,\theta)T_{mn}(\omega,\theta)\gamma_n^*(\omega,\theta)}{\sum_{m=1}^{N}\sum_{n=1}^{N}\gamma_m(\omega,\theta)S_{mn}(\omega,\theta)\gamma_n^*(\omega,\theta)}\right) \tag{7.20}$$

where a matrix $\boldsymbol{T}$ has been introduced as

$$T_{mn}(\omega,\theta) = \exp(i\boldsymbol{k}\boldsymbol{x}_m)\exp(-i\boldsymbol{k}\boldsymbol{x}_n) \tag{7.21}$$
$$= \gamma_{om}^*(\omega,\theta)\gamma_{on}(\omega,\theta) \tag{7.22}$$

The maximum value of eq. (7.20) is equal to the maximum eigenvalue of the matrix $\boldsymbol{S}^{-1}\boldsymbol{T}$. Eq. (7.20) is then the Rayleigh quotient of $\boldsymbol{\gamma}^T(\boldsymbol{T} - \lambda\boldsymbol{S})\boldsymbol{\gamma}^* = 0$

81

whereas

$$\text{maximum} \left(\frac{\boldsymbol{\gamma}^T \boldsymbol{T} \boldsymbol{\gamma}^*}{\boldsymbol{\gamma}^T \boldsymbol{S} \boldsymbol{\gamma}^*} \right) = \lambda_{max} \tag{7.23}$$

where λ_{max} is the maximum eigenvalue. Thus by multiplication of $\gamma^{T^{-1}}$ and $\boldsymbol{S}^{-1}$ and substitution of $\boldsymbol{T}$

$$
\begin{aligned}
\boldsymbol{\gamma}^T \boldsymbol{T} \boldsymbol{\gamma}^* &= \lambda_{max} \boldsymbol{\gamma}^T \boldsymbol{S} \boldsymbol{\gamma}^* \\
\boldsymbol{T} \boldsymbol{\gamma}^* &= \lambda_{max} \boldsymbol{S} \boldsymbol{\gamma}^* \\
\boldsymbol{S}^{-1} \boldsymbol{T} \boldsymbol{\gamma}^* &= \lambda_{max} \boldsymbol{\gamma}^* \\
\boldsymbol{S}^{-1} \boldsymbol{\gamma}_o^* \boldsymbol{\gamma}_o^T \boldsymbol{\gamma}^* &= \lambda_{max} \boldsymbol{\gamma}^*
\end{aligned}
$$

Further by premultiplication by $\boldsymbol{\gamma}_o^T$ yields

$$\boldsymbol{\gamma}_o^T \boldsymbol{S}^{-1} \boldsymbol{\gamma}_o^* \boldsymbol{\gamma}_o^T \boldsymbol{\gamma}^* = \lambda_{max} \boldsymbol{\gamma}_o^T \boldsymbol{\gamma}^* \tag{7.24}$$

Thus

$$\boldsymbol{\gamma}_o^T \boldsymbol{S}^{-1} \boldsymbol{\gamma}_o^* = \lambda_{max} \tag{7.25}$$

It is given from eq. (7.20) that

$$\tilde{S}(\omega, \theta) \propto 1/\lambda_{max}$$

Hence introducing a proportionality factor κ the directional spectrum can be estimated as

$$\tilde{S}(\omega, \theta) = \kappa \left(\boldsymbol{\gamma}_o^T \boldsymbol{S}^{-1} \boldsymbol{\gamma}_o^* \right)^{-1} \tag{7.26}$$

The terms in the RHS of eq. (7.26) are all known when a sample has been carried out. $\boldsymbol{S}$ is the cross-spectrum matrix and is calculated from the time series. γ_o is dependent only on the wavenumber vector and the geometry. The factor κ is used in order to achieve the correct variance (i.e. the measured variance). While the MLM (and BDM) provides reasonable results for directional wave spectra containing incident waves only the methods becomes less reliable when reflections occur. This problem happen because there is a corelation of the phases of the incident and reflected waves. This problem

arises in most methods.

Several methods has been suggested to handle reflection. Common approaches is to either provide information about the location and direction of the reflector i.e. Isobe & Kondo (1984) or by assuming a parametric form of the spreading functions as suggested by Yokoki, Isobe & Watanabe (1992). Hiromune et al. (1992) have done this utilising Mitsuyasu's spreading function. Further the spreading function has the option to imply a reflected wave system which in spreading has the same form as the incoming system but reduced in energy. This method assumes that the waves are reflected along a structure that has a straight front.

7.2 MLM utilising standard spectra

The purpose of the present section is to present the Maximum Likelihood method for estimating directional spectra utilising standard spectra. The presentation is based on Isobe (1990), Yokoki, Isobe & Watanabe (1992) and Christensen & Sørensen (1994). The directional spectrum is given in a standard form in terms of some unknown parameters to be estimated from measured data. In the present section only surface elevations measurements are treated.

The starting point is M surface elevations, $\eta(\mathbf{x}, t)$, measured at M different locations $\mathbf{x}$ at time t. The total elevation processes $\eta_p(\boldsymbol{x}_p, t)$, $p = 1, 2, ..., M$, are modelled as stochastic processes. The processes are assumed to be joint stationary, ergodic and Gaussian distributed. The mean value functions $\mu_{\eta_p}(t)$, $p = 1, 2, \ldots, M$, are assumed to be equal to 0. The M time series can be written as a Fourier-sum as

$$\eta_p(\boldsymbol{x}, t) = \sum_{l=1}^{N} \left(A_{p,l} \cos \omega_l t + B_{p,l} \sin \omega_l t \right), \ p = 1, 2, ..., M \qquad (7.27)$$

where $\omega_l = l\frac{2\pi}{T}$ and T is the length of the time series. The coefficients $A_{p,l}$

and $B_{p,l}$ are given as the stochastic integrals

$$A_{p,l} = \frac{2}{T} \int_{-\frac{T}{2}}^{\frac{T}{2}} \eta_p\left(\boldsymbol{x}_p, t\right) \cos \omega_l t \, dt \qquad l = 1, 2, \ldots, N \; p = 1, 2, \ldots \quad (7.28)$$

$$B_{p,l} = \frac{2}{T} \int_{-\frac{T}{2}}^{\frac{T}{2}} \eta_p\left(\boldsymbol{x}_p, t\right) \sin \omega_l t \, dt \qquad l = 1, 2, \ldots \; N \; p = 1, 2, \ldots \quad (7.29)$$

In eq. (7.27) the term corresponding to $l = 0$ has been omitted as it equals 0.

From eq. (7.28) and eq. (7.29) it is seen that all the coefficients $A_{p,l}$ and $B_{p,l}$ are joint Gaussian distributed stochastic variables.

In the following only the l'th components are considered. The primary aim is to determine the joint distribution of the coefficients $A_{p,l}$ and $B_{p,l}$ $p = 1, 2, \ldots, M$, at the frequency w_l.

The reason for limiting the analysis to a single frequency at a time is that the unknown parameters in $S(\omega, \theta)$ to be estimated may be frequency dependent.

The coefficients are expressed as a vector

$$\begin{aligned} \boldsymbol{A}^T &= [A_1 \; A_2 \; \ldots \; A_M \; B_1 \; B_2 \; \ldots \; B_M] \\ &= [A_1 \; \ldots \; A_M \; A_{M+1} \; \ldots \; A_{2M}] \end{aligned} \qquad (7.30)$$

As the coefficients are joint Gaussian distributed the frequency distribution function is given in terms of the mean value function vector, $E[\boldsymbol{A}]$, and the cross covariance function matrix $\boldsymbol{\kappa}_{\boldsymbol{A}\boldsymbol{A}^T} = E\left[\boldsymbol{A}\boldsymbol{A}^T\right]$. The cross covariance function matrix of size $2M \times 2M$ is symmetric and of the form

$$\boldsymbol{\kappa}_{\boldsymbol{A}\boldsymbol{A}^T} = \begin{bmatrix} \boldsymbol{B} & \boldsymbol{E} \\ \boldsymbol{E}^T & \boldsymbol{D} \end{bmatrix} \qquad (7.31)$$

where the submatrices $\boldsymbol{B}$, $\boldsymbol{E}$ and $\boldsymbol{D}$ are $M \times M$ matrices.

From eq. (7.28) and eq. (7.29) the following results are found

$$E\left[A_{p,l}\right] = \frac{2}{T} \int_{-\frac{2}{T}}^{\frac{2}{T}} E\left[\eta_p\left(\boldsymbol{x}_p, t\right)\right] \cos \omega_l t \, dt = 0 \quad , \quad p = 1, 2, \ldots, M \quad (7.32)$$

and

$$E\left[B_{p,l}\right] = \frac{2}{T} \int_{-\frac{2}{T}}^{\frac{2}{T}} E\left[\eta_p\left(\boldsymbol{x}_p, t\right)\right] \sin \omega_l t \, dt = 0 \quad , \quad p = 1, 2, \ldots, M \quad (7.33)$$

i.e. $E\left[\boldsymbol{A}\right] = \boldsymbol{0}$.

In the following the cross covariance function matrix $E\left[\boldsymbol{A}\,\boldsymbol{A}^T\right]$ will be determined. As an example the submatrix $\boldsymbol{B}$ in eq. (7.31) is considered.

$$
\begin{aligned}
\kappa_{A_{m,l}A_{n,l}}\left(t_1, t_2\right) &= E\left[\frac{2}{T}\int_{-\frac{2}{T}}^{\frac{2}{T}} \eta_m\left(t_1\right) \cos\left(\omega_l t_1\right) dt_1 \cdot \frac{2}{T}\int_{-\frac{2}{T}}^{\frac{2}{T}} \eta_n\left(t_2\right) \cos\left(\omega_l t_2\right) dt_2\right] \\
&= \frac{4}{T^2}\int_{-\frac{2}{T}}^{\frac{2}{T}}\int_{-\frac{2}{T}}^{\frac{2}{T}} E\left[\eta_m\left(t_1\right)\eta_n\left(t_2\right)\right]\,\cos\left(\omega_l t_1\right)\cos\left(\omega_l t_2\right)\,dt_1 dt_2 \\
&= \frac{4}{T^2}\int_{-\frac{2}{T}}^{\frac{2}{T}}\int_{-\frac{2}{T}}^{\frac{2}{T}} \boldsymbol{\kappa}_{mn}\left(t_2 - t_1\right)\cos\left(\omega_l t_1\right)\cos\left(\omega_l t_2\right)\,dt_1 dt_2 \quad (7.34)
\end{aligned}
$$

It is seen, that $\kappa_{A_{cj}^m A_{cj}^n}$ depends on the cross covariance between the elevation processes $\eta_m\left(t_1\right)$ and $\eta_n\left(t_2\right)$. The cross covariance matrix $\boldsymbol{\kappa}_{mn}(\tau)$ is related to the cross spectral density matrix $S_{mn}(\omega)$ in terms of the Wiener-Khinchine relation

$$
\begin{aligned}
G_{mn}(\omega) &= 2S_{mn}(\omega) = 2\int_{-\infty}^{\infty} \boldsymbol{\kappa}_{mn}(\tau)\,e^{-i\omega\tau}\,d\tau \\
&= 2\int_{-\infty}^{\infty} \boldsymbol{\kappa}_{mn}(\tau)\cos\omega\tau\,d\tau - i\cdot 2\int_{-\infty}^{\infty} \boldsymbol{\kappa}_{mn}(\tau)\sin\omega\tau\,d\tau \\
&= C_{mn}(\omega) - i\,Q_{mn}(\omega) \quad (7.35)
\end{aligned}
$$

where $G_{mn}(\omega)$ is a one-sided spectrum.

$$C_{mn}(\omega) = 2 \int_{-\infty}^{\infty} \kappa_{mn}(\tau) \cos \omega\tau \, d\tau$$

and

$$Q_{mn}(\omega) = 2 \int_{-\infty}^{\infty} \kappa_{mn}(\tau) \sin \omega\tau \, d\tau$$

are the co-spectrum and the quad-spectrum, respectively.

Assuming the period T to be "very long" the following result is obtained from eq. (7.34)

$$\kappa_{A_{m,l}A_{n,l}}(t_1, t_2) = \kappa_{A_{m,l}A_{n,l}}(\tau) = \frac{1}{T} C_{mn}(\omega_l) = \frac{\Delta\omega}{2\pi} C_{mn}(\omega_l) = B_{mn}(7.36)$$

It is concluded that $\boldsymbol{B}$ in eq. (7.31) equals $\frac{\Delta\omega}{2\pi}$ multiplied by the co-spectrum of the elevation processes. Further $\boldsymbol{B}$ is time independent.

Using the same procedure the elements $\boldsymbol{E}$ and $\boldsymbol{D}$ of eq. (7.31) can be found and after some calculation the following result is obtained

$$\kappa_{\boldsymbol{A}\boldsymbol{A}^T}(\omega_l) = \frac{\Delta\omega}{2\pi} \begin{bmatrix} \boldsymbol{C} & \boldsymbol{Q} \\ -\boldsymbol{Q} & \boldsymbol{C} \end{bmatrix} = \frac{\Delta\omega}{2\pi} \cdot \boldsymbol{\Omega}(\omega_l) \tag{7.37}$$

i.e. the cross-covariance between the coefficients in eq. (7.27) at a given frequency ω_l is given in terms of the co- and quad-spectra of the elevation processes.

So far expressions have been established for the mean value vector (eq. (7.32) and eq. (7.33)) and the cross covariance matrix eq. (7.37) of the vector $\boldsymbol{A}$. These relations were established at a given frequency ω_l. Besides the frequency the wave pattern is also characterised by a direction of travel. The dependence of the frequency and the direction of travel is expressed in terms of the directional spectrum $S(\omega, \theta)$. The following relation exists between

the one-sided autospectral density $G(\omega)$ and $S(\omega, \theta)$

$$G(\omega) = \int_0^{2\pi} S(\omega, \theta) \, d\theta \qquad (7.38)$$

Furthermore, it can be shown that $S(\omega, \theta)$ is related to the cross spectral density matrix, $G_{mn}(\omega)$, of the elevation processes $\eta_m(\boldsymbol{x}_m, t)$ and $\eta_n(\boldsymbol{x}_n, t)$ as expressed in eq. (7.39)

$$\begin{aligned} G_{mn}(\omega) \quad &= \int_0^{2\pi} S(\omega, \theta) \left\{ \exp(i\boldsymbol{k} \left(\boldsymbol{x}_m - \boldsymbol{x}_n\right)) + r(\omega, \theta) \exp(i\boldsymbol{k} \left(\boldsymbol{x}_m - \boldsymbol{x}_n\boldsymbol{T}\right)) \right. \\ &\left. + r(\omega, \theta) \exp(i\boldsymbol{k} \left(\boldsymbol{x}_m\boldsymbol{T} - \boldsymbol{x}_n\right)) + r^2(\omega, \theta) \exp(i\boldsymbol{k} \left(\boldsymbol{x}_m - \boldsymbol{x}_n\right)\boldsymbol{T}) \right\} d\theta \end{aligned} \qquad (7.39)$$

where $r(\omega, \theta)$ is the reflection coefficient. The modelling of reflected waves is described in Christensen & S>rensen (1994). $\boldsymbol{T}$ is a transformation matrix equal to

$$\boldsymbol{T} = \begin{bmatrix} -1 & 0 \\ 0 & 1 \end{bmatrix} \qquad (7.40)$$

If the directional spectrum $S(\omega, \theta)$ was known eq. (7.39) may be used to calculate $G_{mn}(\omega)$, e.g. by numerical integration.

Based on eq. (7.35) $\boldsymbol{C}$ and $\boldsymbol{Q}$ are identified as the real and the imaginary parts of $\boldsymbol{G}$. Finally $\boldsymbol{\kappa}_{\boldsymbol{A A}^T}(\omega_l)$ can be determined from eq. (7.37). However, $S(\omega, \theta)$ is generally unknown. In the following a method will be presented which can be used to determine a directional spectrum expressed in standard form in terms of some unknown parameters. The method is known as the Maximum Likelihood (ML) method. As expressed earlier the elements in $\boldsymbol{A}$ have a joint normal distribution. The general expression for a density function of a vector $\boldsymbol{A}$ with $2M$ joint Gaussian elements having a mean value vector $\boldsymbol{E}(\boldsymbol{A}) = \boldsymbol{0}$ is

$$p_{\boldsymbol{A}}(\boldsymbol{a}) = \frac{1}{\left(\sqrt{2\pi}\right)^{2M} \left|\boldsymbol{\kappa}_{\boldsymbol{A A}^T}(\tau)\right|^{\frac{1}{2}}} \exp\left(-\frac{1}{2} \boldsymbol{a}^T \boldsymbol{\kappa}_{\boldsymbol{A A}^T}^{-1}(\tau) \boldsymbol{a}\right) \qquad (7.41)$$

where $\left|\boldsymbol{\kappa}_{\boldsymbol{A A}^T}\right|$ and $\boldsymbol{\kappa}_{\boldsymbol{A A}^T}^{-1}$ are the determinant and the inverse matrix of

$\boldsymbol{\kappa}_{\boldsymbol{A}\boldsymbol{A}^T}$ respectively.

If $S(\omega, \theta)$ was given eq. (7.41) could be used to calculate the probability of the observed realisation $\boldsymbol{a}$ of $\boldsymbol{A}$, where $\boldsymbol{a}$ represents the actual Fourier coefficients obtained from a given time-series. Since $S(\omega, \theta)$, or some parameters in $S(\omega, \theta)$, are unknown, a Likelihood function, $L(\cdot)$, will be formulated. Expressed in terms of the Likelihood function the unknown parameters in $S_\eta(\omega, \theta)$ are determined as the values corresponding to the maximum value of L.

In his article Isobe (1990) uses $\mathcal{L}$ time-series at each of the M locations $\boldsymbol{x}_p$, $p = 1, 2, \ldots, M$. Based on each of the $\mathcal{L}$ time-series an estimate $\boldsymbol{a}^{(l)}$, $l = 1, 2, \ldots, \mathcal{L}$, of $\boldsymbol{A}^{(l)}$ is obtained. The probability of $\boldsymbol{a}^{(l)}$ is given by eq. (7.41). Assuming the $\mathcal{L}$ observations to be independent the joint probability for obtaining exactly the $\mathcal{L}$ observed estimates $\boldsymbol{a}^{(l)}$ is given as $p_{\boldsymbol{A}}\left(\boldsymbol{a}^{(1)}\right) \cdot p_{\boldsymbol{A}}\left(\boldsymbol{a}^{(2)}\right) \cdot \ldots \cdot p_{\boldsymbol{A}}\left(\mathbf{a}^{(\mathcal{L})}\right)$. Therefore Isobe (1990) suggested a Likelihood function, $L(\cdot)$, as the $\mathcal{L}$'th root of this product, i.e.

$$L\left(\mathbf{a}^{(1)}, \ldots, \boldsymbol{a}^{(\mathcal{L})}, \boldsymbol{G}\right) = \left\{p_{\boldsymbol{A}}\left(\boldsymbol{a}^{(1)}\right) \cdot \ldots \cdot p_{\boldsymbol{A}}\left(\boldsymbol{a}^{(\mathcal{L})}\right)\right\}^{1/\mathcal{L}}$$

$$= \frac{1}{(\Delta\omega)^M \sqrt{\det(\boldsymbol{\Omega})}} \exp\left(-\frac{1}{2} \sum_{h=1}^{2M} \sum_{l=1}^{2M} \Omega_{hl}^{-1} \tilde{\Omega}_{lh}\right) \qquad (7.42)$$

where

$$\tilde{\Omega}_{lh} = \frac{2\pi}{\Delta\omega \cdot \mathcal{L}} \sum_{m=1}^{\mathcal{L}} a_{ml} a_{mh} \qquad (7.43)$$

where $\tilde{\boldsymbol{\Omega}}$ is the measured cross spectral density matrix.

Eq. (7.42) represents the probability of obtaining exactly the estimates $\boldsymbol{a}^{(l)}$, $l = 1, 2, \ldots, \mathcal{L}$. The unknown quantity in eq. (7.42) is $\boldsymbol{G}$ (or $S(\omega, \theta)$).

The optimal choice of $S(\omega, \theta)$ or (in practice) the unknown parameters in $S(\omega, \theta)$ are determined in order to maximise $L(\cdot)$, i.e. the optimal parameters maximise the probability of obtaining exactly the observed Fourier-coefficients.

7.3 The Bayesian Directional spectrum estimation Method

The Bayesian Directional spectrum estimation Method, BDM, is in principle similar to MLM. However, BDM makes use of a Bayesian approach in order to estimate the most likely estimate of the directional spectrum.

BDM has been presented by Hashimoto et al. (1987). It is assumed, that the directional spreading function $H(\omega, \theta)$ can be expressed as a piecewise-constant function, which takes only positive values. The directional spreading function is discretized into K intervals. Defining $x_l(\omega)$ as

$$x_l(\omega) = \ln H(\omega, \theta_l) \qquad l = 1, 2, ..., K \qquad K\Delta\theta = 2\pi \qquad (7.44)$$

$H(\omega, \theta)$ can be approximated to

$$H(\omega, \theta) \simeq \sum_{l=1}^{K} \exp(x_l(\omega))I_l(\theta) \qquad I_l = \begin{cases} 1 & (l-1)\Delta\theta \leq \theta < k\Delta\theta \\ 0 & \text{otherwise} \end{cases} \quad (7.45)$$

The relationship between the cross-spectrum and the directional spectrum has been deducted to

$$S_{mn}(\omega) = \int_0^{2\pi} S(\omega, \theta) \exp(-ikr_{mn} \cos(\theta - \beta_{mn}))d\theta \qquad (7.46)$$

Inserting the approximation eq. (7.45) and dividing by $S(\omega)$ leads to

$$\frac{S_{mn}(\omega)}{S(\omega)} \simeq \int_0^{2\pi} \sum_{l=1}^{K} \exp(x_l(\omega))I_l(\theta) \exp(-ikr_{mn} \cos(\theta - \beta_{mn}))d\theta$$

$$\simeq \sum_{l=1}^{K} \exp(x_l(\omega)) \exp(-ikr_{mn} \cos(\theta_l - \beta_{mn}))\Delta\theta \qquad (7.47)$$

If M wave gauges are available, eq. (7.47) can be applied to $N = M(M+1)/2$ spectra of which M will be autospectra. However, considering the N complex equations as two separate equations, i.e. the real term and the imaginary term, $2N$ real equations are obtained. Expressing these in an arbitrary order

eq. (7.47) can be rearranged to

$$S_j(\omega) = \sum_{l=1}^{K} \exp(x_l(\omega))\alpha_{jl}(\omega) + \varepsilon_j(\omega) \quad j = 1, 2, \ldots, M \qquad (7.48)$$

where an error $\varepsilon_{mn}(\omega)$ of the cross-spectrum $S_{mn}(\omega)$ has been added, and

$$\alpha_{jl}(\omega) = \frac{\exp(-ikr_{mn}\cos(\theta_l - \beta_{mn}))\Delta\theta}{\sqrt{S_{mm}(\omega)S_{nn}(\omega)}} \qquad (7.49)$$

$$S_j(\omega) = \frac{S_{mn}(\omega)}{S(\omega)\sqrt{S_{mm}(\omega)S_{nn}(\omega)}} \qquad (7.50)$$

$$\varepsilon_j(\omega) = \frac{\varepsilon_{mn}(\omega)}{\sqrt{S_{mm}(\omega)S_{nn}(\omega)}} \qquad (7.51)$$

where it is suggested that $1 \le j \le N$ denote real parts and $N < j \le 2N$ denote imaginary parts. However, the number of equations involved can be altered at will.

It is assumed that $\varepsilon_j : N(0; \sigma^2)$, hence when omitting the argument ω

$$\varepsilon_j = S_j - \sum_{l=1}^{K} \exp(x_l)\alpha_{jl} \qquad : N(0; \sigma^2)$$

S_j's and α_{jl}'s are given. σ^2 and x_l's are to be estimated.

The probability density function for ε_j is

$$p(\varepsilon_j) = \frac{1}{\sqrt{2\pi}\sigma} \exp\left(-\frac{\varepsilon_j^2}{2\sigma^2}\right)$$

The likelihood function is then

$$
L(\varepsilon_1, \varepsilon_2, ..., \varepsilon_{2N}; \sigma) = \prod_{j=1}^{2N} \frac{1}{\sqrt{2\pi}\sigma} \exp\left(-\frac{\varepsilon_j^2}{2\sigma^2}\right)
$$

$$
= \frac{1}{(2\pi\sigma^2)^N} \exp\left(-\sum_{j=1}^{2N} \frac{\varepsilon_j^2}{2\sigma^2}\right)
$$

$$
= \frac{1}{(2\pi\sigma^2)^N} \exp\left(\frac{-1}{2\sigma^2} \sum_{j=1}^{2N} \left(S_j - \sum_{l=1}^{K} \exp(x_l)\alpha_j\right)^2\right) \quad (7.52)
$$

$$
L(x_1, x_2, ..., x_K; \sigma) = L(\varepsilon_1, \varepsilon_2, ..., \varepsilon_{2N}; \sigma) \tag{7.53}
$$

for the given $S_j, \ j = 1, 2, ..., 2N$.

As the estimate of $H(\omega, \theta)$ becomes smoother, it is assumed, that the differences of second order of $x_l - 2x_{l-1} + x_{l-2}$ decrease, i.e. the value

$$
\sum_{l=1}^{K} (x_l - 2x_{l-1} + x_{l-2})^2 \tag{7.54}
$$

where $x_0 = x_K$ and $x_{-1} = x_{K-1}$, decreases as well.

Maximising the likelihood eq. (7.52) and minimising eq. (7.54) lead to the estimate which also maximises

$$
\ln L(x_1, x_2, ..., x_K; \sigma) - \frac{u^2}{2\sigma^2} \sum_{l=1}^{K} (x_l - 2x_{l-1} + x_{l-2})^2
$$

where u is introduced as a hyperparameter. Further applying the exponential function leads to the alternative expression

$$
L(x_1, x_2, ..., x_K; \sigma) \exp\left(-\frac{u^2}{2\sigma^2} \sum_{l=1}^{K} (x_l - 2x_{l-1} + 2x_{l-2})^2\right) \tag{7.55}
$$

At this stage the Bayesian approach is introduced utilising $p(y|\boldsymbol{x}) \propto L(y|\boldsymbol{x})p(y)$. When normalised the second term in eq. (7.55) can be regarded as the joint

distribution of $\boldsymbol{x} = (x_1, x_2, ..., x_K)$

$$p(\boldsymbol{x}|u^2, \sigma^2) = \left(\frac{u}{\sqrt{2\pi}\sigma}\right)^K \exp\left(-\frac{u^2}{2\sigma^2}\sum_{l=1}^{K}(x_l - 2x_{l-1} + x_{l-2})^2\right) \quad (7.56)$$

This correspond to the prior distribution and is known, when an estimate of $\boldsymbol{x}$ is given and u and σ have been estimated. Maximising eq. (7.55) leads to the posterior distribution, when inserting into $p(y|\boldsymbol{x}) \propto L(y|\boldsymbol{x})p(y)$, i.e.

$$p_{post}(\boldsymbol{x}|u, \sigma^2) \propto L(\boldsymbol{x}, \sigma^2)p_{prior}(\boldsymbol{x}|u, \sigma^2) \quad (7.57)$$

Hence minimising the following quantity determine the value of $\boldsymbol{x}$, which maximises eq. (7.57)

$$\frac{1}{2\sigma^2}\sum_{j=1}^{2N}\left(S_j - \sum_{l=1}^{K}\exp(x_l)\alpha_{jl}\right)^2 + \frac{u^2}{2\sigma^2}\left(\sum_{l=1}^{K}(x_l - 2x_{l-1} + x_{l-2})^2\right)$$

I.e. σ can be omitted reducing the above quantity to

$$\sum_{j=1}^{2N}\left(S_j - \sum_{l=1}^{K}\exp(x_l)\alpha_{jl}\right)^2 + u^2\left(\sum_{l=1}^{K}(x_l - 2x_{l-1} + x_{l-2})^2\right) \quad (7.58)$$

During the derivation of BDM it has been presumed that

- All values in the spreading functions are larger than zero

- The spreading functions are smooth (the smoothness being dependent on one parameter)

- The errors on the spectral estimates are outcomes of a Gaussian distribution function

The BDM turns out to be a very useful and reliable method for estimation of directional wave spectra. But some inaccuracy arises when the wave samples contain reflections, which in worst cases results in non-converging results. Similarly to the MLM it is possible to create additional constraints to the shape of the directional spreading function or make some assumptions about location and direction of the reflector.

7.4   Tests of the presented methods

In principle all methods for estimating reflected waves should be tested upon:

- Ability to process data correctly

- Robustness to possible errors

- Reliability of results from real wave data

In this section the performance of the methods are evaluated with numerical data in situations where the reflection is known, and no possible noise (errors) on the data are included.Moreover, the application of the BDM method to data from physical model tests is demonstrated.

7.4.1   MLM utilising standard spectra on numerical data

In the numerical tests performed, the generated data were simultaneous realizations of surface elevation time series recorded in a CERC5 wave gauge array with a radius of 1.0 m positioned at a water depth of 4.0 m, see fig. 7.2.

Two tests were performed: One in which no reflection occurred and one in which a wall with a reflection coefficient of $r=0.5$ was positioned at $x=0.0$ m, see fig. 7.2.
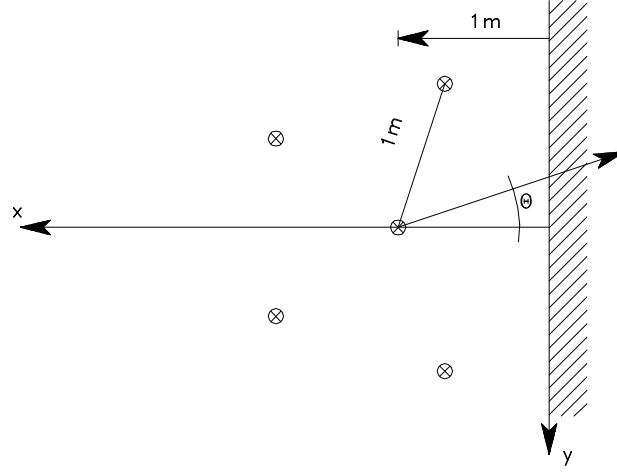
Figure 7.2: Wave gauge arrangement for numerical tests.

In both tests, the incident wave fields were irregular waves corresponding to a Pierson-Moskowitz spectrum ($f_p = 0.5Hz$, $H_s = 0.5m$) with a Mitsuyasu-type spreading function ($\theta_0 = \pi/3$, $s = 6$). A sample frequency of $f_s = 4Hz$ was applied.

Measured cross covariance matrices were determined from a total of 45 surface elevation subseries each of length $T=128$ s.

The estimated value of the auto spectral density $S_\eta(\omega)$ and the maximum likelihood estimates of the parameters θ_0 , s and r are given in fig. 7.3 and fig. 7.4. For comparison, the target values are plotted.

In both tests, the estimated values of the parameters are in good agreement with the target values. However, in the test involving reflection the method has some problems separating incident and reflected waves at some frequencies resulting in larger estimated values of the auto spectral density, see fig. 7.4 compared to the results obtained without reflection, see fig. 7.3.
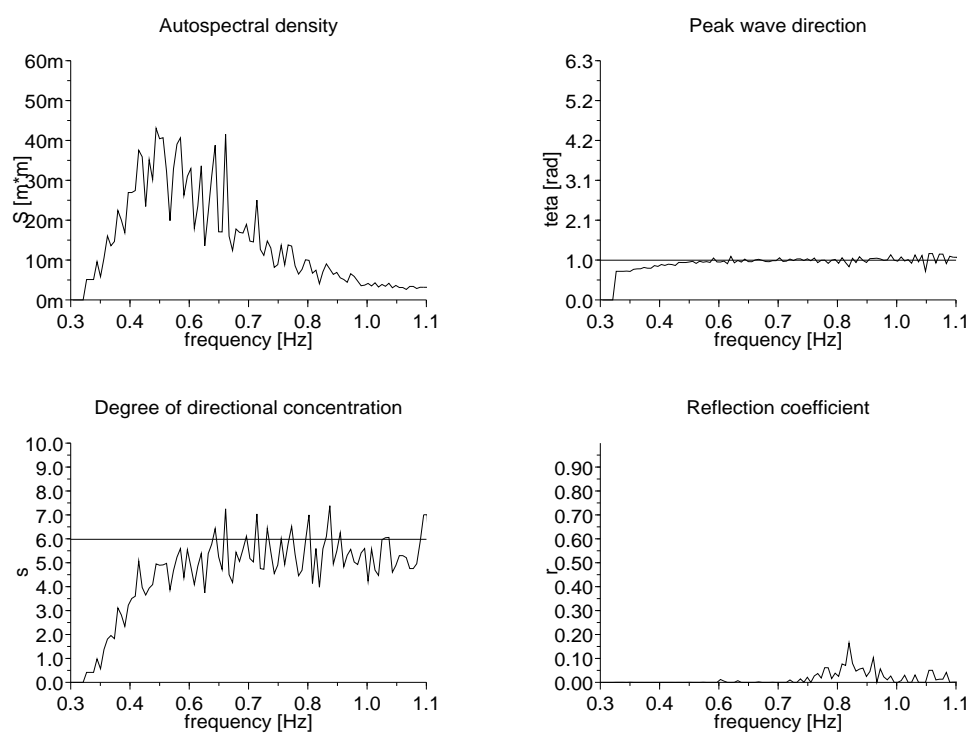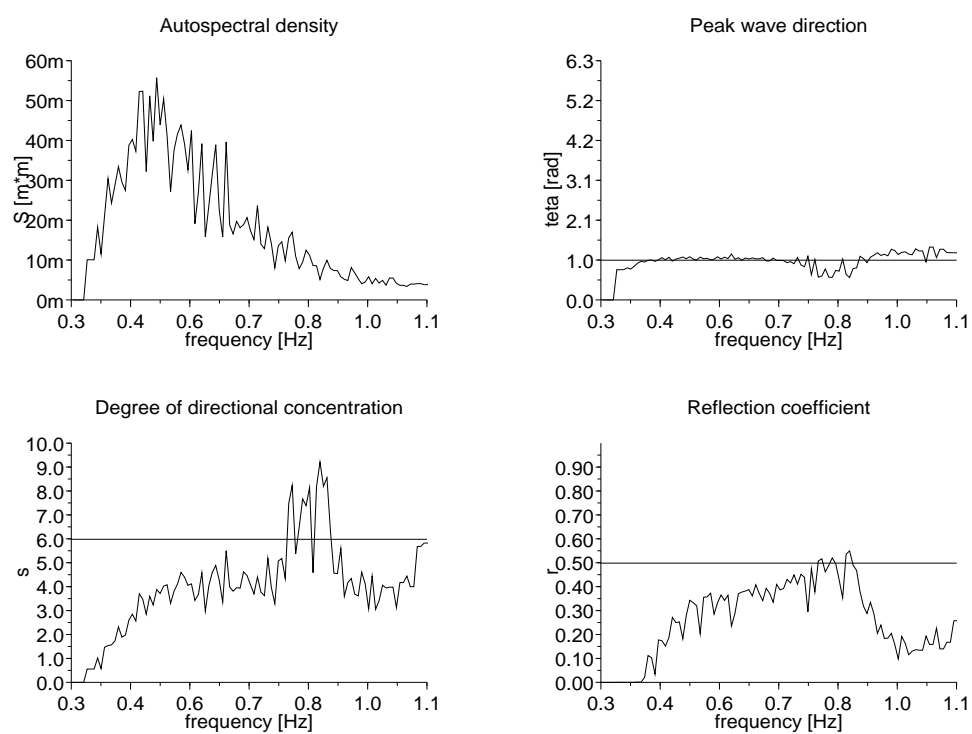
Figure 7.3: Numerical test results (no reflection).

Figure 7.4: Numerical test results (with reflection).

7.4.2 BDM on numerical data

The BDM method has been tested utilising numerical simulations of an unimodal wave field and a bi-modal wave field.

Only the bi-directional wave field test is shown, see fig. 7.5. In this case it is seen that both peaks are estimated well. Though the narrow peak is estimated most accurate.
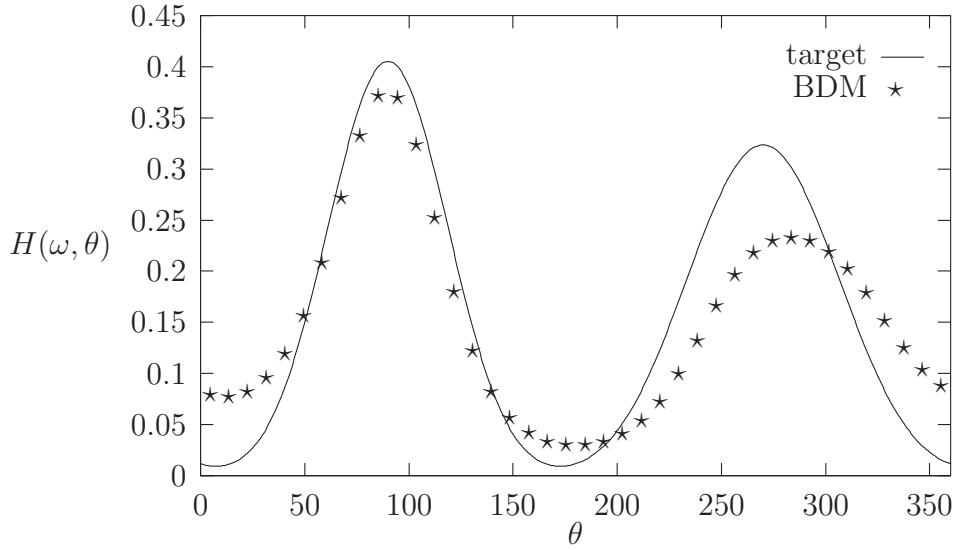

Figure 7.5: Test with simulated bi-directional wave field.

Data. Test 1.	
Date of sample	070893
Depth of water	$200m$
Radius of array	$26m$
Sample frequency	$4Hz$
Duration	$720sec.$
Quantity	Elevation
Autospectrum	P–M,
$T_p = 10s, \ H_s = 4.0m$	
Directional spreading function Mits.,	
$s_1 = 5, s_2 = 8, \theta_1 = -90°, \theta_2 = 90°$	

7.4.3 BDM on Model Test Data

In fig. 7.6 a test from Aalborg University's 3D wave basin is shown. The main direction of the incident waves is 290 degrees and the mean direction of the reflected waves should be 70 degrees.
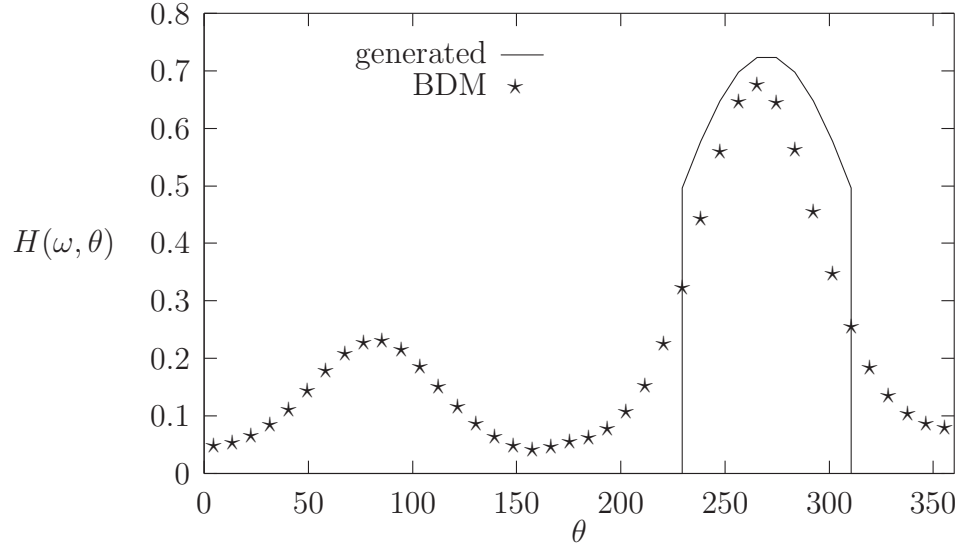

Figure 7.6: Test with reflected waves in 3D wave basin. Test 2.

Data. Test 2.	
Date of sample	090193
Depth of water	$0.6m$
Radius of array	$0.25m$
Sample frequency	$10Hz$
Duration	$720sec.$
Quantity	Elevation
Autospectrum	JONSWAP,
$T_p = 0.8s, \ H_s = 0.1m$	
Directional spreading function Mits.,	
truncated $s_1 = 3, \theta_1 = -90°$	

The BDM method estimates the incident wave energy to be spread over a wider range. This is reasonable considering the conditions in the basin, i.e. limitations due to boundary conditions. The mean direction of the reflected waves though deviate about 20 degrees.

7.5   Conclusion

Several different methods for estimating reflection have been presented and tested in the previous chapters.

The methods for estimating reflection are divided into groups:

- *Frequency domain* methods for 2-dimensional waves.

- *Time domain* methods for 2-dimensional waves.

- *Frequency domain* methods for 3-dimensional waves.

The *frequency domain* methods give the incident wave spectrum and the reflected wave spectrum. The *time domain* methods give the incident waves as function of time.

Some of the methods take into account the 3-dimensionality of the waves. If waves on location are 3-dimensional it is necessary to use a method for 3-dimensional waves, though because the methods for estimating reflection in 3-dimensional waves introduce the directional spreading function with many degrees of freedom, they become less statistically reliable.

Chapter 8

Wave Groups

A wave group is generally defined as a sequence of consecutive high waves in a random wave train.

In sea wave recordings, group formations of high waves occur from time to time. This phenomenon corresponds to a non-zero correlation between successive waves. Information concerning this correlation is of importance when reproducing waves in the laboratory in order to determine the response of the modelled structure. Normally, irregular waves are reproduced in accordance with a specific energy spectrum solely defining the distribution of the variances. The grouping of waves is determined by the distribution of the phases. Hitherto, independence between successive waves have been applied and the phases are treated as independent random variables, each with a uniform probability density on the interval $[0;2\pi]$ leading to a sea surface that is Gaussian distributed. However, if the waves during wave propagation become more non-linear there will be some coupling and thus dependence of the phases of the component waves at different frequencies, which eventually will modify the wave grouping.

To illustrate the effect of randomly assigned phases two wave trains are generated from the same energy spectrum. These two wave conditions are depicted in Figure 8.1.

Figure 8.1 shows different groupiness characteristics, and clearly it is important to have information on the wave grouping when coastal structures respond differently when exposed to the distinctive wave patterns. Especially, the stability of rubble mound structures appears to be significantly affected by the wave grouping, but also the slow drift oscillations of moored vessels is highly dependent on the wave grouping.

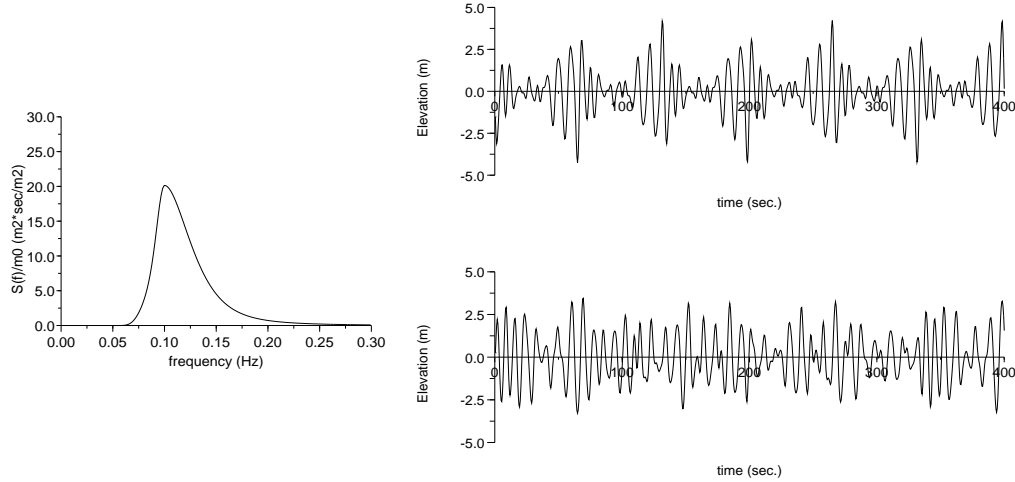Burcharth (1979) and Johnson et al. (1978) found that the wave grouping

Figure 8.1: *Wave energy spectrum and generated grouped and non-grouped wave trains.*

significantly affects the stability of rubble mound breakwaters as well as the run-up. Johnson et al., (1978) compared the effects of a grouped and a non-grouped time series generated from the same energy spectrum, thus having the same statistical properties. Conclusively, the model tests showed that the breakwater response to the two different wave trains was quite different, with the grouped wave train causing severe damage and the non-grouped only causing minor rocking of the armour units. Similar significant influence on the wave grouping was found in the tests performed by Burcharth (1979).

In irregular seas, model tests by Spangenberg (1980) showed that the wave grouping has a significant influence on the slow drift motion of moored platforms and vessels. This influence might be explained by the fact that the period of the slow drift oscillations practically corresponds to the wave group period where the wave grouping is pronounced.

Both examples illustrate the importance of a correct modelling of natural sea waves in the laboratory if the structural responses are sensitive to the wave grouping. A characterization of the wave grouping seems therefore evident.

8.1 Description of Wave Groups

A measure of the wave grouping is obtained by defining the wave envelope to the time signal. Due to the presence of small waves in the signal the wave envelope is difficult to determine. However, if the time signal is squared, the squaring procedure will suppress the relative influence of the small waves present, and furthermore, a slowly varying part appears which may be inter-

preted as the square envelope.

Assuming that the sea surface elevation at a given point is a realization of a linear stationary Gaussian process defined by its one-sided spectrum $S_\eta(f)$, it can be represented by an ordinary sum of a finite number of waves

$$\eta(t) = \sum_{n=1}^{N} c_n \cos(\omega_n t + \varepsilon_n) \tag{8.1}$$

where c_n = amplitude, ω_n = cyclic frequency, and ε_n = phase angle. By squaring the time signal following equation is obtained

$$\eta^2(t) = \sum_{n=1}^{N}\sum_{m=1}^{N} c_n c_m \cos(\omega_n t + \varepsilon_n)\cos(\omega_m t + \varepsilon_m) \tag{8.2}$$

$$= \sum_{n=1}^{N}\sum_{m=1}^{N}\{c_n c_m(\frac{1}{2}\cos((\omega_n + \omega_m)t + (\varepsilon_n + \varepsilon_m)) +$$

$$\frac{1}{2}\cos((\omega_n - \omega_m)t + (\varepsilon_n - \varepsilon_m)))\} \tag{8.3}$$

Equation (8.3) represents a splitting of $\eta^2(t)$ into a slowly varying part (represented by the difference-frequencies) and a more rapid oscillating part (represented by the summation-frequencies).

By use of symmetry of the double summation, equation (8.3) can be expressed in terms of four separate contributions

$$\eta^2(t) = \frac{1}{2}\sum_{n=1}^{N} c_n^2 + \frac{1}{2}\sum_{n=1}^{N} c_n^2 \cos(2\omega_n t + 2\varepsilon_n)$$

$$+ \sum_{n=1}^{N}\sum_{m=n+1}^{N} c_n c_m \cos((\omega_n + \omega_m)t + (\varepsilon_n + \varepsilon_m))$$

$$+ \sum_{n=1}^{N}\sum_{m=n+1}^{N} c_n c_m \cos((\omega_n - \omega_m)t + (\varepsilon_n - \varepsilon_m))) \tag{8.4}$$

The four terms on the right-hand side of equation (8.4) are identified as follows: The first term consists of a constant off-set component. The second and third term constitutes the superharmonic components, i.e. the summation-frequency terms, and the fourth term constitutes the subharmonic components, i.e. the difference-frequency terms. It is the latter that describes the

slowly varying part of the squared time signal and the term which may be interpreted as the square envelope. By means of Bartlett filtering the superharmonic components on the right-hand side of equation (8.4) may be filtered out after subtraction of the constant off-set as done by Funke and Mansard (1979).

Funke and Mansard denoted the filtered square of the time signal the SIWEH (Smoothed Instantaneous Wave Energy History) function as the function provides a measure of the instantaneous wave energy in the time signal.

The effect of the Bartlett filtering corresponds to a digital low pass filtering and the efficiency of the SIWEH analysis can best be interpreted by examination of the energy spectrum of the stochastic process in (8.1) and the energy spectrum of the squared process.
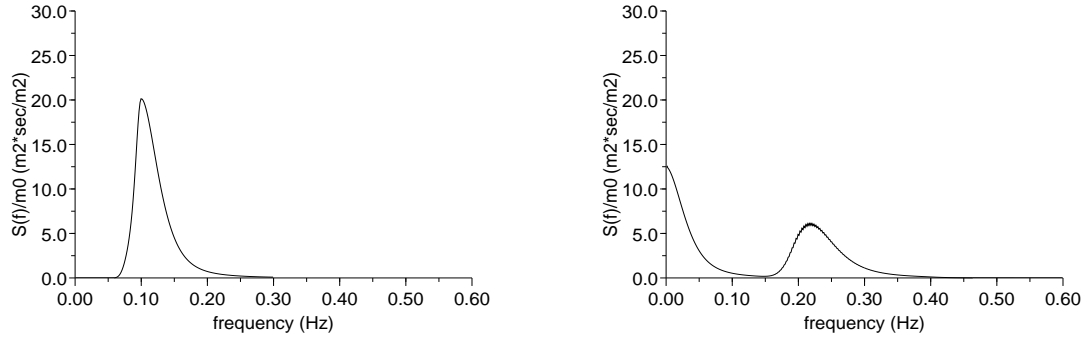

Figure 8.2: a) *JONSWAP energy spectrum for a linear stochastic process and* b) *energy spectrum for the squared process.*

From figure 8.2 it is understood that the SIWEH analysis does not exactly isolate the slowly varying part; also contributions from the superharmonic components occur and not the complete amount of energy from the subharmonic components is included. Only when the process is narrow-banded does the SIWEH analysis perform well but as the process becomes more and more broad-banded the SIWEH function is a poor estimator of the wave envelope, see Hupspeth and Medina (1988).

Instead of using a Bartlett window to isolate the subharmonic components, a wave envelope function defined on basis of the time series and its Hilbert transform isolates exactly the subharmonic components.

104

8.2 Hilbert Transform Technique

From the sea surface elevation $\eta(t)$ a conjugate signal $\hat{\eta}(t)$ is uniquely obtained by shifting the phase of each elementary harmonic component of $\eta(t)$ by $\pm\frac{\pi}{2}$. When the phase angles of all components of a given signal are shifted $\pm\frac{\pi}{2}$, the resulting function $\hat{\eta}(t)$ is known as the Hilbert transform of the original signal $\eta(t)$. The Hilbert transform is defined by

$$\hat{\eta}(t) = \frac{1}{\pi} \int_{-\infty}^{\infty} \frac{\eta(t)}{t-\tau} d\tau \tag{8.5}$$

From the definition of the Hilbert transform it is noted that $\hat{\eta}(t)$ is simply the convolution of $\eta(t)$ with a linear filter with the impulse response function $h(t) = \frac{1}{\pi t}$ [1]. Since a convolution of two functions in the time domain are transformed into a multiplication of their Fourier transforms in the frequency domain [2] a frequency response function $H(f)$ is related to the impulse response function. The frequency response function provides an equally characterization of the linear time-invariant input and output system in (8.5) and does furthermore visualize the effect of the Hilbert transform operation. Through the Fourier transform the frequency response of the Hilbert transformer becomes

$$H(f) = \mathcal{F}[\frac{1}{\pi t}] = -i\,\text{sgn}(f) = \begin{cases} -i & f > 0 \\ 0 & f = 0 \\ i & f < 0 \end{cases} \tag{8.6}$$

The gain of this frequency response function is $\sqrt{\text{re}^2(H(f)) + \text{im}^2(H(f))}$ resulting in unity in magnitude, and thus, the amplitudes of the signal does not change. The phase angle is $\arctan(\frac{\text{im}(H(f))}{\text{re}(Hf))})$ resulting in a phase angle of $-\frac{\pi}{2}$ for $f > 0$ and $+\frac{\pi}{2}$ for $f < 0$. Such a system is denoted an ideal 90-degree phase shifter.

Consequently, applying the Hilbert transform operation to the sea surface elevation in (8.1) the cosine function simply shifts to the sine function

$$\hat{\eta}(t) = \sum_{n=1}^{N} c_n \sin(\omega_n t + \varepsilon_n) \tag{8.7}$$

Associated with the Hilbert transform is the complex analytical signal defined

---

[1] The convolution of the functions $g(t) * h(t)$ is: $g(t) * h(t) \equiv \int_{-\infty}^{\infty} g(\tau)h(t-\tau)d\tau$

[2] The convolution theorem: $g(t) * h(t) \Leftrightarrow G(f)H(f)$

from the original signal $\eta(t)$ and the Hilbert transform $\hat{\eta}(t)$

$$
\begin{aligned}
\tilde{\eta}(t) &= \mid \tilde{\eta}(t) \mid \; \exp(i\psi(t)) = \mid \tilde{\eta}(t) \mid \; \cos(\psi(t)) + i \mid \tilde{\eta}(t) \mid \; \sin(\psi(t)) \\
&= \eta(t) + i\hat{\eta}(t)
\end{aligned} \tag{8.8}
$$

where the envelope or the modulation $\mid \tilde{\eta}(t) \mid = \sqrt{\eta^2(t) + \hat{\eta}^2(t)}$ and the associated phase $\psi(t) = \arctan(\frac{\hat{\eta}(t)}{\eta(t)})$. The properties of the Hilbert transform operation entail that the slowly varying difference-frequency terms in the second order expression $\eta^2(t)$ are separated mathematically by the expression

$$
E(t) \equiv \mathrm{re}(\tilde{\eta}^*(t)\tilde{\eta}(t)) = \mid \tilde{\eta}(t) \mid^2 \tag{8.9}
$$

where $\tilde{\eta}^*(t) = $ the complex conjugate and $E(t) = $ the square wave envelope function.

In order to visualize the effect of the defined envelope function the Hilbert transform of the sea surface elevation is squared and rewritten by use of trigonometry and symmetry of the double summation similar to $\eta^2(t)$

$$
\begin{aligned}
\hat{\eta}^2(t) &= \sum_{n=1}^{N}\sum_{m=1}^{N} c_n c_m \sin(\omega_n t + \varepsilon_n)\sin(\omega_m t + \varepsilon_m) \tag{8.10} \\
&= \sum_{n=1}^{N}\sum_{m=1}^{N}\{c_n c_m(\frac{1}{2}\cos((\omega_n - \omega_m)t + (\varepsilon_n - \varepsilon_m)) - \\
&\quad \frac{1}{2}\cos((\omega_n + \omega_m)t + (\varepsilon_n + \varepsilon_m)))\} \tag{8.11} \\
&= \frac{1}{2}\sum_{n=1}^{N} c_n^2 - \frac{1}{2}\sum_{n=1}^{N} c_n^2 \cos(2\omega_n t + 2\varepsilon_n) \\
&\quad - \sum_{n=1}^{N}\sum_{m=n+1}^{N} c_n c_m \cos((\omega_n + \omega_m)t + (\varepsilon_n + \varepsilon_m)) \\
&\quad + \sum_{n=1}^{N}\sum_{m=n+1}^{N} c_n c_m \cos((\omega_n - \omega_m)t + (\varepsilon_n - \varepsilon_m))) \tag{8.12}
\end{aligned}
$$

Remembering that the squared time signal is given by (8.4), the square wave envelope function, according to (8.9), then becomes

$$
E(t) = \sum_{n=1}^{N} c_n^2 + 2\sum_{n=1}^{N}\sum_{m=n+1}^{N} c_n c_m \cos((\omega_n - \omega_m)t + (\varepsilon_n - \varepsilon_m)) \tag{8.13}
$$

Introducing $\frac{1}{\sqrt{2}}$ in the complex analytical signal $\tilde{\eta}(t) = \frac{1}{\sqrt{2}}(\eta(t) + i\hat{\eta}(t))$ leads to the definition of an envelope function which may be interpreted as half the square envelope.

$$E(t) = \mid \tilde{\eta}(t) \mid^2 = \frac{1}{2}(\eta^2(t) + \hat{\eta}^2(t)) \tag{8.14}$$

This envelope function isolates exactly the slowly varying part of the squared time signal plus the constant off-set similar to what approximately is achieved by the SIWEH analysis.

The present method seems to be more convenient than the SIWEH analysis and it does not require the narrow-band spectrum assumption. The disadvantage of this method is however that the sea surface must be described by a linear model.

8.2.1 Computation of half the square envelope

To compute the Hilbert transform numerically the continuous-time convolution integral in (8.5) is approximated by a discrete-time Hilbert transformation. Furthermore, as the Hilbert transformation is non-banded, approximations limiting the impulse response function are made. A tool to handle the ideal Hilbert transformation of the sea surface elevation is by using FIR approximations. In such approximations the 90-degree phase shift is conserved exactly.

The principle in the FIR approximation is that the convolution integral in (8.5) is represented by a summation over a finite number of coefficients where the coefficients are fitted to represent the impulse response function. Taking an even number of coefficients, easily extended to an odd number, the non-causal FIR approximation can be written

$$\hat{\eta}_j = \sum_{k=-N_c/2}^{N_c/2-1} c_k \eta_{j-k} = \sum_{k=0}^{N_c-1} c_k \eta_{j+k-N_c/2} \tag{8.15}$$

where c_k = the k'th coefficient, N_c = number of coefficients or filter length, $\hat{\eta}_j$ is the Hilbert transform corresponding to the time step j, and $\eta_{j+k-N_c/2}$ are the input elevations to the filter system. The reason why the index on the filter coefficients remain unchanged is that the coefficients are mirrored in the Nyquist frequency, i.e. the frequency corresponding to half the filter length. The coefficients are derived from the frequency response function by FFT

to obtain a least-square fit of the coefficients. Opposite the centered format definition of the Fourier transformation, the FFT is based on a one-sided format

$$c_k = \frac{1}{N_c} \sum_{j=0}^{N_c-1} X_j \exp(i\omega_j k \Delta t) = \frac{1}{N_c} \sum_{j=0}^{N_c-1} X_j \exp(i\frac{2\pi jk}{N_c}) \qquad (8.16)$$

where ω_j is the cyclic frequency corresponding to the j'th coefficient and X_j is the desired sampled frequency response of the system. By using the one-sided format a time delay corresponding to half the filter length is introduced

$$\tau = \frac{N_c}{2}\Delta t \qquad (8.17)$$

The corresponding phase delay may then be found as

$$\psi_\tau = \tau\omega_j = \tau\frac{2\pi j}{N_c\Delta t} = \pi j \qquad (8.18)$$

To compensate for the phase delay the original frequency response function given by (8.6) only needs to be multiplied by a linear phase shift operator $\exp(-i\pi k)$ and X_j might be interpreted as

$$X_j = H(f_j)\exp(-i\pi j) = G(f_j)\cos(\psi_j - \pi j) + iG(f_j)\sin(\psi_j - \pi j) \qquad (8.19)$$

where $G(f_j)$ is the gain of the input amplitude to equal the output amplitude and $\psi_j - \pi j$ is the phase difference between the input and the output signal.

To sample the frequency response function the frequency band is subdivided into N_c discrete frequencies where $f_j = j\frac{f_s}{N_c}$ and f_s is the sample frequency. Since the phase $\psi_j = -\frac{\pi}{2}$ for $0 < f_j < f_{Nq}$ and $\psi_j = \frac{\pi}{2}$ for $f_{Nq} < f_j < 2f_{Nq}$ the sampled discrete frequency response function becomes

$$H(f_j) = \begin{cases} G(f_j)\cos(-\frac{\pi}{2} - \pi j) + iG(f_j)\sin(-\frac{\pi}{2} - \pi j) & 0 < f_j < f_{Nq} \\ 0 & f_j = 0, f_{Nq} \\ G(f_j)\cos(-\frac{\pi}{2} - \pi j) - iG(f_j)\sin(-\frac{\pi}{2} - \pi j) & f_{Nq} < f_j < 2f_{Nq} \end{cases} \qquad (8.20)$$

Due to the truncation of the Fourier transformation, the filter frequency response will differ from the desired frequency response. To illustrate the effect of the least-square fit, both the gain and phase characteristic of a linear FIR Hilbert filter are plotted in figure 8.3.
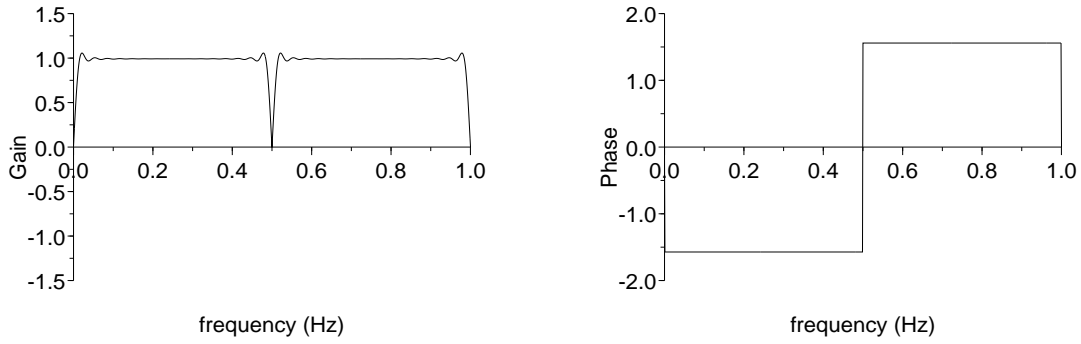
Figure 8.3: *Gain and phase characteristic of linear FIR Hilbert filter with a filter length $N_c = 64$ and $f_s = 1.0$ Hz.*

To compare the FIR approximated Hilbert transform with the theoretical Hilbert transform an irregular time signal is generated from the JONSWAP spectrum and the two transforms are depicted in figure 8.4. Generally very good accordance is observed also at the edges where a zone of half the filter length normally is disturbed.
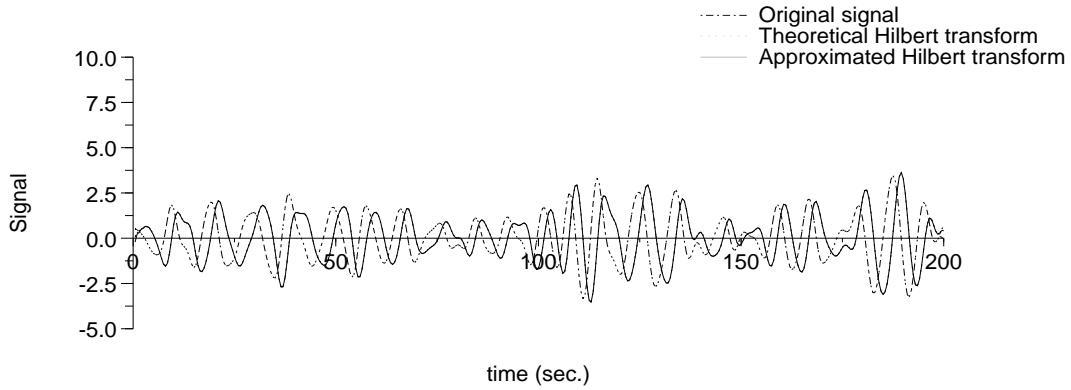

Figure 8.4: *Comparison of theoretical and FIR approximated, $N_c = 64$, Hilbert transform. The signal is generated from the JONSWAP spectrum, $f_p = 0.1$ Hz and $\gamma = 3.3$.*

To illustrate the envelope function, $E(t)$ is plotted together with half the squared elevation in figure 8.5 for a time signal generated from the JONSWAP spectrum.
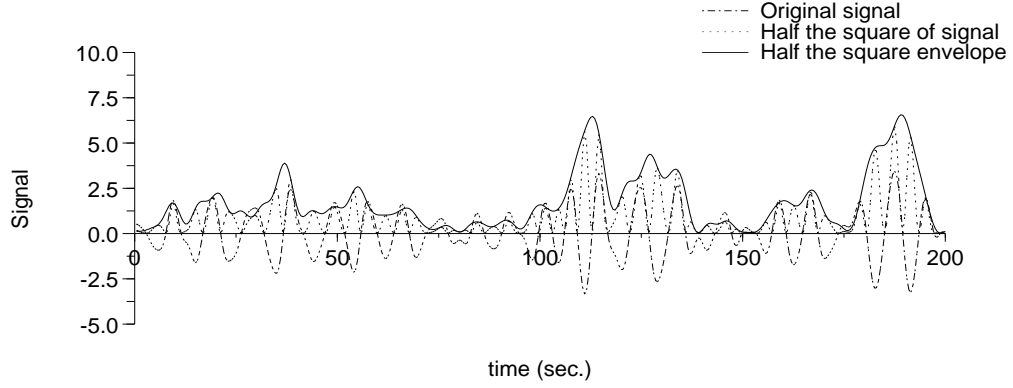
Figure 8.5: *Comparison of half the square envelope $E(t)$ and $\frac{1}{2}\eta^2(t)$ for signal generated from a JONSWAP spectrum, $f_p = 0.1$ Hz, $\gamma = 3.3$, and $N_c = 64$.*

8.3 Groupiness Factor

To characterize the actual groupiness of a wave train the energy spectrum $S_{\hat{\eta}}(f)$ of half the square envelope function can be evaluated. However, a simpler measure is the groupiness factor that is defined as the standard deviation of half the square envelope relative to the variance of the original time signal

$$GF = \frac{\sigma[E(t)]}{\sigma^2[\eta(t)]} \tag{8.21}$$

For a monochromatic (sinusoidal) signal the envelope function $E(t)$ is constant leading to a groupiness factor $GF = 0$. Taking a completely Gaussian signal the expected value of the groupiness factor can be shown to be equal to 1.0 independent of the spectrum shape. The actual values for time signals generated from a JONSWAP spectrum including approximately 500 periods are approximately 1.0 in mean with a standard deviation of approximately $\sigma = 0.13$.

Instead of computing one value of the groupiness factor over the complete length of the time signal, the groupiness factor can be evaluated as instantaneous values by computing an average groupiness factor over a time moving window. The length of the window in time is dependent on the desired degree of smoothing of the computed groupiness factor function.

In figure 8.6 to figure 8.9 the groupiness factor function is plotted for both a narrow-banded and a broad-banded JONSWAP spectrum for two different window sizes.
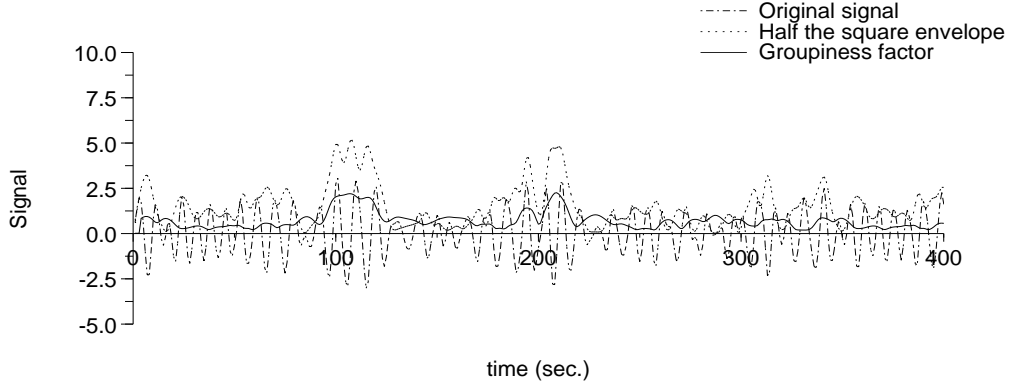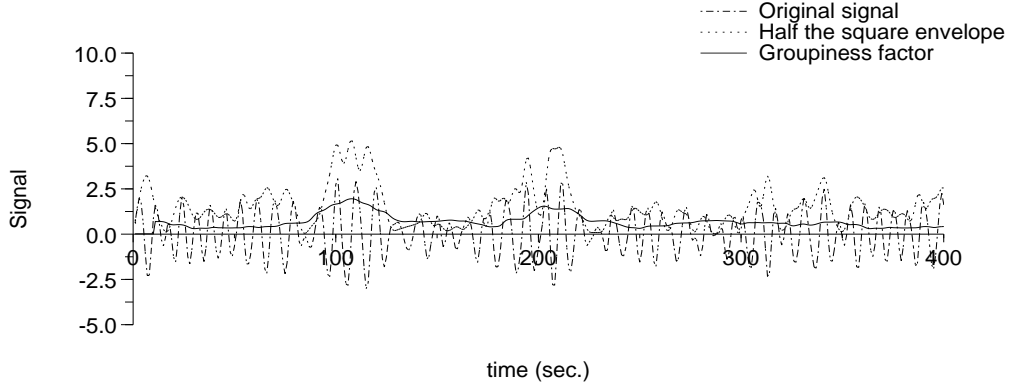
Figure 8.6: *Groupiness factor function GF(t) for signal generated from JON-SWAP spectrum, f_p = 0.1 Hz, f_s = 1.0 Hz, γ = 10.0, N_c = 64, and window size = T_m.*

Figure 8.7: *Groupiness factor function GF(t) for signal generated from JON-SWAP spectrum, f_p = 0.1 Hz, f_s = 1.0 Hz, γ = 10.0, N_c = 64, and window size = $3T_m$.*

Generally, a more smooth groupiness factor function is obtained for a window size of 3 mean periods and only the largest wave groups are separated as high and smooth peaks. It should though be noted that the sample frequency is 1.0 Hz and that a higher sample frequency eventually will lead to smoother groupiness factor function for smaller window sizes.
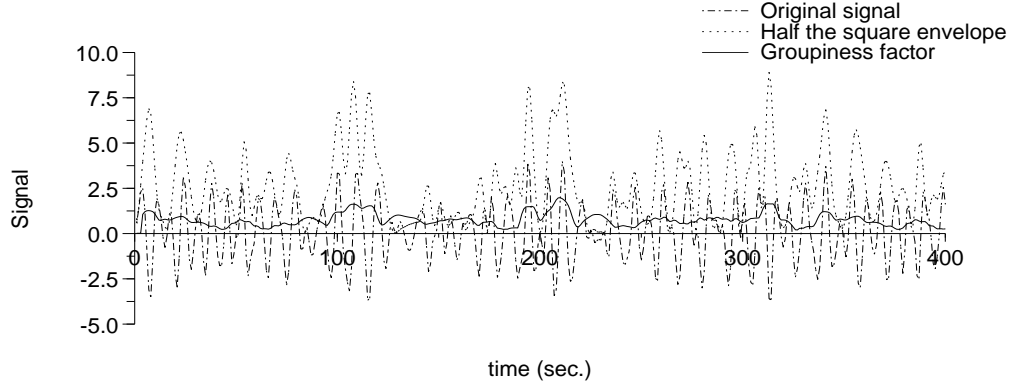
Figure 8.8: *Groupiness factor function GF(t) for signal generated from JON-SWAP spectrum, $f_p = 0.1$ Hz, $f_s = 1.0$ Hz, $\gamma = 1.0$, $N_c = 64$, and window size $= T_m$.*
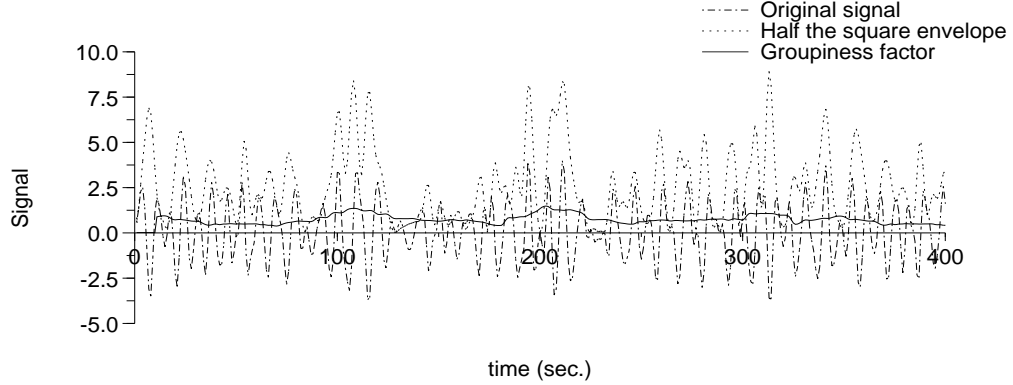

Figure 8.9: *Groupiness factor function GF(t) for signal generated from JON-SWAP spectrum, $f_p = 0.1$ Hz, $f_s = 1.0$ Hz, $\gamma = 1.0$, $N_c = 64$, and window size $= 3T_m$.*

8.4 Conclusions and Further Use

Based on a linear assumption a method for calculating the instantaneous wave energy history and the groupiness factor function has been presented. The method is based on a temporal Hilbert filter and this approach enables an exact isolation of the 2nd order subharmonics which describe the slowly varying part of the time signal. This Hilbert filter approach is thus more efficient than the SIWEH analysis. The groupiness factor has proven to be ineffective in describing Gaussian distributed sea surfaces and the groupiness factor function is defined. Also discussions regarding the implementation of the Hilbert filter using FIR approximations and choice of window sizes for computing the groupiness factor functions are made.

The method can easily be extended to a three-dimensional motion but a physical interpretation of the more slowly varying part must then be revised.

The groupiness factor function enables computations of instantaneous groupiness factors in time and hence, the function is suitable for comparing the correlation between the damage development of e.g. a breakwater and the wave grouping in the wave train causing the damage.

A further application is the possibility to evaluate the change in wave grouping due to shoaling and thus also the change in phase distribution from deep to shallow water.

Chapter 9

References

Aalborg University, 2012.
WaveLab 3 homepage. http://www.hydrosoft.civil.aau.dk/wavelab/

Battjes, J. A. and Groenendijk, H. W.
Wave height distributions on shallow foreshores.
Coastal Engineering, Vol. 40, 2000, pp. 161-182.

Brorsen, M. and Frigaard, P., 1992.
Active Absorption of Irregular Gravity Waves in BEM-models. Boundary Elements XIV, Vol.1 Editors: Brebbia, Dominiquez and Paris. Computational Mechanics Publications, Southampton.

Christensen, M. and N. B. Sørensen, 1994.
"Maximum Likelihood Estimation of Directional Spectrum Expressed in Standard Form"
Aalborg University.

Davis, Russ E. and Regier, Lloyd A., 1977.
"Methods for estimating directional wave spectra from multi-element arrays".
Journal of Marine Research.

Frigaard, P. and Brorsen, M., 1993.
"A time-domain method for Separating Incident and Reflected Irregular Waves.
Coastal Engineering, Vol. 24, Nos. 3 and 4.

Frigaard, P., Helm–Petersen, J., Klopman, G., Stansberg, C.T., Benoit, M., Briggs, J., Miles, M., Santas, J., Schäffer, H.A. and Hawkes, P.J., 1997.
IAHR List of Sea State Parameters – an update for multidirectional waves.
IAHR Seminar Multidirectional Waves and their Interaction with Structures, IAHR Congress, San Francisco.

Grønbech, J., Jensen, T. and Andersen, H. (1996).
Reflection Analysis with Separation of Cross Modes.
Proc. 25th Int. Conf. on Coastal Eng., Orlando, Florida, USA, pp. 968-980.

Goda, Y. and Suzuki, Y., 1976.
"Estimation of Incident and Reflected Waves in Random Wave Experiments"
Proceedings, 15th International Conference on Coastal Engineering, Vol. 1, pp. 828-845, Honolulu, Hawaii.

Goda, Y., 1986.
Effect of wave tilting on zero-crossing wave heights and periods.
Coastal Engineering in Japan, Vol. 29, pp. 79-90.

Goda, Y., 2010.
Random Seas and Design of Maritime Structures, 3rd Edition.
Advanced Series on Ocean Eng., Vol. 38, World scientific publishing.

Hashimoto, N. and Kobune, K., 1988.
"Directional spectrum estimation from a Bayesian approach".
Proceedings, 21st Conference on Coastal Engineering, Vol. 1, pp 62-76, Costa del Sol-Malaga, Spain.

Helm–Petersen, J., 1993.
"The Bayesian Directional Spectrum Estimation Method"
Master Thesis, Aalborg University

Isobe, M., 1990.

"Estimation of Directional Spectrum Expressed in Standard Form"
Proc. 22nd Int. Conf on Coastal Eng., pp. 647-660.

Isobe, M. and K. Kondo, 1984.
"Method for Estimating Directional Wave Spectrum in Incident and Reflected Wave Field"
Proc. 19th Int. Conf on Coastal Eng., pp. 467-483.

Isobe, M., Kondo, K. and Horikawa, K., 1984.
"Extension of MLM for estimating directional wave spectrum".
University of Tokyo, Japan.

Karl, John H., 1989.
"An Introduction to Digital Signal Processing"
Academic Press, San Diego.

Klopmann, G. and Stive, M.J.F., 1989.
"Extreme waves and wave loading in shallow water."
E & P Forum, Report No. 3.12/156.

Mansard, E. and Funke, E., 1980.
"The Measurement of Incident and Reflected Spectra Using a Least Squares Method"
Proceedings, 17th International Conference on Coastal Engineering, Vol. 1, pp 154-172, Sydney, Australia.

Nelder, J. A. and R. Mead, 1965.
Computer Journal, vol. 7, p. 308.

Neu, H.J.A., 1982.
"11-year deep water wave climate of Canadian Atlantic waters."
Canadian Tech. Rept. of Hydrography and Ocean Sciences, 13.

Newland, D.E., 1975.
"In introduction to random vibrations and spectral analysis."
Longman, London, 1975.

Ochi, Michel K. 1998
"Ocean Waves - The Stochastic Approach"
Cambridge University Press, Cambridge. ISBN: 0-521-56378

Press, W. H., B. P. Flannery, S. A. Teukolsky and W. T. Vetterling, 1989.
"Numerical Recipes in Pascal".
Cambridge University Press, Cambridge.

Raunholt, L. & Skjærbæk, P. 1990
Optimering af lodrette perforerede plader som bølgeabsorber (in Danish)
Master Thesis, Aalborg University

Stive, M.J.F., 1986.
"Extreme shallow water conditions."
Delft Hydraulics, Intern Report H533.

Tucker, M.J., 1991.
"Waves in ocean engineering: measurement, analysis, interpretation".
Ellis Horwood Ltd.

Yokoki, H., M. Isobe and A. Watanabe, 1992.
"A Method for Estimating Reflection Coefficient in Short Crested Random Seas"
Proc. 23rd Int. Conf on Coastal Eng., pp. 765-776.

Young, I.R., 1999
"Wind Generated Ocean Waves."
Elsevier, Kidlington, Oxford 1999. ISBN: 0-08-04331

Zelt, J.A. and Skjelbreia, J., 1992.
"Estimating Incident and Reflected Wave Fields Using an Arbitrary Number of Wave Gauges"
Proceedings, 23th International Conference on Coastal Engineering, Vol. 1, pp 777-789, Venice, Italy.